DEVELOPMENT AND APPLICATION OF MICROPATTERNED LIPID BILAYER ARRAYS USING FLUORESCENCE MICROSCOPY AND SUM-FREQUENCY VIBRATIONAL IMAGING

by

Kathryn Alice Smith

A dissertation submitted to the faculty of
The University of Utah
in partial fulfillment of the requirements for the degree of

Doctor of Philosophy

Department of Chemistry

The University of Utah

December 2012

The University of Utah Graduate School

STATEMENT OF DISSERTATION APPROVAL

The dissertation of **Kathryn Alice Smith**

has been approved by the following supervisory committee members:

John C. Conboy	, Chair	**7/19/2012** Date Approved
Jennifer S. Shumaker-Parry	, Member	**7/19/2012** Date Approved
Joel M. Harris	, Member	**7/19/2012** Date Approved
Michael H. Bartl	, Member	**7/19/2012** Date Approved
Bruce K. Gale	, Member	**7/19/2012** Date Approved

and by **Henry S. White** , Chair of the Department of **Chemistry**

and by Charles A. Wight, Dean of The Graduate School.

ABSTRACT

The importance of lipid bilayers to the structure and function of cellular membranes coupled with their inherent complexity has driven the development of analytical techniques capable of high-throughput investigation of these surfaces. This work describes a continuous flow microspotter (CFM) that was modified to create micropatterned lipid bilayer arrays (MLBAs). This dissertation is divided into four main parts, with the first chapter focusing on the characterization of MLBAs using fluorescence microscopy to ensure bilayer formation and integrity. The individually addressable nature of the CFM was also demonstrated using a multi-ligand array containing ganglioside GM_1, dinitrophenyl (DNP) and biotin. A multiple protein-ligand assay was performed using the ligand array to detect three different fluorescently labeled proteins (cholera toxin b (CTb), anti-DNP antibody and NeutrAvidin) from solution simultaneously.

The second part of this dissertation concentrates on creating stable MLBAs using a polymerizable lipid, poly(bis-SorbPC) in order to generate a more robust biosensing platform. The poly(lipid) arrays were compared directly to the MLBAs prepared without the polymerizable lipids using fluorescence microscopy to demonstrate their superior stability. A multiple protein-ligand assay was also performed to demonstrate the utility of these arrays and their potential application as a sensor substrate.

Next, the MLBAs were used to investigate the impact of fifteen different lipid components on small molecule-membrane binding. The lipophilic dye merocyanine 540 (MC540) was used as a model small molecule and its binding was monitored by fluorescence microscopy. These studies demonstrate the potential of using MLBAs to investigate drug membrane interactions while preserving time and cost-effectiveness.

Finally, sum-frequency vibrational imaging (SFVI) was developed to provide a surface specific noninvasive, analytical technique capable of monitoring lipid structure and dynamics in a high-throughput manner. The vibrational sensitivity of SFVI was investigated with an asymmetric lipid bilayer patterned by ultraviolet (UV) radiation lithographically. The phase behavior of three different binary mixtures in a MLBA was successfully investigated using SFVI. The SFVI setup had the sensitivity, resolution and field of view required for exploring lipid bilayer properties in an array format.

This dissertation presents a new approach for assembling lipid bilayer arrays in combination with a powerful analytical technique to allow exploration of the physical properties of lipid membranes in a high-throughput and noninvasive manner.

TABLE OF CONTENTS

LIST OF FIGURES

LIST OF ABBREVIATIONS

CFM	Continuous flow microspotter
PSLBs	Planar supported lipid bilayers
MLBAs	Micropatterned lipid bilayer arrays
DNP	Dinitrophenyl
CTb	Cholera toxin b
TRITC-SA	Tetramethylfhodamine-labeled streptavidin
Rh	Lissamine rhodamine B sulfonyl
MC540	Merocyanine 540
DSPC	1,2-Distearoyl-*sn*-glycero-3-phosphocholine
DSPC-d_{70}	1,2-Distearoyl(d70)-*sn*-glycero-3-phosphocholine
DOPC	1,2-Dioleoyl-*sn*-glycero-3-phosphocholine
DMPC	1,2-Dimyristoyl-*sn*-glycero-3-phosphocholine
DPPC	1,2-Dipalmitoyl -*sn*-glycero-3-phosphocholine
SOPC	1-Stearoyl-2-oleoyl-*sn*-glycero-3-phosphocholine
POPC	1-Palmitoyl-2-oleoyl-*sn*-glycero-3-phosphocholine
Bis-SorbPC	1,2-bis[10-(2′,4′-hexadienoloxy)decanolyl]-*sn*-glycero-3-phosphocholine
GM_1	Ganglioside
PS	Phosphatidylserine
T_m	Phase transition temperature

l.c.	liquid-crystalline
CHO	Cholesterol
BSA	Bovine serum albumin
FRAP	Fluorescence Recovery after photobleaching
SFVI	Sum-frequency vibrational imaging
SFVS	Sum-frequency vibrational spectroscopy
UV	Ultraviolet
PDMS	Poly(dimethylsiloxane)
LB	Langmuir-Blodgett
LS	Langmuir-Schaefer
SUV	Small unilamellar vesicle
PBS	Phosphate buffered saline
USAF	United States Air Force

ACKNOWLEDGEMENTS

I would like to acknowledge those who have helped make this dissertation possible. Foremost, special thanks go to my advisor Prof. John C. Conboy for the opportunity to take part in his research and for guiding me to become a competent analytical chemist. I also appreciate the support from my collaborator, Prof. Bruce K. Gale, for supplying the CFM along with his encouragement, which made this research possible. I thank all the past and present Conboy group members for their help and technical support in lab, as well as insightful discussion about the theory of our research. In particular, I thank Dr. Grace Stokes for her help and advice in setting up the SFVI instrumentation, as well as editing papers and this dissertation and helpful discussion. In addition, I thank Ms. Krystal Brown for her help with learning nonlinear spectroscopy, as well as editing my manuscripts and dissertation.

The important role my family played in my approaching and completing graduate school cannot be overstated. Much of the strength and determination necessary to pursue such an ambitious degree comes from my mother Kathleen. She has taught by example that by hard work and never giving up, anything is possible. I also acknowledge the tough love of Edward McGuire, who has been like a father to me and always encouraged me to continually raise the bar. I would never have made it this far in life without the unconditional love and support of my siblings Joanna, Kerry and Bryan. Furthermore, none of this would have been possible without my twin sister, Dr.

Joanna Smith, at my side, who I have always looked up to and aspire to be like in life. Special thanks go to my brother-in-law, Dr. Jason Boyle, who has taught me how to work smart and play hard and my graduate experience would have never been the same without him.

CHAPTER 1

INTRODUCTION

There is an increasing interest in the development of microarray based assays for high-throughput analysis and detection of biomolecules.[1-3] These array-based analyses have proven extremely useful for DNA detection and sequencing.[1,2,4] The general versatility of microarrays for multi-variable, high-throughput analysis has also been applied to solve analytical problems in the emerging field of proteomics.[1,2] One area of chemical and biological research that could potentially benefit from the use of microarrays is the study of biological membranes. Cell membranes facilitate many vital biological processes including protein-ligand interactions, endocytosis/exocytosis, immune response and controlling the transport of ions, nonelectrolytes, and pharmaceutical drugs into and out of the cell.[5,6] Challenges remain because cell membranes are supported by a complex lipid matrix containing over a hundred different types of lipids uniquely distributed throughout.[5] In order to overcome this difficulty, an extensive amount of work has been done to develop model membranes that possess characteristics of biological structures, such as fluidity and biocompatibility, without the complexity of natural cellular membranes. Furthermore, placing model lipid bilayers in a microarray format is extremely desirable because a high-throughput platform for the investigation of specific biological and chemical interactions can be realized. The

development and characterization of such an assay platform is presented in this dissertation.

Planar supported lipid bilayers (PSLBs) serve as good model membranes and allow a diverse assortment of biological and chemical interactions to be explored in a controlled manner. PSLBs are also an attractive platform for performing biological assays due to their intrinsic resistance to nonspecific biomolecule adsorption and non-fouling nature.[7,8] One key attribute of PSLBs that makes them desirable biocompatible substrates and model models is the fluid nature of these 2D macromolecular assemblies; however, this property of PSLBs also makes it challenging to create arrays of lipid bilayers as adjacent bilayers can fuse and combine their contents.[9]

There are many examples of corralling PSLB into array format presented in the literature and include, microcontact printing,[10-12] pre-patterned substrates,[13-15] UV photolithography,[16] robotic printing[17] and microfluidics.[16,18,19] Most of these techniques require multiple steps or expensive equipment to generate multicomponent. Microfluidics is the exception, requiring only one step to create individually addressable PSLB arrays. The microfluidic systems previously presented in the literature utilize a 2D arrangement to produce a 1D array of lipid bilayers (Figure 1.1a); however, arranging the microfluidic system into a 3D structure would allow for a higher density of lipid spots better utilizing the available real-estate (Figure 1.1b). Presented in this dissertation is the use of a 3D continuous flow microspotter (CFM) for generating 2D multiplexed PSLB arrays.

In Chapter 2, the CFM is applied to the creation of high density PSLB arrays by vesicle fusion. The PSLB arrays were characterized using fluorescence microscopy to

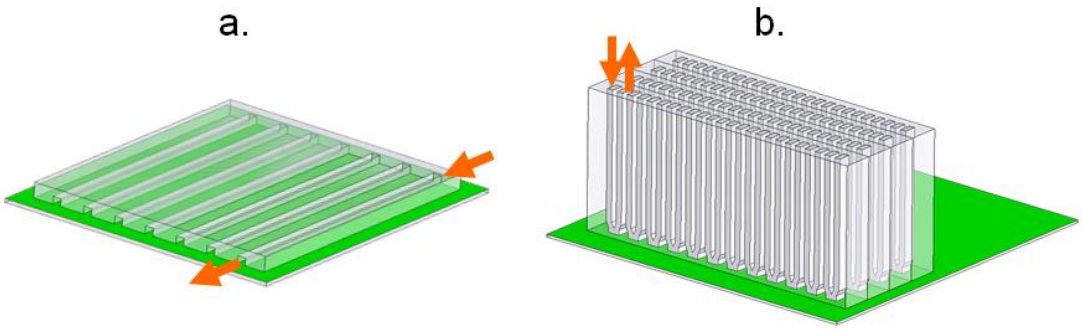

Figure 1.1. Schematic illustration of a (a) 2D and (b) 3D microfluidic system. Arrows represent the direction of solution flow within each microchannel. Images were provided by Prof. Bruce K. Gale, Department of Mechanical Engineering.

ensure bilayer formation and membrane fluidity. The functionality of these arrays was first demonstrated with a multicomponent fluorescent array using fluorescently-labeled-lipids incorporated into individual lipid domains. Finally, the practical use of these arrays was tested by performing a rapid multiple protein assays using a multicomponent ligand array. Chapter 2 presents the use of the CFM as a straight forward alternative for the production and high-throughput analysis utilizing PSLBs.

While high-density MLBAs are an appealing platform for biosensing, this application is precluded by a lack of robustness and stability.[9,20-22] For example, when these arrays are introduced through an air/water interface they will desorb from the surface.[23] Chapter 3 focuses on developing stable MLBAs using the polymerizable lipid bis-SorbPC. The air-stability of the poly(lipid) bilayer arrays were compared to unpolymerizable lipid bilayer arrays using fluorescence microscopy. A multiplexed ligand array was prepared using the poly(lipid) bilayer arrays to detect multiple proteins in solution simultaneously. Furthermore, these arrays were also shown to be reusable after being exposed to a protein denaturing solution and air. These studies present poly(lipid) bilayer arrays as a robust platform for high-throughput biomolecule detection, providing an alternative to the traditional MLBAs.

The ability to create lipid bilayer arrays containing an assortment of lipid compositions could also accelerate the study of small molecule association with specific membrane components. Small molecule-membrane interactions with MLBAs are explored in Chapter 4. The lipophilic fluorescent dye merocyanine 540 (MC540) was used to model a small molecule and fluorescence microscopy was used to simultaneously study its interaction with fifteen different bilayer compositions. This

chapter demonstrates that MLBAs are a useful tool for preparing high density, reproducible bilayer arrays to study small-molecule membrane interaction in a high-throughput manner.

Thus far, fluorescence microscopy has been used to characterize the MLBAs and study biomolecule interaction with the lipid arrays; however, there are many drawbacks to using a fluorescent label. Attaching an extrinsic label to any biomolecule can modify the native molecule's chemistry resulting in inaccurate measurements of its physical properties, as well as its interactions with other biomolecules. For this reason, sum-frequency vibrational imaging (SFVI) was developed here to image MLBAs. SFVI provides a surface specific, label-free technique for investigating the physical properties of the lipid bilayer arrays in a high-throughput manner. The different vibrational transitions of the lipids in a patterned asymmetrically prepared lipid bilayer composed of 1,2-distearoyl-*sn*-glycero-3-phosphocholine (DSPC):1,2-distearoyl(d70)-*sn*-glycero-3-phosphocholine (DSPC-d_{70}) were successfully imaged. Finally, SFVI was used to probe the phase behavior of three different binary mixtures in a MLBA. This work demonstrates that SFVI provides sensitive chemical imaging capabilities, spatial resolution and field of view required for exploring lipid membranes in a high-throughput array based assay.

The enormous complexity of biological membranes has motivated the development of MLBAs. The work presented in this dissertation demonstrates the successful application of the CFM for preparing 2D MLBAs and its use for high-throughput experiments. Furthermore, the coupling of SFVI with the MLBAs provides a powerful means to explore the physical properties of lipids in a controlled manner without the

need of a label. This new tool can hasten the exploration of lipid chemistry and biological events in applications such as screening potential drug candidates and investigating drug-membrane interactions.

1.1 References

(1) *Microarray Technology and Its Applications*; Muller, U. R.; Nicolau, D. V., Eds.; Springer-Verlag: Berlin 2005.

(2) *Microarray Technology Through Applications*; Falciani, F., Ed.; Taylor and Francis Group: New York, 2007.

(3) Zhang, F.; Gates, R. J.; Smentkowski, V. S.; Natarajan, S.; Gale, B. K.; Watt, R. K.; Asplund, M. C.; Linford, M. R. *J. Am. Chem. Soc.* **2007**, *129*, 9252.

(4) *Integrated Biochips for DNA Analysis*; Liu, R. H.; Lee, A. P., Eds.; Landes Bioscience and Springer Science+Business Media: New York, 2007.

(5) Gennis, R. B. *Biomembranes: Molecular Structure and Function*; Springer-Verlag: New York, 1989.

(6) Keller, P.; Toomre, D.; Diaz, E.; White, J.; Simons, K. *Nature Cell Biology* **2001**, *3*, 140.

(7) *Proteins at Interfaces: Physicochemical and Biochemical Studies*; Brash, J. L.; Horbett, T. A., Eds.; American Chemical Society: Washington, DC, 1987.

(8) Chapman, D. *Langmuir* **1993**, *9*, 39.

(9) Cremer, P. S.; Boxer, S. G. *J. Phys. Chem. B* **1999**, *103*, 2554.

(10) Hovis, J. S.; Boxer, S. G. *Langmuir* **2001**, *17*, 3400.

(11) Kung, L. A.; Kam, L.; Hovis, J. S.; Boxer, S. G. *Langmuir* **2000**, *16*, 6773.

(12) Ross, E. E.; Joubert, J. R.; Wysocki, R. J., Jr.; Nebesny, K.; Spratt, T.; O'Brien, D. F.; Saavedra, S. S. *Biomacromolecules* **2006**, *7*, 1393.

(13) Groves, J. T.; Ulman, N.; Boxer, S. G. *Science* **1997**, *275*, 651.

(14) Lenz, P.; Ajo-Franklin, C. M.; Boxer, S. G. *Langmuir* **2004**, *20*, 11092.

(15) Cremer, P. S.; Yang, T. *J. Am. Chem. Soc.* **1999**, *121*, 8130.

(16) Shi, J.; Yang, T.; Cremer, P. S. *Anal. Chem.* **2008**, *80*, 6078.

(17) Yamazaki, V.; Sirenko, O.; Schafer Robert, J.; Nguyen, L.; Gutsmann, T.; Brade, L.; Groves Jay, T. *BMC Biotechnol* **2005**, *5*, 18.

(18) Kam, L.; Boxer, S. G. *J. Am. Chem. Soc.* **2000**, *122*, 12901.

(19) Yang, T.; Jung, S.; Mao, H.; Cremer, P. S. *Anal. Chem.* **2001**, *73*, 165.

(20) Ross, E. E.; Rozanski, L. J.; Spratt, T.; Liu, S.; O'Brien, D. F.; Saavedra, S. S. *Langmuir* **2003**, *19*, 1752.

(21) Albertorio, F.; Diaz, A. J.; Yang, T.; Chapa, V. A.; Kataoka, S.; Castellana, E. T.; Cremer, P. S. *Langmuir* **2005**, *21*, 7476.

(22) Sisson, T. M.; Lamparski, H. G.; Koelchens, S.; Elayadi, A.; O'Brien, D. F. *Macromolecules* **1996**, *29*, 8321.

(23) Holden, M. A.; Jung, S.-Y.; Yang, T.; Castellana, E. T.; Cremer, P. S. *Journal of the American Chemical Society* **2004**, *126*, 6512.

CHAPTER 2

MICROPATTERNED FLUID LIPID BILAYER ARRAYS CREATED USING A CONTINUOUS FLOW MICROSPOTTER

2.1 Introduction

The previous chapter described the importance of studying lipid bilayers in a high-throughput manner but asserted that there is still a need for effective techniques to create multicomponent arrays. Current methods used to create micropatterned lipid bilayer arrays (MLBAs) include micro-contact printing,[1,2] deep ultraviolet photolithography (UV),[3] the use of pre-patterned substrates,[4] a combination of pre-patterned substrates with a robotic spotter system,[5] and 2D microfluidics.[6] Many of these approaches are discussed in a recent review by Castellana et al.[7] Microcontact printing was first introduced by Kumar et al. for creating arrays of self-assembled monolayers.[8] A lithographically patterned poly(dimethylsiloxane) (PDMS) stamp is used to transfer the material onto a substrate. Microcontact printing has since become a common method for patterning PSLBs.[1,2,9] Yang et al. demonstrated that a PDMS mold can also be used to displace portions of a continuous PSLB followed by the generation

of addressable compartments above each patterned bilayer array.[10] The use of deep-UV radiation is another way to create lipid bilayer arrays by directing light through a photomask onto a continuous lipid bilayer resulting in localized photochemical degradation of the exposed lipid bilayers.[3,11,12] Small unilamellar vesicle (SUV) solutions can also be manually pipetted into corrals created on pre-patterned substrates[4] or the same approach can be mechanized, with the aid of robotics, to create spatially addressed bilayers.[5] The polymer lift-off technique patterns a layer of Parylene, a polyxylylene polymer, on a substrate using photolithography. Vesicles are then fused to the polymer-patterned substrate and the polymer is removed to generate a patterned bilayer.[13,14] The air bubble collapse technique patterns lipids by removing a portion of a bilayer with a clean air bubble, creating a monolayer of lipids at the bubble's air water interface. The lipid covered air bubble is then brought into contact with a substrate where the air is removed, causing the monolayer to collapses on itself and resulting in the formation of a bilayer.[15]

Many of the methods mentioned above employ backfilling with vesicles to create multi-composition arrays, significantly limiting the number of bilayers with distinct compositions. Majd et al. demonstrated a method to create multicomponent arrays for micro-contact printing by manual hand pipetting SUV solutions but a drawback to this is the need for large spot sizes (~1 mm). Robotics can generate multicomponent membrane arrays with small spot sizes (250 μm) but this approach has drawbacks as well. Due to the extremely small volume size (nanoliters), this type of deposition process must be performed in a humidity chamber (~98% humidity) to prevent evaporation during SUV delivery.

The use of 2D microfluidics is a more recent approach for the creation of lipid arrays which involves introducing a solution of vesicles through a single plane of microchannels imbedded within PDMS producing parallel lanes of PSLBs.[6,14,16-21] Microfluidics offers a simple and cheap alternative for creating multi-composition arrays. The use of microfluidics simplifies sample handling and eliminates problems associated with solvent evaporation. The addressable microchannels also allow for the rapid production and interrogation of numerous multicomponent bilayers, limited only by the density and number of channels in the microfluidic device.

Microfluidics has proven to be a promising method for producing patterned PSLBs; however, the 2D nature of these devices limits the addressable elements in an array to linear channels on the surface. In this chapter, a 3D Continuous Flow Microspotter™ (CFM) system capable of producing higher density multicomponent arrays compared to traditional 2D microfluidics is used to prepare multianalyte PSLB arrays (Figure 2.1). The PDMS microspotter consists of a series of inlet and outlet wells connected by pairs of microfluidic channels embedded within the polymer. When the PDMS print-head contacts the substrate, one continuous channel is formed between the inlet and outlet pairs resulting in the continuous flow of solution over the substrate (Figure 2.1). Each channel is individually addressable, allowing the production of 2D PSLB arrays. The microfluidic system does not require the use of a pre-patterned substrate because PSLBs are effectively corralled into discrete micron-sized domains by the residual PDMS deposited on the silica substrate from the PDMS print head.[22-25] Other attractive features include an easy washing process after vesicle fusion and the ability to address each element of the array individually if the print head is maintained in contact with the

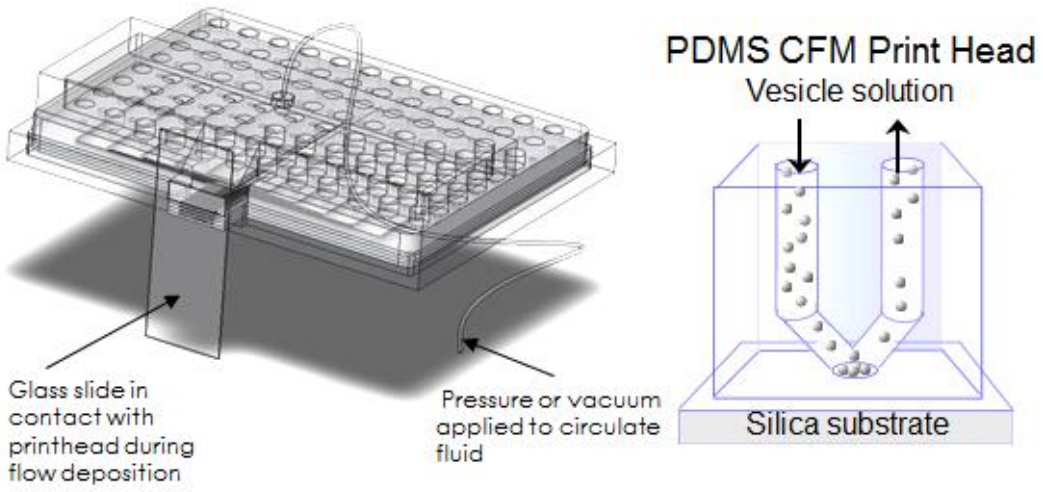

Figure 2.1. Schematic of the CFM apparatus and close-up of the CFM print head in contact with a silica substrate used for bilayer formation. The arrows represent the direction of fluid flow in the sealed channel created by contacting the PDMS print head with the silica substrate.

substrate, or upon removal of the print head the entire array can be queried for multiply analytes in a high-throughput fashion.

In this chapter, the CFM was applied to generate lipid bilayer arrays by vesicle fusion and was characterized using fluorescence microscopy to ensure bilayer formation and membrane fluidity. The highly customizable nature of the MLBAs was demonstrated utilizing three different fluorescently labeled lipids to generate a multiple component lipid array. Finally, the functionality of these arrays was tested by modeling a multiple protein-ligand binding assay. The model protein-ligand pairs chosen were cholera toxin B/ganglioside GM_1, antidinitrophenyl (DNP) antibody/DNP, and NeutrAvidin/biotin. The multicomponent patterned bilayers were functionalized with GM_1, DNP and biotin lipids, and binding curves were generated by recording surface fluorescence versus increasing concentration of membrane bound ligands. It is shown here that the CFM is a convenient way of producing fluid and functional lipid bilayer arrays.

2.2 Experimental

2.2.1 Materials

1,2-dioleoyl-*sn*-glycero-3-phosphocholine (DOPC), 1,2-dioleoyl-*sn*-glycero-3-phosphoethanolamine-N-(lissamine rhodamine B sulfonyl) (Rh-DOPE), 1,2-dipalmitoyl-*sn*-glycero-3-phosphoethanolamine-N-(lissamine rhodamine B sulfonyl) (Rh-DPPE), 1-palmitoyl-2-[12-[(7-nitro-2-1,3-benzoxadiazol-4-yl)amino]dodecanoyl]-*sn*-glycero-3-phosphocholine (NBD-PC), 1,2-dipalmitoyl-*sn*-glycero-3-phosphoethanolamine-N-[6-[(2,4-dinitrophenyl)amino]caproyl] (DNP-cap-PE), GM_1

Ganglioside (Brain, Ovine-Ammonium Salt) and 1,2-dioleoyl-*sn*-glycero-3-phosphoethanolamine-N-(Cap Biotinyl) (Biotin-cap-DOPE) were obtained from Avanti Polar Lipids and used as received. Marina Blue® 1,2-dihexadecanoyl-*sn*-glycero-3-phosphoethanolamine (Marina Blue-DHPE) and Oregon Green® 488 1,2-dihexadecanoyl-*sn*-glycero-3-phosphoethanolamine (Oregon Green-DHPE) were purchased from Invitrogen. Alexa Fluor 350 labeled NeutrAvidin (~4 mole dye per mole protein), Alexa Fluor 555 labeled cholera toxin subunit b (~5 mole dye per mole protein) and Alexa Fluor 488 labeled anti-dinitrophenyl-KLH rabbit IgG antibodies (~7 mole dye per mole protein) were also purchased from Invitrogen. The water used in these studies was obtained from a Nanopure™ Infinity Ultrapure water purification system with a minimum resistivity of 18.2 Mohm-cm. Quartz microscope slides (Chemglass) and glass cover slips (VWR International) were also used.

2.2.2 Small Unilamellar Vesicle (SUV) Preparation

To prepare SUVs, lipids were dissolved in chloroform followed evaporation of the bulk chloroform under a stream of N_2(g) and placed under a vacuum for at least 2 hours to remove any residual chloroform. The dried lipids were re-suspended by vortexing in phosphate buffered saline (PBS, pH 7.4, 140 mM NaCl, 3 mM KCl, 10 mM Na_2HPO_4, 2 mM KH_2PO_4 and 1 mM NaN_3) to a final concentration of 0.5 mg/mL. The solution was then bath sonicated for 10 - 30 min to clarify. The solutions were stored at 4°C and used within 3 days.

2.2.3 MLBA Preparation

The quartz microscope slides or glass cover slips used for MLBA preparation were cleaned in 70% -18 M sulfuric acid / 30 % - 30 % H_2O_2 (piranha solution) followed by rinsing with a copious amount of nanopure water. (*Caution! Piranha solution is a strong oxidant and highly corrosive; reacts violently with organic solvents and should be handled with extreme care.*) The slides were dried in a 120 °C oven and then plasma cleaned (Harrick PDC-32G) with Ar for 3 min.

MLBAs were prepared by vesicle fusion utilizing a Continuous Flow Microspotter™ (CFM). Details of the microspotter construction can be found elsewhere.[26] Briefly, the CFM is capable of producing up to 48 spots, each spot is a 400 x 400 μm^2 square with a pitch of 875 μm. However, the pitch may vary slightly due to deformities inherent within the PDMS print-head, variations between print-heads or spreading of the lipid bilayer patches. The PDMS print-head is approximately 5 x 12 mm^2. The PDMS microspotting plate was degassed under vacuum before use to help prevent the formation of air bubbles within the microchannels during the experiment. MLBAs were assembled by introducing numerous solutions of DOPC SUVs through the microchannels simultaneously, allowing them to fuse to a silica slide or coverslip with an incubation time of 15 min followed by the cycling of vesicle solutions back and forth over the substrate by changing the flow direction. Excess vesicles were rinsed away by flowing nanopure water or PBS buffer through the channels. The rinse cycle was repeated three times by discarding and then refilling the solution in the microchannels for each cycle while ensuring the channels are never completely empty. The CFM print-head was then removed from the substrate in a reservoir of water and

assembled into a custom built Teflon flow cell. Once formed, the MLBA was maintained in an aqueous environment. The MLBAs are stable for at least one day assuming a successful pattern was fabricated resulting in well corralled lipid bilayers.

2.2.4 Verification of Lipid Bilayer Formation

In order to verify a bilayer structure is formed by vesicle fusion using the CFM, fluorescence microscopy was used to quantitatively compare the emission intensity of a symmetric lipid bilayer of DOPC + 0.5 mol % NBD-PC prepared by the Langmuir-Blodgett/Langmuir-Schaefer (LB/LS) method and by vesicle fusion using the CFM. The bilayers were formed on a cleaned quartz slide. For the LB/LS method, the substrate was placed in the water subphase of a KSV Instruments Minitrough and a 1 mg/mL lipid solution (DOPC + 0.5 mol % NBD-PC) in chloroform was spread onto the air/water interface. The lipid film was transferred onto the substrate by pulling the slide out of the subphase (LB layer). The same glass slide was then horizontally passed through the air/water interface into the same subphase to deposit the LS layer. All depositions were carried out at a surface pressure of 35 mN/m, which roughly corresponds to a bilayer surface pressure of a bilayer prepared by vesicle fusion (30-35 mN/m).[27] For comparison, an array of DOPC bilayers containing 0.5 mol % NBD-PC was patterned onto a cleaned quartz substrate using the CFM. The fluorescence intensity of the micropatterned lipid bilayer array was measured by averaging two separately prepared arrays, each array consisting of approximately 24 spots. The fluorescence of each spot was obtained by averaging over the entire bilayer area. The fluorescence of the LB/LS bilayer was measured by averaging the fluorescence

intensities of two separately prepared LB/LS bilayers. The fluorescence intensities of each bilayer was obtained by averaging the fluorescence intensity over a 400 x 400 μm^2 area in the center of the image for approximately 15 different areas on the substrate. The fluorescence measurements were performed on the same day using similar quartz substrates. The samples were all placed in the same flow cell in order to minimize problems associated sample alignment in the microscope, background fluorescence and other sources of errors. All fluorescence images were acquired with the same exposure times. This procedure allowed for the direct comparison of absolute fluorescence intensities between experiments while minimizing errors. For comparison, the fluorescence intensity of the lipid bilayer prepared by the LB/LS method and the fluorescence of the MLBAs were both normalized to the average fluorescence of the micropatterned lipid bilayer arrays.

2.2.5 Fluorescence Recovery After Photobleaching (FRAP)

A solution of DOPC SUVs doped with 1 mol % Rh-DOPE was introduced through the microchannels of the CFM to create a patterned substrate on a coverslip. After removal from the PDMS print-head the coverslip was placed in a custom built Teflon® flow cell. Using an Olympus 1X71 inverted microscope and a 100x objective (NA 1.4) a 5 μm spot was bleached within a 400 μm bilayer patch using a 488 nm high powered Argon ion laser (50 mW) with an exposure time of between 0.2-0.5 seconds. The fluorescence recovery was monitored by obtaining 3 pre-event and 32 post-event images with a Sony Interline CoolSNAP$_{HQ}$ CCD camera (Roper Scientific) using a Rh filter set and 100W mercury arch lamp as the excitation light source. The fluorescence

recovery within the bleached spot was measured over time using ImagePro software to yield the fluorescence intensity profile for each time and the intensity data were fit to the 2D diffusion equation described by Soumpasis[28]

$$f(t) = e^{-2\tau_D/t}\left[I_0\left(\frac{2\tau_D}{t}\right) + I_1\left(\frac{2\tau_D}{t}\right)\right] \tag{2.1}$$

where I_0 and I_1 are modified Bessel functions, $\tau_D = r^2 / 4D$ is the characteristic diffusion time, and r is the radius at half-height of the bleached area at $t = 0$. FRAP experiments were performed at room temperature in PBS (pH 7.5), with a phosphate concentration of 0.01M and 0.15 M NaCl. The diffusion coefficient reported represents the average of two different bilayer patches from two different MLBAs with six trials performed within each element.

2.2.6 Multiple Protein-Ligand Binding Assay

Patterned DOPC bilayers containing varying concentrations of one of three functionalized lipids (biotin-cap-DOPE, GM_1 and DNP-cap-PE) were prepared. NeutrAvidin labeled with Alexa Fluor 350 was used to monitor avidin/biotin binding. Cholera toxin subunit b (CTb) labeled with Alexa Fluor 555 was used to monitor CTb/GM_1 binding. Anti-dinitrophenyl-KLH (anti-DNP) labeled with Alexa Fluor 488 was used to monitor anti-DNP/DNP binding. The functionalized MLBA was assembled in a custom built Teflon flow cell and then incubated with a 2 mg/mL bovine serum albumin (BSA) solution to block the hydrophobic PDMS residue from the CFM print-head and prevent nonspecific adsorption of protein. A protein mixture of 500 nM

NeutrAvidin, 200 nM CTb and 500 nM anti-DNP all dissolved in PBS was introduced into the Teflon flow cell containing the multiligand MLBA and incubated for at least 40 min. The cell was then rinsed with PBS and the adsorption of protein to the MLBA elements was measured by fluorescence microscopy.

2.2.7 Fluorescence Microscopy

Fluorescence images were recorded using an Olympus BX40 equipped with a Photometrics CoolSNAP$_{cf}$ (Roper Scienctific) color camera. Three filter sets were used to pass the excitation/emission wavelengths of each fluorophore: 510/526 nm for Oregon Green/NBD/Alexa Fluor 488, 557/571 nm for Rhodamine/Alex Fluor 555 and 365/460 nm for Marina Blue/Alexa Fluor 350. Images were taken with a 10x objective (NA, 0.30), which fits one 400 μm spot per field of view, and were used to obtain quantitative fluorescence intensity measurements. Typically, images showing more than one bilayer spot were pieced together from images taken under a 4x (NA, 0.10) or 10x objective using Canvas X software. The 10x objective was used to obtain fluorescence measurements instead of a 4x because of the more uniform light intensity profile located in the center of the image. The use of a 10x objective also allowed for a more precise assessment of lipid and protein coverage within an individual lipid spot, facilitating a more accurate determination of protein binding. In the future a macroscope or other high-throughput imaging system, such as that employed by Castellana et al., could be employed to provide increased light gathering capabilities and a larger field of view facilitating the interrogation of multiple bilayer patched simultaneously.[29] However, for the sake of characterization of the newly described

MLBAs, the imaging method described above was employed. The fluorescence intensity average and standard deviation for each spot were measured using the software package Voodoo Incantation 1.2 provided by Photometrics. All the fluorescence images were background corrected.

2.3 Results and Discussion

2.3.1 Characterization of MLBAs

The MLBAs created using the CFM were characterized to assure both bilayer formation and membrane fluidity. In order to verify that lipid bilayers were indeed created using the CFM, the fluorescence intensity from a symmetric lipid bilayer of DOPC containing 0.5 mol% NBD-PC prepared by the LB/LS method was compared to the fluorescence intensity measured from a MLBA using the CFM prepared by vesicle fusion from the same lipid solution (Figure 2.2a). The fluorescence intensities in both images were normalized to the average fluorescence of the MLBA. The fluorescence intensities observed from LB/LS bilayer and the MLBA bilayer spots are not significantly different at the 95 % confidence level, strongly supporting the formation of only a single bilayer structure utilizing the CFM deposition methods. The bar graph shown in Figure 2.2a represents the average fluorescence of two separately prepared LB/LS bilayers and two separately prepared 24 spot MLBAs.

Fluorescence recovery after photobleaching (FRAP) experiments were performed to validate the fluidity of the PSLBs created by the CFM. A lipid array was created using DOPC + 1 mol % Rh-DOPC. A 5 μm diameter spot was bleached into one 400 μm

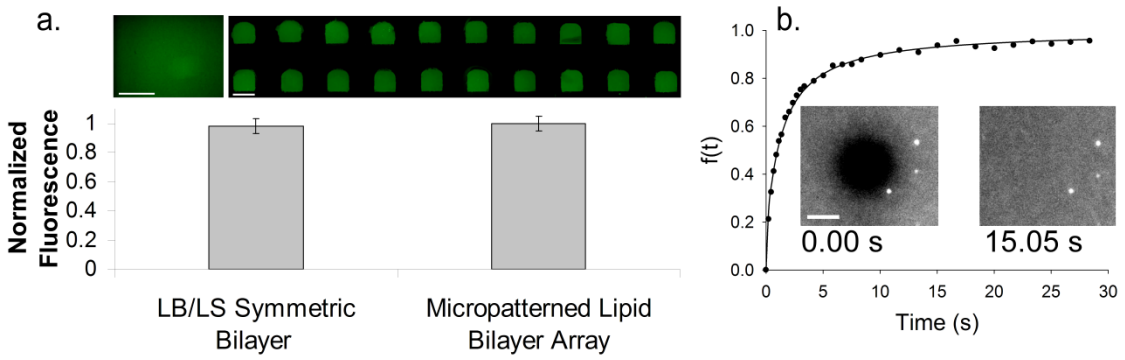

Figure 2.2. Characterization of a bilayer created with the CFM: (a) is a comparison of the normalized fluorescence intensity of CFM patterned DOPC membranes containing 0.5 mol % NBD-PC (1.00 ± 0.05), and a symmetric DOPC + 0.5 mol % NBD-PC LB/LS bilayer (0.98 ± 0.05) with the fluorescence images of both shown in the insert. The scale bar represents 400 μm. (b) is the FRAP recovery curve with corresponding fluorescence images at times t = 0 and t = 15.05 seconds. The line is the fit to the data using a 2-D diffusion model (Equation 1). The scale bar represents 3 μm.

membrane patch. The recovery of the fluorescence intensity was monitored over time (Figure 2.2b). A diffusion coefficient of 1.4 (± 0.30)x10^{-8} cm^2/sec was calculated using a 2D lateral diffusion model (Eq. 1).[28] This value represents the average diffusion coefficient measured on two different bilayer patches on two separately prepared MLBAs with six different areas on each bilayer patch being analyzed. The measured diffusion coefficient is in good agreement with previously reported values for the diffusion of similar lipids in PSLBs and are within the same order of magnitude (although several times slower) of solution phase liposomes.[15,30-32] These results demonstrate that the intrinsic fluidity of the bilayer is maintained during array formation with essentially no immobile fraction indicated by nearly full fluorescence recovery (97 ± 1%).

2.3.2 MLBA Concentration Gradient

The reproducibility of the vesicle fusion method as well as the addressable nature of the CFM method was demonstrated by preparing a concentration gradient of Rh-DPPE lipids in a DOPC MLBA. Lipid bilayer arrays were generated from eight SUV solutions with increasing concentrations of Rh-DPPE ranging from 0.0 to 2.1 mol %. The SUV solutions were introduced through a total of 24 microchannels simultaneously. The array was replicated three times (in three rows) on the same substrate (Figure 2.3). In addition to the fluorescence image of the MLBA in Figure 2.3, a graph illustrating the linear trend of fluorescence versus mol % Rh-DPPE is also shown. The data points represent the average fluorescence of three spots prepared with

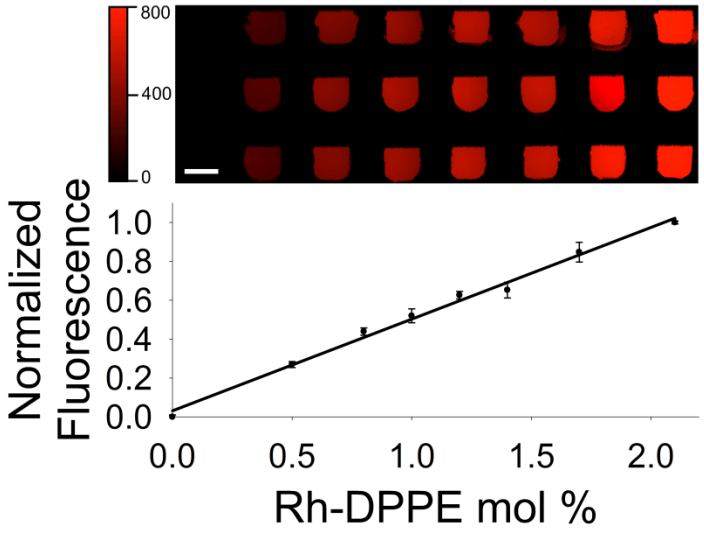

Figure 2.3. Micropatterned concentration gradient of Rh-DPPE doped in DOPC at 0.0, 0.5, 0.8, 1.0, 1.2, 1.4, 1.7 and 2.1 mol %, corresponding to the images starting from left to right, respectively. The concentration gradient was reproduced over three rows (top to bottom). The scale bar to the left of the image represents the raw fluorescence intensity. The graph represents the linear trend of fluorescence versus mol % of Rh-DPPE in the DOPC SUVs. The graph was normalized to the maximum fluorescence value of 800 at 2.1 mol % Rh-DPPE, seen in the fluorescence image. The data points are the average fluorescence intensity with the standard deviation obtained for three spots located in the same column. Scales bar corresponds to 400 μm.

the same SUV solution along with the corresponding standard deviation. Vesicle fusion performed in different microchannels results in approximately the same number of lipids per area as suggested by the reproducibility of fluorescence measured for the various bilayer spots prepared by the same SUV solutions. The graph also shows that as the mol % of Rh-DPPE doubles, the fluorescence intensity increases approximately two fold. This shows that liposomes created with discrete lipid composition, in this case the addition of Rh-DPPE, are accurately transferred to the substrate with high fidelity and there is no apparent cross-talk between the channels.

2.3.3 Multiple Component MLBAs

The use of the CFM for the formation of a MLBA allows for the composition of each bilayer element to be controlled individually, opening up the possibility for multi-analyte assays. A multiple component array was generated using DOPC SUVs containing one of three different fluorescent probes, 1.0 mol% Rh-DPPE, 1.0 mol % Oregon Green-DHPE or 3.0 mol % Marina Blue-DHPE, in order to visually demonstrate the multicomponent array capability of the CFM. The three SUV solutions were simultaneously delivered to the substrate surface, producing a multi-color lipid bilayer array with the red, green and blue spots corresponding to Rh-DPPE, Oregon Green-DHPE and Marina Blue-DHPE functionalized bilayers, respectively. A true color fluorescence image of the MLBA is shown in Figure 2.4. Figure 2.4 shows 48 high quality bilayers with very few defects indicated by the uniform fluorescence of each spot. The PSLBs in Figure 2.4 are clearly separated from one another with little spreading, demonstrating the stability of the individual bilayer domains. These

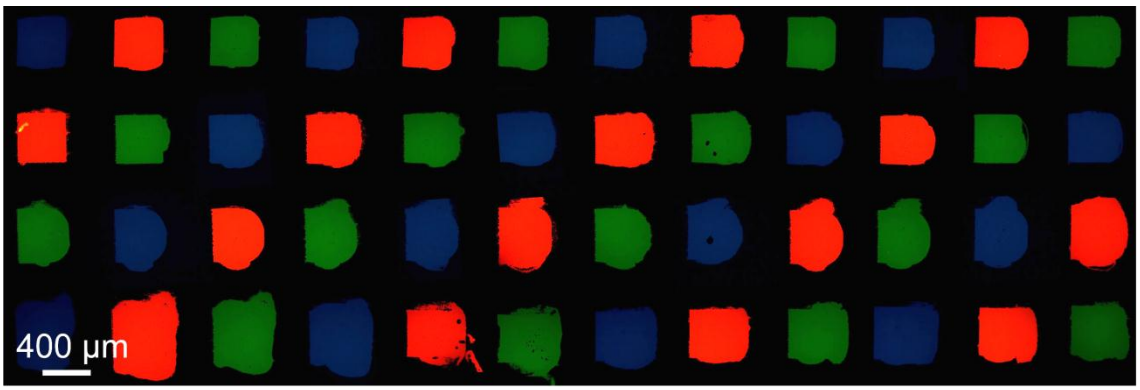

Figure 2.4. A 48 element MLBA of DOPC containing either 1.0 mol % Rh-DPPE (red), 1.0 mol % Oregon Green-DHPE (green) or 3.0 mol % Marina Blue-DHPE (blue).

experiments demonstrate that MLBAs with spatially addressed compositions can easily be prepared using a CFM.

2.3.4 Multiple Protein-Ligand Binding Assay

PSLBs have long been known to be inherently biocompatible substrates that are ideally suited for performing biological assays.[33,34] Bilayer surfaces containing phosphocholine headgroups have been shown to be highly resistant to nonspecific protein adsorption due in part to their charge neutrality and hydration of the headgroups.[35-38] Additionally, assays may be performed utilizing PSLBs by functionalizing the membrane with receptor sites. The avidin/biotin, CTb/GM_1 and anti-DNP antibody/DNP systems were used to demonstrate that these features are maintained with the MLBAs prepared by the CFM in a multiple protein-ligand binding assay. The ligand array was generated by simultaneously introducing DOPC SUVs containing different molar ratios of functionalized lipids through 48 microchannels, with each ligand type designated to one row (Figure 2.5). A solution containing CTb (200 nM), NeutrAvidin (500 nM) and anti-DNP (500 nM) was incubated with the surface and fluorescence microscopy used to quantify binding. The high protein concentrations used in this study were employed to ensure surface saturation of NeutrAvidin and CTb[17,39] and facilitate rapid equilibrium of the sample. While saturation concentrations of anti-DNP to PSLBs containing DNP-cap ligands has been shown to be in the μM range,[40] 500 nM anti-DNP was sufficient to obtain high fluorescence signal while reducing the cost of performing the assay. Shown in Figure 2.5 are the representative fluorescence images of a single MLBA imaged with three

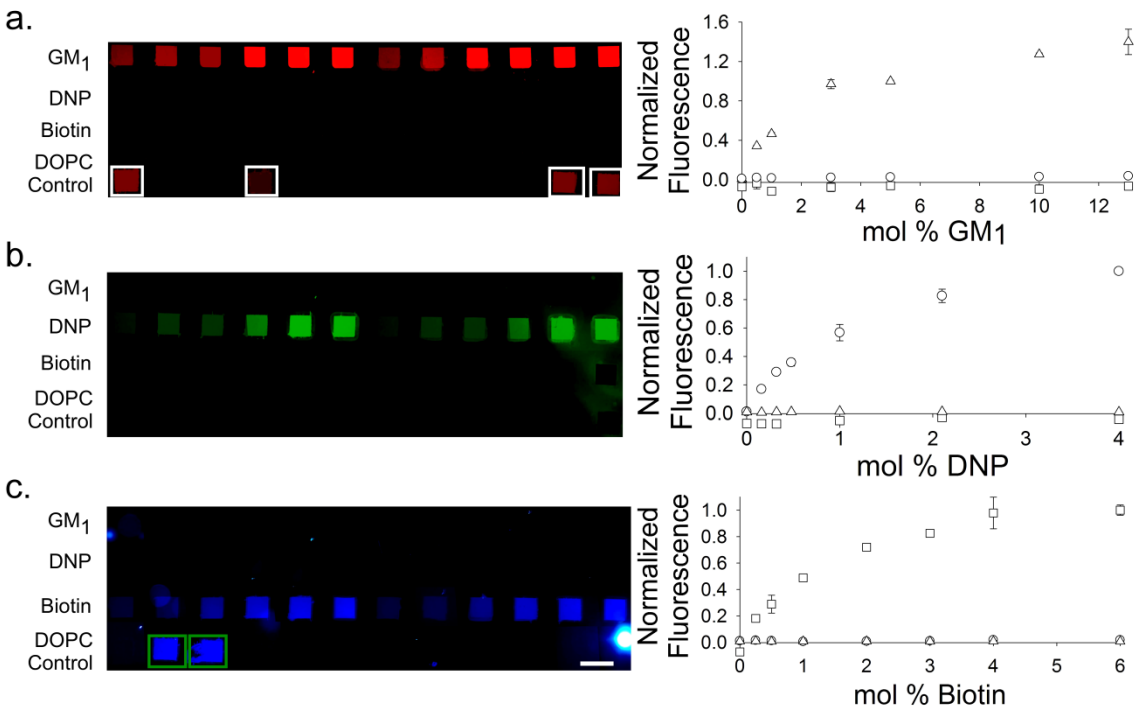

Figure 2.5. A multiligand MLBA containing: (row 1) GM_1 at 0.5, 1.0, 3.0, 5.0, 10.0 and 13.0 mol % in DOPC, (row 2) DNP-cap-PE at 0.2, 0.3, 0.5, 1.0, 2.1 and 4 mol % in DOPC and (row 3) biotin-cap-DOPE at 0.25, 0.5, 1.0, 2.0, 3.0 and 4.0 mol % in DOPC. Each ligand concentration is present in two sequential sets going from the left to right in each row. Row 4 contains six control DOPC spots with no ligands present. There are also four DOPC + 1 mol % Rh-DOPE spots which were used as position finders at the beginning of the experiment (outlined by open white squares). In order to increase the concentration range of biotin relative to the other ligands, two 6.0 mol % biotin-cap-DOPE spots (outlined by green open squares) were also prepared in row 4. The array was imaged under the red (a), green (b) and blue (c) filter sets to obtain the images shown. The representative binding curves to the right of the images represent the average fluorescence intensity of the duplicate bilayers from rows 1, 2, 3, and 4 obtained under the red (open triangles), green (open circles) and blue (open squares) filter sets. The scale bar represents 600 μm.

filter sets, one for each of the fluorescently labeled proteins. CTb is in the red (Figure 2.5a), anti-DNP is in the green (Figure 2.5b) and NeutrAvidin is in the blue channel (Figure 2.5c). Each row in the image represents a specific ligand, GM_1 for CTb, DNP for anti-DNP and biotin for NeutrAvidin. Each row has two series of increasing concentration of ligand (two adjacent sets) from left to right. Also shown is a control lane containing reference markers used to register the array and pure DOPC bilayers for controls. A minimal amount of nonspecific adsorption to the solid support is observed for each of the protein. There was some anti-DNP that bound to the PDMS residue in the lower right of Figure 2.5b possibly due to a leaky spot during MLBA preparation. This does not affect the other bilayer patches and is apparent by the contrast of fluorescence around the patterned spots. The bright spot in Figure 2.5c is most likely the result of contamination of dust particles which fluoresce upon excitation with ultraviolet light. More importantly, no cross-reactivity or nonspecific protein binding is observed to lipid bilayer elements not containing the protein-specific ligand. This is apparent by the minimal fluorescence observed for rows containing a ligand other than the one required by the protein-ligand couple of interest.

Also shown in Figure 2.5 are the binding curves of each protein to increasing concentrations of ligand doped in the DOPC bilayers. The plotted data represent the average of the two reproduced bilayer spots of identical lipid composition whereas the data plotted for the DOPC control represent the average of six spots. The fluorescence of individual bilayer spots were obtained by spatially averaging the fluorescence intensity of the entire bilayer patch. The relative uncertainties of the fluorescence signal within the individual spots were <5 % for the CTb and DNP functionalized bilayers.

The standard deviation within each biotin containing lipid patch ranged from 25 to 5 % relative uncertainty from low to high biotin mol % bilayers respectively. The high standard deviation at low concentration of biotin is due to the weaker fluorescence measured with NeutrAvidin versus anti-DNP and CTb. However, the standard deviation within each spot remains relatively constant through the experiment (2.2 ± 0.4) for the unnormalized fluorescence signal), thus explaining the high relative uncertainty at lower signal. The comparatively low relative error suggests that the proteins bind uniformly over the bilayers.

The CTb/GM_1 binding curve presented in Figure 2.5a shows increasing amounts of CTb binding to DOPC bilayers with increasing mol % of GM_1. The amount of nonspecifically adsorbed CTb to the DOPC controls (0.0 mol % GM_1) was <1 % of the normalized signal. Figure 2.5b shows that anti-DNP increases in surface coverage up to 4 mol % DNP-cap-PE. The amount of nonspecifically adsorbed antibody to the DOPC control bilayers was ~1 % relative to the fluorescence signal near surface saturation. The surface coverage of NeutrAvidin onto biotin functionalized bilayers increased until saturation at 4 mol %. The fluorescence of the DOPC control spots was at background levels, indicating minimal amounts of NeutrAvidin adsorption. There was essentially no cross-reactivity of protein with other ligand functionalized bilayers as shown by the lack of signal when imaged under the remaining two filter sets. The MLBA shows a minimal amount of nonspecific protein adsorption, consistent with the non-fouling nature of the DOPC membranes.

The reproducibility of the multiple protein-ligand assays was tested by performing three independent binding experiments on freshly prepared MLBAs. The data plotted

in Figure 2.6 represent the average of six spots whereas the DOPC controls are averaged from ~18 spots. The three separate experiments were first normalized and then pooled together to determine the reproducibility in the binding trends. These results show good reproducibility of the arrays from day to day demonstrated by the small standard deviations associated with the average fluorescence with the exception of CTb for GM_1 concentrations ≥ 10 mol %. The relatively large scatter could be attributed to the clustering of the GM_1 lipids at high GM_1 concentrations.[17,41] The binding curves for CTb, anti-DNP and NeutrAvidin were compared to similar binding curves presented by Cremer and cowokers.[17,39,40] The program g3data (for Linux) were used to extract data from the published graphs in references [17, 39 and 40]. These data were then used to obtain the data points in shown in Figure 2.6. For the anti-DNP/DNP and CTb/GM_1 data (references 26 and 48), the binding data at the highest protein concentrations (saturation levels), ~28 μM for anti-DNP and 6 nM for CTb, were used.[17,40] For the streptavidin/biotin assay (reference 47), the data from the graph reporting fluorescence data at a saturation concentration (0.01 mg/mL) of streptavidin were used.[39] All the data presented in Figure 2.6b and c were normalized to the fluorescence at the highest reported ligand concentration. The data for CTb/GM_1 were normalized to the fluorescence at 5 mol % GM_1 because of the large scatter at 10 mol % GM_1.

The binding curves obtained here for CTb, anti-DNP and avidin on the MLBAs correlate extremely well with similar binding curves obtained by Cremer and coworkers (see Figure 2.6) with the exception of CTb binding to GM_1 at high ligand densities (>5 mol%). This discrepancy is likely due to GM_1 domain formation, as mentioned

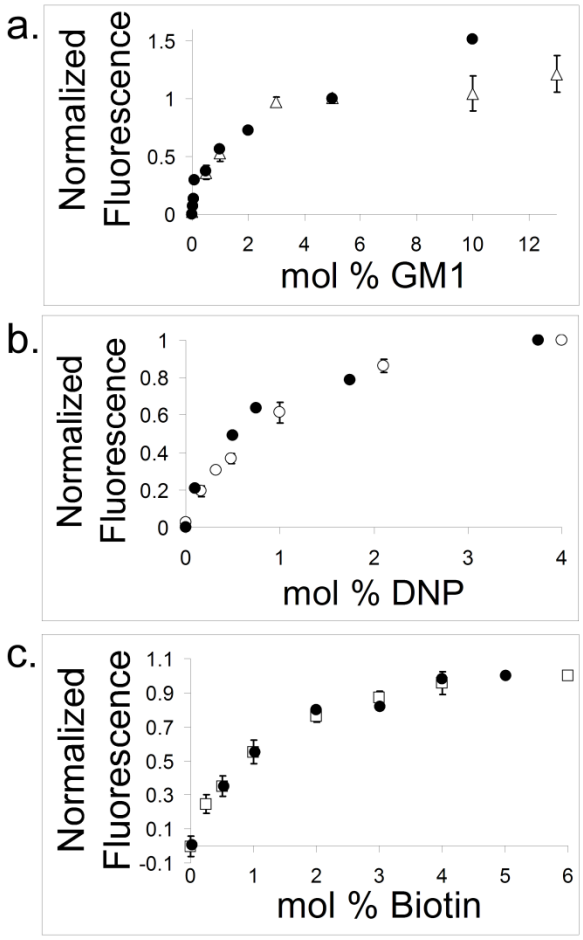

Figure 2.6. The average binding curves of three independent MLBAs (open shapes) for CTb/GM_1 (a), anti-DNP/DNP (b) and NeutrAvidin/biotin (c). The data obtained from Cremer and coworkers[17,39,40] for similar systems (see text) are overlaid as closed circles.

previously. The similar results obtained for protein binding studies performed using the MLBA and those reported by a different research group using lipid bilayers in a different experimental platform; strongly suggest that the integrity and functionality of the lipid bilayers prepared here are equivalent in nature. Additionally, the protein binding experiments reported by Cremer and coworkers were performed within a bilayer coated microfluidic network while the binding experiments presented in this paper were performed in a flow cell where the entire sensing surface could be addressed simultaneously. The important conclusions to be drawn from this comparison are that the lipid patterning process by the CFM has little effect on protein binding to the MLBAs prepared with the CFM and the MLBAs created have the potential to increase the number of assays performed by increasing the usable real estate on the sensor surface.

2.4 Conclusion

We have demonstrated that the CFM provides a powerful way to create fluid and functionalized MLBAs. The fluorescence of lipid membranes prepared by the CFM was nearly identical to the intensity of a LB/LS prepared bilayer, suggesting the formation of lipid bilayers on the substrate surface. The lipid bilayer patches remain well corralled on the substrate as confined by the PDMS residue of the CFM printhead to prevent the spreading of lipids while still retaining their fluid nature. A diffusion coefficient of 1.4 ($\pm$ 0.3)x10^{-8} cm^2/sec was calculated from the FRAP experiments for lipid diffusion in the lipid membranes prepared by the CFM. Vesicle fusion utilizing the CFM has been shown to be a reliable deposition method for patterning lipid bilayers

while maintaining a high level of experimental control and reproducibility. The linear response of bilayer fluorescence vs. mol % Rh-DPPE in DOPC SUVs demonstrates that discrete lipid compositions are successfully transferred from vesicles to the substrate. The standard deviation in the fluorescence between the different bilayer spots prepared from the same SUV solution were small, demonstrating the reproducibility in the packing of the lipids within the 400 x 400 μm^2 area. Multiple component MLBAs were also prepared utilizing three fluorescently labeled lipid probes for visualization. On average, a 7% relative error in the fluorescence within each of the three sets of functionalized DOPC bilayers, Rh-DPPE, Oregon Green-DHPE and Marina Blue-DHPE was obtained, again illustrating the reproducibility of bilayer formation within an array. A simultaneous multiple protein-ligand binding experiment was also obtained using CTb, anti-DNP and avidin binding, to varying mol % of GM_1, DNP-cap-PE and biotin-cap-DOPE, respectively. The MLBAs were shown to resist nonspecific protein adsorption and have minimal amounts of cross-reactivity. The high density MLBAs we have demonstrated here have potential applications in many fields such as biosensing, drug discovery, proteomics and clinical diagnostics.

2.5 References

(1) Kung, L. A.; Kam, L.; Hovis, J. S.; Boxer, S. G. *Langmuir* **2000**, *16*, 6773.

(2) Majd, S.; Mayer, M. *Angew. Chem., Int. Ed.* **2005**, *44*, 6697.

(3) Yee, C. K.; Amweg, M. L.; Parikh, A. N. *Advanced Materials* **2004**, *16*, 1184.

(4) Cremer, P. S.; Yang, T. *J. Am. Chem. Soc.* **1999**, *121*, 8130.

(5) Yamazaki, V.; Sirenko, O.; Schafer Robert, J.; Nguyen, L.; Gutsmann, T.; Brade, L.; Groves Jay, T. *BMC Biotechnol* **2005**, *5*, 18.

(6) Yang, T.; Jung, S.; Mao, H.; Cremer, P. S. *Anal. Chem.* **2001**, *73*, 165.

(7) Castellana, E. T.; Cremer, P. S. *Surf. Sci. Rep* **2006**, *61*, 429.

(8) Kumar, A.; Whitesides, G. M. *Appl. Phys. Lett.* **1993**, *63*, 2002.
(9) Hovis, J. S.; Boxer, S. G. *Langmuir* **2001**, *17*, 3400.

(10) Yang, T.; Simanek, E. E.; Cremer, P. *Anal. Chem.* **2000**, *72*, 2587.

(11) Yu, C.-h.; Parikh, A. N.; Groves, J. T. *Advanced Materials* **2005**, *17*, 1477.

(12) Yee, C. K.; Amweg, M. L.; Parikh, A. N. *J. Am. Chem. Soc.* **2004**, *126*, 13962.

(13) Orth, R. N.; Kameoka, J.; Zipfel, W. R.; Ilic, B.; Webb, W. W.; Clark, T. G.; Craighead, H. G. *Biophys. J.* **2003**, *85*, 3066.

(14) Moran-Mirabal, J. M.; Edel, J. B.; Meyer, G. D.; Throckmorton, D.; Singh, A. K.; Craighead, H. G. *Biophys. J.* **2005**, *89*, 296.

(15) Mager, M. D.; Melosh, N. A. *Langmuir* **2007**, *23*, 9369.

(16) Burridge, K. A.; Figa, M. A.; Wong, J. Y. *Langmuir* **2004**, *20*, 10252.

(17) Shi, J.; Yang, T.; Kataoka, S.; Zhang, Y.; Diaz, A. J.; Cremer, P. S. *J. Am. Chem. Soc.* **2007**, *129*, 5954.

(18) Phillips, K. S.; Cheng, Q. *Anal. Chem.* **2005**, *77*, 327.

(19) Kam, L.; Boxer, S. G. *Langmuir* **2003**, *19*, 1624.

(20) Kam, L.; Boxer, S. G. *J. Am. Chem. Soc.* **2000**, *122*, 12901.

(21) Perez, T. D.; Nelson, W. J.; Boxer, S. G.; Kam, L. *Langmuir* **2005**, *21*, 11963.

(22) Glasmaestar, K.; Gold, J.; Andersson, A.-S.; Sutherland, D. S.; Kasemo, B. *Langmuir* **2003**, *19*, 5475.

(23) Groves, J. T.; Ulman, N.; Boxer, S. G. *Science* **1997**, *275*, 651.

(24) Ross, E. E.; Joubert, J. R.; Wysocki, R. J., Jr.; Nebesny, K.; Spratt, T.; O'Brien, D. F.; Saavedra, S. S. *Biomacromolecules* **2006**, *7*, 1393.

(25) Foley Jennifer, O.; Fu, E.; Gamble Lara, J.; Yager, P. *Langmuir* **2008**, *24*, 3628.

(26) Chang-Yen, D. A.; Myszka, D. G.; Gale, B. K. *Journal of Microelectromechanical Systems* **2006**, *15*, 1145.

(27) Marsh, D. *Biochim. Biophys. Acta, Rev. Biomembr.* **1996**, *1286*, 183.

(28) Soumpasis, D. M. *Biophys. J.* **1983**, *41*, 95.

(29) Castellana, E. T.; Cremer, P. S. *Biointerphases* **2007**, *2*, 57.

(30) Tamm, L. K.; McConnell, H. M. *Biophysical Journal* **1985**, *47*, 105.

(31) Przybylo, M.; Sykora, J.; Humpolickova, J.; Benda, A.; Zan, A.; Hof, M. *Langmuir* **2006**, *22*, 9096.

(32) Lapinski, M. M.; Castro-Forero, A.; Greiner, A. J.; Ofoli, R. Y.; Blanchard, G. J. *Langmuir* **2007**, *23*, 11677.

(33) Sackmann, E. *Science* **1996**, *271*, 43.

(34) Brian, A. A.; McConnell, H. M. *Proc. of the Natl. Acad. of Sci. U. S. A.* **1984**, *81*, 6159.

(35) Murphy, E. F.; Lu, J. R.; Brewer, J.; Russell, J.; Penfold, J. *Langmuir* **1999**, *15*, 1313.

(36) Glasmastar, K.; Larsson, C.; Hook, F.; Kasemo, B. *J. Colloid Interface Sci.* **2002**, *246*, 40.

(37) Chen, S.; Zheng, J.; Li, L.; Jiang, S. *J. Am. Chem. Soc.* **2005**, *127*, 14473.

(38) Ross, E. E.; Spratt, T.; Liu, S.; Rozanski, L. J.; O'Brien, D. F.; Saavedra, S. S. *Langmuir* **2003**, *19*, 1766.

(39) Mao, H.; Yang, T.; Cremer, P. S. *Anal. Chem.* **2002**, *74*, 379.

(40) Yang, T.; Baryshnikova, O. K.; Mao, H.; Holden, M. A.; Cremer, P. S. *J. Am. Chem. Soc.* **2003**, *125*, 4779.

(41) Vie, V.; Van Mau, N.; Lesniewska, E.; Goudonnet, J. P.; Heitz, F.; Le Grimellec, C. *Langmuir* **1998**, *14*, 4574.

CHAPTER 3

STABLE, LIGAND-DOPED, POLY(bis-SorbPC) LIPID BILAYER ARRAYS FOR PROTEIN BINDING AND DETECTION

NOTE: Reprinted (adapted) with permission from Joubert, J. R.; Smith, K.A.; Johnson, E.; Keogh, J.P.; Wysocki, V.H.; Gale, B.K.; Conboy, J.C.; Saavedra, S.S. *ACS Appl. Mater. Interfaces*, **2009**, *1*, 1310–1315. The second author conducted all experimental work reported in collaboration with the first author.

3.1 Introduction

MLBAs have shown increasing potential as a high-throughput analytical device for the detection of a variety biomolecules such as proteins.[1-3] Furthermore, the last chapter showed the MLBAs prepared from the CFM system to be useful in detecting multiple proteins in solution simultaneously; however, the stability is limited for any bilayer array composed of fluid lipids. Lipid bilayers are self-associated and adsorbed to planar substrates by weak, noncovalent interactions that render them unstable to drying, surfactants, organic solvents, heat, and mechanical stress, all of which limit their commercial applications.[4-7] A variety of stabilization techniques exist including covalently attaching one leaflet to the substrate,[8,9] tethering a floating bilayer to the

substrate,[10-14] attaching proteins to the upper surface of the lipid bilayer,[15] using lipopolymers[6] and polymerizing reactive lipids.[7] A variety of polymerizable lipids have been used, including methacryloyl, diacetylenic, and dienoyl lipids.[16-18] Extremely stable planar supported lipid bilayers (PSLBs) have been formed using 1,2-bis[10-(2′,4′-hexadienoloxy)decanoyl]-*sn*-glycero-3-phosphocholine (bis-SorbPC),[19] and functionalization of these bilayers with water-soluble and transmembrane proteins has been described.[20,21]

In this chapter, a CFM is used to produce microarrays of poly(bis-SorbPC) bilayers that are stable to air and vacuum exposure. Poly(bis-SorbPC) arrays were doped with GM_1 and 1,2-dioleoyl-*sn*-glycero-3-phosphoethanolamine-N-biotinyl (biotin-DOPE). These arrays bound their respective, fluorolabeled protein targets from a dissolved mixture with little cross-talk. Gradient arrays of ganglioside GM_1 were created, and the extent of cholera toxin subunit b (CTb) binding was correlated with the mole percentage of GM_1 in the poly(lipid) spots. Exposure of GM_1 gradient arrays to denaturants removed CTb and regenerated the array, which maintained its CTb binding capacity even after multiple regeneration cycles as well as air drying.

3.2 Experimental

3.2.1 Materials

1,2-Dioleoyl-*sn*-glycero-3-phosphocholine (DOPC), 1,2-dipalmitoyl-sn-glycero-3-phosphoethanolamine-N-(lissamine rhodamine B sulfonyl) (Rh-DPPE), biotin-DOPE, and GM_1 were purchased from Avanti Polar Lipids. Bis-SorbPC was synthesized as previously described.[22] Phosphate-buffered saline (PBS), pH 7.4, was made containing

the following components: 140 mM sodium chloride, 3 mM potassium chloride, 10 mM dibasic sodium phosphate, 2mM monobasic potassiumphosphate, and 1 mM sodium azide. Bovine serum albumin (BSA) was obtained from Sigma-Aldrich. Tetramethylrhodamine-labeled streptavidin (TRITC-SA) with a 3:1 dye/protein ratio was obtained from Pierce Biotechnology. CTb labeled with Alexa Fluor 488 (Alexa488CTb) at a 5:1 dye/protein ratio was obtained from Invitrogen. Quartz microscope slides from Chemglass and silicon wafers from Wacker Chemie AG were used. Water from a Nanopure Infinity Ultrapure purification system or a Barnstead Nanopure system with a minimum resistivity of 18MΩ·cm was used. A regeneration solution of 6 M urea, 0.1 M glycine, and 0.2 M NaCl adjusted to pH 3 with hydrochloric acid was made using chemicals from Sigma-Aldrich.

3.2.2 Preparation of Small Unilamellar Vesicles (SUVs)

Dopant lipids (Rh-DPPE, biotin-DOPE, or GM_1) were mixed with bis-SorbPC or DOPC at appropriate molar ratios (expressed below as the mole percentage) in benzene or chloroform. The organic solvent was removed from lipid stock solutions under a stream of argon or nitrogen, followed by vacuum drying for at least 2 h. The lipids are then rehydrated with PBS to a concentration of 0.5 mg/mL, vortexed to suspend the lipid, and then sonicated in either a bath sonicator or a Branson sonicator with a cup horn, at a temperature above the lipid main-phase transition temperature, until no longer cloudy.

3.2.3 PSLB Microarray Formation

Quartz slides were cleaned in a piranha solution (3:7 30% H_2O_2/18 M H_2SO_4) and rinsed thoroughly in water. Each slide was then oven-dried at 120 °C, plasma-cleaned (Harrick PDC-32G) with Ar for 3 min and assembled into the CFM. The details of the CFM construction as well as MLBA preparation are given in Chapter 2. After the SUVs were introduced through the microchannels and rinsed with PBS, a low-pressure mercury pen lamp with a rated intensity of 4500 μW/cm2 at 254 nm was directed through a bandpass filter (330 nm, 140 nm fwhm; U-330, Edmund Optics) and through the quartz slide for 15 min to polymerize bis-SorbPC. The slide was removed from the CFM underwater and assembled into an epifluorescence flow cell. A solution of 2 mg/mL of BSA in PBS was then injected over the array and allowed to adsorb for 20 min to the PDMS residue between PSLB spots. Binding assays were performed by incubating PSLB arrays with solutions of Alexa488CTb (14 μg/mL) in PBS, TRITC-SA (0.1 mg/mL) in PBS, or a mixture thereof. In all cases, protein solutions were incubated with arrays for 45 min before washing with PBS.

Experiments were also performed on extended PSLBs. Silicon wafers were cleaned in a piranha solution and rinsed thoroughly in water. The wafers were dried with a stream of nitrogen, covered in a SUV solution for 15 min to form PSLBs, and placed in a container of excess water for rinsing. UV irradiation was used as described above to polymerize bis-SorbPC. The wafers were then removed from water, rinsed with water, and dried with a nitrogen stream. Binding assays were performed as described above.

3.2.4 Fluorescence Microscopy

Arrays were imaged using an Olympus BX40 microscope equipped with a Photometrics CoolSNAP color camera (Roper Scientific) and 4× and 10× objectives. Two optical filter sets with excitation/emission wavelengths of 510/526 and 557/571 nm were used for fluorescence imaging of Alexa488 and rhodamine, respectively. Images were acquired at 4× and, in some cases, spliced together into larger images using either GIMP or Canvas X software. Intensities of images captured at 10× were analyzed using Image J software, available online from NIH. Intensity data were corrected for background using images taken before exposure of PSLBs to fluorescent proteins.

3.3 Results and Discussion

3.3.1 PSLB Microarray Formation and Stability

The CFM was used to generate a microarray of poly(bis-SorbPC) PSLB spots doped with 1.9% Rh-DPPE on a quartz slide. For comparison purposes, an array of DOPC PSLB spots doped with 1.0% Rh-DPPE was also formed. An epifluorescence image of the arrays after UV irradiation is shown in Figure 3.1, rows a and b. Both exhibit uniform fluorescence, indicating the presence of a continuous PSLB in each spot. Variations in the geometry of the channel openings where the CFM head contacts the quartz slide account for differences in the spot shape, and differences in the Rh-DPPE mole percentage account for variations in brightness.

The stability of the PSLB spots was examined by injecting air into the epifluorescence cell at a rate of approximately 1 mL/min for 1 min, followed by a static

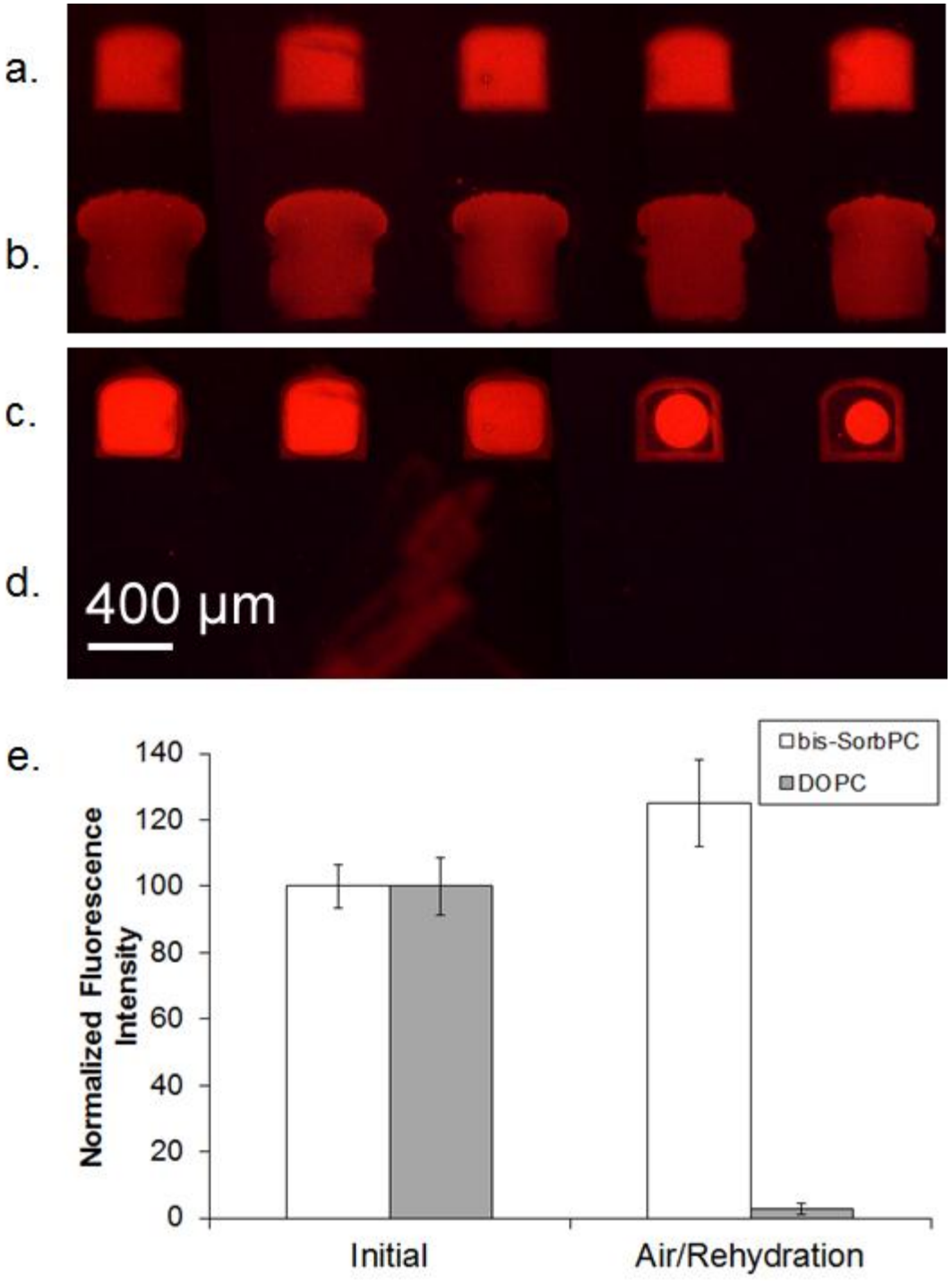

Figure 3.1. Epifluorescence images of a PSLB microarray consisting of UV-irradiated Rh-DPPE/bis-SorbPC (a and c) and Rh-DPPE/DOPC (b and d) before (a and b) and after (c and d) exposure to air. The Rh-DPPE loadings in bis-SorbPC and DOPC bilayers are 1.9% and 1.0% (mol/mol), respectively. (e) Plot of normalized average intensities of the two types of PSLB spots before and after air exposure. The error bars represent the standard deviations of five trials.

incubation period of ca. 5 min, after which the cell was refilled with PBS at a rate of 1 mL/min for 1 min. An image of the resulting array is shown in Figure 3.1, rows c and d. Row c, consisting of Rh-DPPE/poly(bis-SorbPC) bilayers, remained mostly intact with large areas of uniform fluorescence, although some lipid was removed at the edges of the spots adjacent to the regions where the PDMS print head contacted the slide. The underlying cause of this observation is not clear, but one possibility is that low-molecular-weight components in PDMS contaminate the surface of the slide adjacent to the edges of the bulk PDMS and thereby disrupt adhesion of the PSLB to the slide. After exposure to air, the Rh-DPPE/DOPC bilayers were almost completely removed, with little discernible fluorescence (Figure 3.1, row d). A square region of interest (ROI) slightly smaller than the uniformly bright area of the rightmost spot of Figure 3.1, row c, was used to determine the average intensity within each spot before and after the air/PBS treatment. These data were averaged to generate the plot in Figure 3.1e, which shows that the Rh-DPPE/DOPC spots were nearly quantitatively desorbed while the Rh-DPPE/poly(bis-SorbPC) spots remained largely intact. Previous work has shown that unpolymerized bis-SorbPC PSLBs are also completely desorbed when removed from water.[19] There was a measurable increase in Rh-DPPE/poly(bis-SorbPC) fluorescence after drying/rehydrating. It may have been caused by redistribution of Rh-DPPE within the polymerized bilayer, resulting in a lower level of self-quenching after rehydration.

3.3.2 CTb Binding to a GM_1 Gradient Microarray

The CFM was used to construct a PSLB array composed of poly(bis-SorbPC) doped with GM_1 at mole percentages ranging from 0% to 10%. A solution of Alexa488CTb was subsequently injected and allowed to adsorb to the array before a PBS rinse was performed to remove unbound protein. An epifluorescence image of the resulting array is shown in Figure 3.2a. The mean intensity within the same ROI in each spot was averaged to generate the plot in Figure 3.2b, which shows that the fluorescence intensity due to bound Alexa488CTb is correlated with the GM_1 mole percentage in the respective PSLB spot.

3.3.3 Simultaneous Multianalyte Detection

Multianalyte detection using microarrays bearing different ligands at spatially distinct locations was also investigated. The CFM was used to prepare an array of PSLB spots composed of 10% GM_1 in poly(bis-SorbPC) and 30% biotin-DOPE in poly(bis-SorbPC) along with control spots containing pure DOPC and bis-SorbPC. A mixture of Alexa488CTb and TRITC-SA was then injected and allowed to adsorb to the array before PBS rinsing. A larger mole percentage of biotin-DOPE was used because a significant decrease in streptavidin binding after UV irradiation of 30% biotin-DOPE/poly(bis-SorbPC) PSLBs was observed (up to 90% loss), presumably because of photodegradation of biotin (this information comes from discussions with the first author of the manuscript). Figure 3.3 shows the fluorescence images of a single array acquired using the (a) rhodamine and (b) Alexa488 filter sets. Figure 3.3c displays normalized fluorescence intensities of Alexa488CTb and TRITC-SA adsorbed to pure

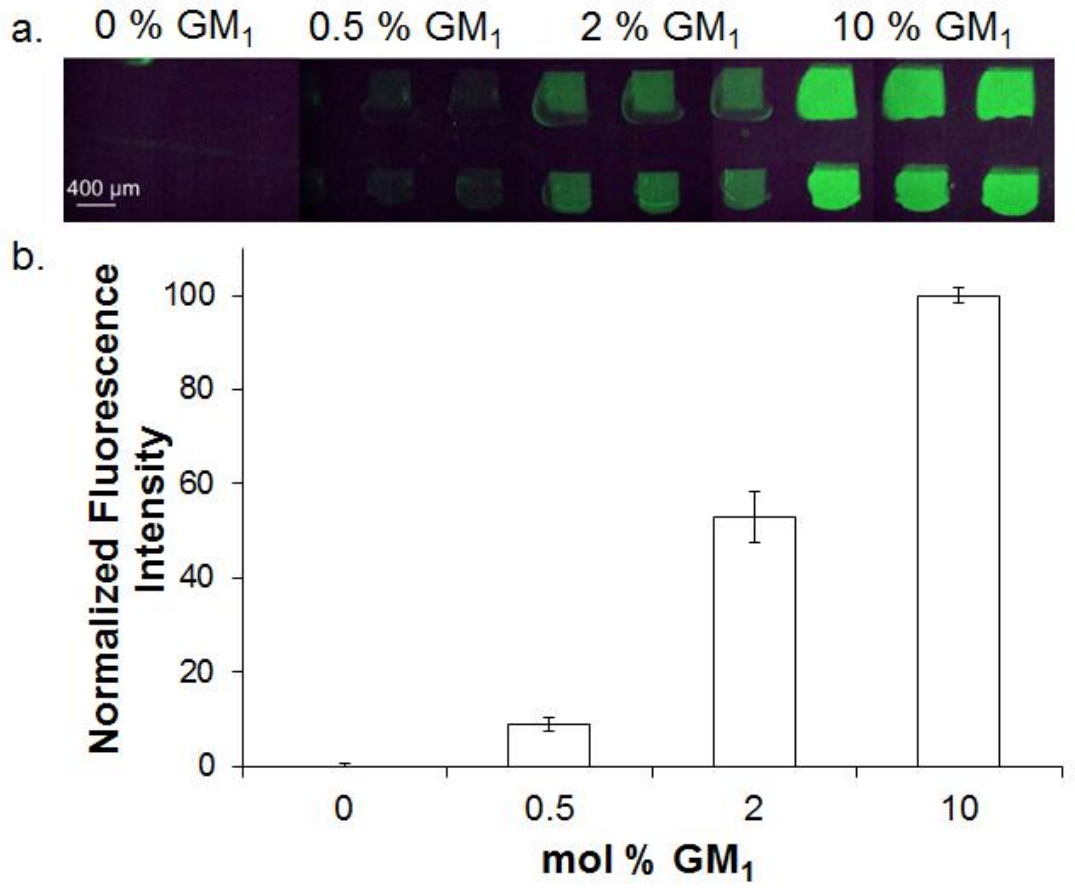

Figure 3.2. (a) Epifluorescence images of a lipid microarray of 0%, 0.5%, 2%, and 10% GM_1 in poly(bis-SorbPC) after adsorption of Alexa488CTb. (b) Plot of the normalized average intensities of the gradient array shown in part a. The error bars represent the standard deviations of six trials.

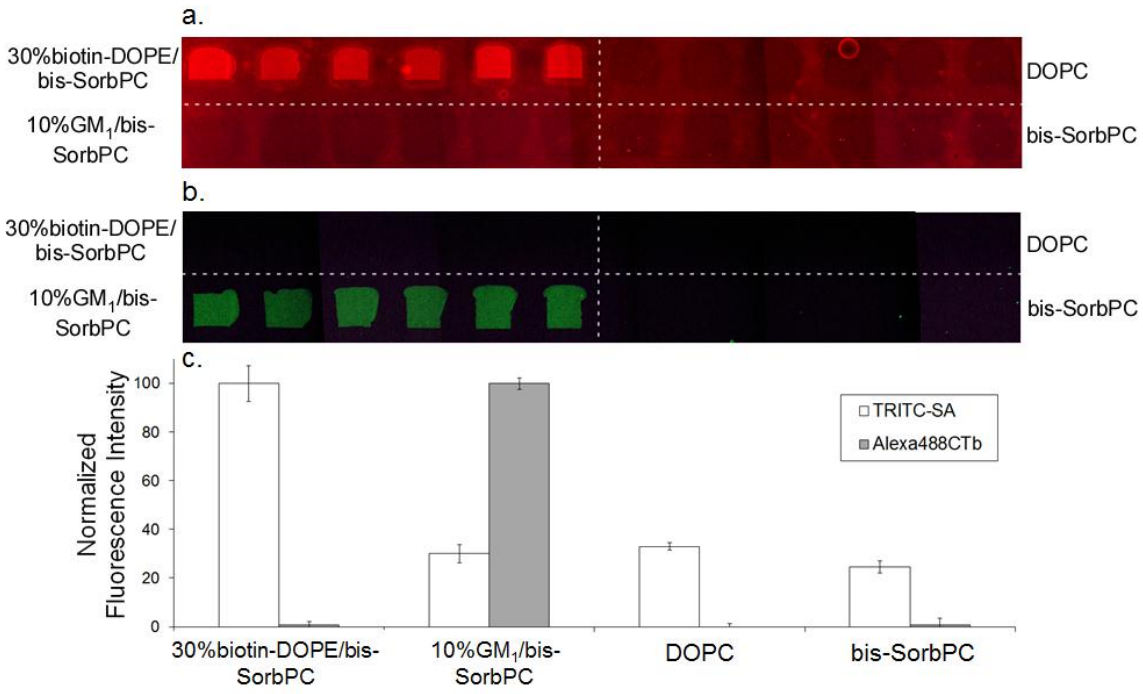

Figure 3.3. Epifluorescence images of a lipid microarray of 30 mol % biotin-DOPE/bis-SorbPC, 10 mol % GM_1/bis-SorbPC, DOPC and pure bis-SorbPC taken using the (a) rhodamine and (b) Alexa488 filter sets. (c) Plot of normalized average fluorescence intensities of Alexa488CTb and TRITC-SA adsorbed from a mixture of the two proteins to a lipid microarray. The error bars represent the standard deviations of six trials.

DOPC, poly(bis-SorbPC), 10% GM1/poly(bis-SorbPC), and 30% biotin-DOPE/poly(bis-SorbPC). A relatively high level of Alexa488CTb binding occurs on the spots containing 10% GM_1 but not on the spots containing 30% biotin-DOPE, demonstrating specificity and a lack of cross-talk. Minimal fluorescence of Alexa488CTb is observed on pure DOPC, poly(bis-SorbPC) and 30% biotin-DOPE, indicating very low nonspecific adsorption. In contrast, TRITC-SA shows a higher degree of nonspecific adsorption on pure DOPC, poly(bis-SorbPC) and 10% GM_1. This higher level can be understood as follows: As noted above, UV irradiation destroys most of the specific binding capacity of a 30% biotin-DOPE/poly(bis-SorbPC) bilayer. This reduces the ratio of specific binding to nonspecific adsorption to about 2. Because the data in Figure 3.3 are normalized to the total amount of TRITC-SA bound to 30% biotin-DOPE, the apparent level of nonspecific adsorption on bilayers lacking biotin-DOPE appears to be high because the specific binding on 30% biotin-DOPE is relatively low. Despite the problem with UV degradation of biotin-DOPE, overall these results demonstrate the ability to distinguish among multiple protein analytes bound to poly(bis-SorbPC) microarrays.

3.3.3 Regeneration and Reuse

The ability to regenerate and reuse these arrays would enhance their utility for commercial applications and was also examined. A 10% GM_1/poly(bis-SorbPC) PSLB array was prepared, exposed to an Alexa488CTb/TRITC-SA solution mixture, rinsed with PBS, and then exposed to a denaturing solution (urea, glycine, and NaCl at pH 3) for 10 min to remove the bound Alexa488CTb, followed by another PBS rinse. This

cycle was repeated three times. Mean fluorescence intensities for the PSLB spots in contact with PBS measured before and after each regeneration are plotted in Figure 3.4. The Alexa488CTb fluorescence decreased to ca. one-tenth the initial value after exposure to the denaturing solution, indicating that most of the bound CTb was removed. Reintroduction of the protein solution produced intensities equivalent to those measured in the first cycle, demonstrating that the GM_1-CTb binding activity was retained through multiple regeneration cycles. After the third regeneration, the slide was transferred from solution into air, reassembled into the epifluorescence cell, and flushed with PBS before being exposed again to the Alexa488CTb/TRITCSA solution. The mean emission intensity (last column of Figure 3.4) was unchanged from the previous cycles, demonstrating that drying and rehydration had no measurable effect on the capacity of GM_1-doped PSLBs to bind Alexa488-CTb. The 0% GM_1 spots [pure poly(bis-SorbPC)] in the array exhibited minimal fluorescence signals after air and Alexa488CTb/TRITC-SA exposure, indicating that specific binding of CTb to GM_1 rather than nonspecific adsorption was responsible for the data shown in Figure 3.4. Overall, these experiments demonstrate the ability to regenerate and reuse poly(bis-SorbPC) arrays for capturing and detecting CTb without loss in ligand binding capacity. However, they do not address whether the specific activity of GM_1 is affected by polymerization, drying, and rehydration; this topic will be the subject of future studies.

3.4 Conclusion

Microarrays composed of polymerized lipid bilayers were formed using a CFM and shown to be highly stable and resistant to nonspecific protein adsorption. Arrays doped

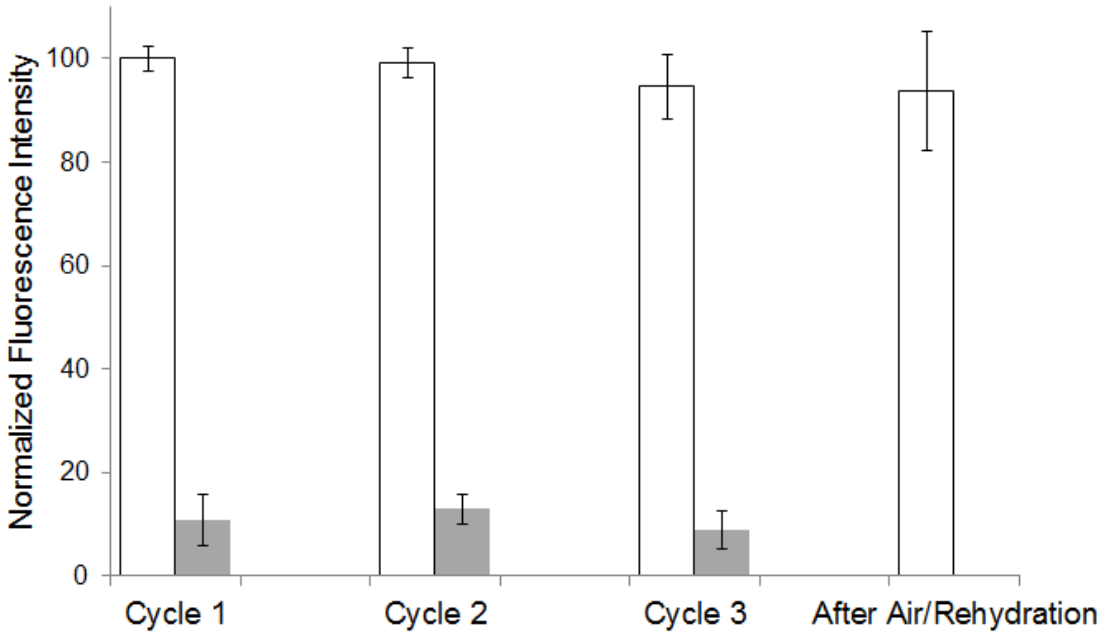

Figure 3.4. Plot of the average fluorescence intensity of Alexa488CTb adsorbed to a 10% GM_1/poly(bis-SorbPC) PSLB through three regeneration cycles followed by air exposure. The error bars represent the standard deviations of four to six trials.

with ligand-bearing lipids selectively capture their respective protein targets from dissolved mixtures, and the extent of target binding is correlated with the mole percentage of dopant. These arrays can be regenerated and reused multiple times and even maintain specific binding, with no apparent change in binding capacity, after exposure to air. In summary, these results show that poly(PSLB) microarrays have considerable potential for use in membrane based binding assays with applications in high-throughput pharmacological screening and disease diagnosis.

3.5 References

(1) Sackmann, E.; Tanaka, M. *Trends in Biotechnology* **2000**, *18*, 58.

(2) Fang, Y.; Frutos, A. G.; Lahiri, J. *J. Am. Chem. Soc.* **2002**, *124*, 2394.

(3) Bayley, H.; Cremer, P. S. *Nature* **2001**, *413*, 226.

(4) Cremer, P. S.; Boxer, S. G. *J. Phys. Chem. B* **1999**, *103*, 2554.

(5) Ross, E. E.; Spratt, T.; Liu, S.; Rozanski, L. J.; O'Brien, D. F.; Saavedra, S. S. *Langmuir* **2003**, *19*, 1766.

(6) Albertorio, F.; Diaz, A. J.; Yang, T.; Chapa, V. A.; Kataoka, S.; Castellana, E. T.; Cremer, P. S. *Langmuir* **2005**, *21*, 7476.

(7) Sisson, T. M.; Lamparski, H. G.; Koelchens, S.; Elayadi, A.; O'Brien, D. F. *Macromolecules* **1996**, *29*, 8321.

(8) Parikh, A. N.; Beers, J. D.; Shreve, A. P.; Swanson, B. I. *Langmuir* **1999**, *15*, 5369.

(9) Meuse, C. W.; Krueger, S.; Majkrzak, C. F.; Dura, J. A.; Fu, J.; Connor, J. T.; Plant, A. L. *Biophys. J.* **1998**, *74*, 1388.

(10) Raguse, B.; Braach-Maksvytis, V.; Cornell, B. A.; King, L. G.; Osman, P. D. J.; Pace, R. J.; Wieczorek, L. *Langmuir* **1998**, *14*, 648.

(11) Naumann, R.; Schiller, S. M.; Giess, F.; Grohe, B.; Hartman, K. B.; Kaercher, I.; Koeper, I.; Luebben, J.; Vasilev, K.; Knoll, W. *Langmuir* **2003**, *19*, 5435.

(12) Terrettaz, S.; Mayer, M.; Vogel, H. *Langmuir* **2003**, *19*, 5567.

(13) Janshoff, A.; Steinem, C. *Analytical and Bioanalytical Chemistry* **2006**, *385*, 433.

(14) Atanasov, V.; Knorr, N.; Duran, R. S.; Ingebrandt, S.; Offenhaeusser, A.; Knoll, W.; Koeper, I. *Biophys. J.* **2005**, *89*, 1780.

(15) Holden, M. A.; Jung, S.-Y.; Yang, T.; Castellana, E. T.; Cremer, P. S. *Journal of the American Chemical Society* **2004**, *126*, 6512.

(16) O'Brien, D. F.; Armitage, B.; Benedicto, A.; Bennett, D. E.; Lamparski, H. G.; Lee, Y.-S.; Srisiri, W.; Sisson, T. M. *Accounts of Chemical Research* **1998**, *31*, 861.

(17) Mueller, A.; O'Brien, D. F. *Chem. Rev.* **2002**, *102*, 727.

(18) Bader, H.; Dorn, K.; Hupfer, B.; Ringsdorf, H. *Advances in Polymer Science* **1985**, *64*, 1.

(19) Ross, E. E.; Rozanski, L. J.; Spratt, T.; Liu, S.; O'Brien, D. F.; Saavedra, S. S. *Langmuir* **2003**, *19*, 1752.

(20) Ross, E. E.; Joubert, J. R.; Wysocki, R. J., Jr.; Nebesny, K.; Spratt, T.; O'Brien, D. F.; Saavedra, S. S. *Biomacromolecules* **2006**, *7*, 1393.

(21) Subramaniam, V.; Alves, I. D.; Salgado, G. F. J.; Lau, P.-W.; Wysocki, R. J., Jr.; Salamon, Z.; Tollin, G.; Hruby, V. J.; Brown, M. F.; Saavedra, S. S. *J. Am. Chem. Soc.* **2005**, *127*, 5320.

(22) Sells, T. D.; O'Brien, D. F. *Macromolecules* **1994**, *27*, 226.

CHAPTER 4

USING MICROPATTERNED LIPID BILAYER ARRAYS TO MEASURE THE EFFECT OF MEMBRANE COMPOSITION ON MEROCYANINE 540 BINDING

Reprinted from *Biochimica et Biophysica Acta*, *1808*, Smith, K. A.; Conboy, J. C. 1611–1617., Copyright 2011, with permission from Elsevier B.V.

4.1 Introduction

As mentioned already in Chapter 1, one major function of biomembranes is to provide a selectively permeable barrier for the binding of small solute molecules, such as ions, nonelectrolytes, and pharmaceutical drugs.[1] These types of molecules can absorb to the surface or partition into the membrane and diffuse across the bilayer to the other side.[1] Understanding these membrane interactions is of interest to many areas of research, in particular, drug discovery. For example, the way in which drugs permeate the cell membrane is important to the pharmacological activity of a drug and its effectiveness in reaching its target site.[1-3] Chapters 2 and 3 demonstrated the CFM as a useful tool for creating MLBAs to investigate multiple ligand-protein interactions and will also be particularly useful in the study of small molecule-membrane interactions. The aim of the study presented here is to demonstrate the use of MLBAs for the high-

throughput investigation of various membrane constituents on small molecule association using the well-studied membrane-associating molecule merocyanine 540 (MC540).[4-10]

In this study, the use of the MLBAs has been expanded upon to investigate small-molecule membrane interactions. As mentioned previously, cellular membranes are complex, containing well over 100 unique lipid compositions with different headgroup and acyl group portions whose properties such as charge and lipid packing will impact small molecule penetration into the membrane.[1,3,11] Glycerophospholipids represent the majority of membrane lipids with the zwiterrionic phosphatidylcholine (PC) headgroup being the most common. Cell membranes also contain a significant amount of the anionic phosphatidylserine (PS) headgroup with PS representing ~10% of lipids in human erythrocyte membranes.[12] The acyl chains differ in length and degree of saturation, which has an impact on membrane segregation, fluidity and the phase transition temperature (T_m). The T_m is the temperature at which the lipids change from the gel phase characterized by dense, tightly packed chains, to the liquid-disordered phase where the lipids are randomly and loosely packed.[13] Generally, saturated lipids tend to exist in the gel phase at room temperature with longer chains having a higher T_m due to increased van der Waals interactions. Unsaturated lipids exist in the liquid-disordered or liquid-crystalline (l.c.) phase as the *cis* double bond introduces kinks in the chain to disorder the packing. Cholesterol is another major component in biological membranes. Constituting ~30% of the membrane lipids in animal cell plasma membranes, cholesterol is known to influence the physical properties of cellular membranes.[1,14] For example, cholesterol has a condensing effect on membrane lipids

which decreases the surface area per lipid molecule.[14] Cholesterol also influences the miscibility of lipid components and modulates the T_m.[14,15]

In the work presented here, a MLBA was used for the high-throughput investigation of the various membrane properties mentioned above on the binding of the fluorescent anionic dye MC540 (Figure 4.1). MC540 is used as a model amphipathic low molecular weight molecule, a characteristic of many drug compounds, with its nonpolar parts having an affinity for the hydrophobic portion of the lipid membranes. The fluorescence characteristics of MC540 are sensitive to the polarity of the local environment.[5] When MC540 is located in the aqueous environment surrounding the polar headgroup, it is in its weakly fluorescent dimer form with an absorbance maximum at 530 nm.[8] When the dye is incorporated into a lipid bilayer, it partitions as a monomer slightly above the glycerol backbone with its butyl groups extending into hydrocarbon chain, resulting in a red shift in the absorbance maxima to 568 nm and an increase in the fluorescence quantum yield.[5,8]

Fluorescence microscopy can be used to obtain information on MC540 binding with respect to membrane properties as the fluorescence intensity is related to the location of the dye within the membrane. MC540 has been used to probe membrane properties such as molecular packing of lipid bilayers, with increased MC540 fluorescence in loosely packed (l.c. phase) lipid bilayers as opposed to closely packed (gel phase) membranes.[4-7] MC540 has also demonstrated sensitivity to the membrane surface potential, showing a decrease in MC540 monomer binding to negatively charged membranes.[5,9,10,16,17] MC540 is an excellent candidate to validate the efficacy of

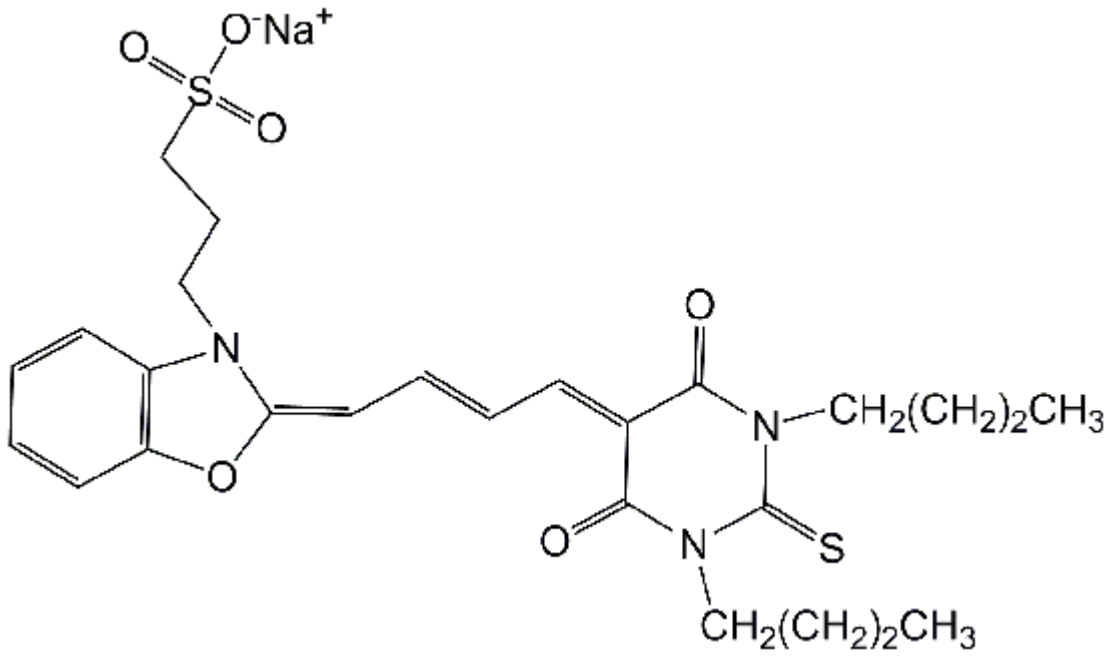

Figure 4.1. Structure of merocyanine 540 (MC540).

MLBAs for monitoring small molecule-membrane interactions due to its abundant use on bilayer systems in the literature.

In the experiments reported here MLBAs composed primarily of lipids with the zwitterionic PC headgroup with different alkyl chains along with varying ratios of cholesterol and phosphatidylserine (PS) lipids were examined. Fluorescence microscopy was used to measure the effect of lipid composition on MC540 binding. Lipids with saturated, unsaturated or mixed chains were used to investigate the effects of gel and l.c. phases of the lipid-small molecule interactions using the following glycerophospholipid (chain length:number of double bonds); myristoyl (14:0), palmitoyl (16:0), stearoyl (18:0), oleoyl (18:1) and mixed stearoyl-oleoyl (18:0-18:1) and palmitoyl-oleoyl (16:0-18:1). The lipids mentioned above were also prepared in binary mixtures with cholesterol to study its effect on small molecule association. Finally, the PC membranes were doped with varying concentrations of PS to study the effect of charged membranes on MC540 binding.

4.2 Experimental

4.2.1 Materials

1,2-Dimyristoyl-*sn*-glycero-3-phosphocholine (DMPC), 1,2-dipalmitoyl-*sn*-glycero-3-phosphocholine (DPPC), 1,2-distearoyl-*sn*-glycero-3-phosphocholine (DSPC), 1,2-dioleoyl-*sn*-glycero-3-phosphocholine (DOPC), 1-stearoyl-2-oleoyl-*sn*-glycero-3-phosphocholine (SOPC), 1-palmitoyl-2-oleoyl-*sn*-glycero-3-phosphocholine (POPC), and 1,2-dioleoyl-*sn*-glycero-3-phospho-L-serine (sodium salt) (DOPS) were obtained from Avanti Polar Lipids. MC540 was obtained from Fluka. Bovine serum albumin

(BSA) and cholesterol (CHO) were purchased from Sigma-Aldrich. All materials were used as received. The water used in these studies was obtained from a Nanopure Infinity Ultrapure water purification system with a minimum resistivity of 18.2 MΩ· cm. Quartz microscope slides (Chemglass) were used as the supporting substrate for the MLBAs.

4.2.2 Small Unilamellar Vesicle (SUV) Preparation

The SUV preparation described in Chapter 2 was used here.

4.2.3 MLBA Preparation

Details of the MLBA preparation as well as substrate cleaning procedure are described in Chapter 2. Briefly, the various SUV solutions at a 0.5 mg/mL lipid concentration were simultaneously introduced through the microchannels at least 15°C above the T_m and circulated over the substrate for at least 20 min. The SUV solutions were removed and the channels were rinsed with nanopure water, making sure the channels never completely empty. The substrate was removed from the PDMS printhead in a reservoir of a 0.2% (w/v) BSA solution in PBS and incubated for 20 min. BSA adsorbs to the hydrophobic PDMS residue from the printhead along with any areas of bare glass, corralling the bilayer spots to prevent lipid spreading.[18] The substrate was then transferred in a water bath to a custom built Teflon flow cell.

4.2.4 MC540 Binding Experiments

Patterned membranes were prepared with one of the primary phospholipids (DMPC, POPC, DPPC, DSPC, SOPC and DOPC) containing 0 or 33 mol % cholesterol. Patterned DOPC membranes doped with 0-25 mol % of DOPS were also prepared on the same substrate. The MLBA was incubated with 18 μM MC540 in PBS for 20 min in the dark. The substrate was then reassembled into a new flow cell in a PBS bath to eliminate background fluorescence from MC540 staining the bottom of the flow cell. This procedure was repeated for the ionic strength dependent experiments with the exception of modifying the PBS to contain 500 mM NaCl. The binding of MC540 to the different lipid compositions was measured by fluorescence microscopy. All binding experiments were performed at room temperature (~25°C).

4.2.5 Fluorescence Microscopy

An Olympus BX40 microscope equipped with a Photometrics CoolSNAP$_{cf}$ (Roper Scienctific) color camera was used to image the MLBAs under a 10x objective (NA, 0.30). The bandpass filter set used for MC540 has a center excitation/emission wavelength of 550/615 nm with a passband width of 30/45 nm, respectively. The excitation/emission wavelengths of the MC540 dimer and monomer are 530/570 and 568/590 nm, respectively.[4] Fluorescence images were analyzed and background corrected using the software package Voodoo Incantation 1.2 provided by Photometrics. The brightness and contrast of the fluorescent images were adjusted for presentation purposes. The micropatterned bilayer images were pieced together using Canvas X software. The use of a 10× objective allowed for the more precise assessment of

MC540 fluorescence within an individual lipid spot, facilitating a more accurate determination of small-molecule binding along with the possibility of observing any inhomogeneous distribution of MC540 as a result of lipid phase segregation or domain formation in the binary mixtures.

4.2.6 UV-Vis Absorbance

The results from the MC540 binding experiment were verified by performing a similar binding experiment on SUVs using absorbance spectroscopy. The liposome stock solutions were prepared at a 2.7 mM lipid concentration. The MC540 stock solution of 29 μM was prepared in PBS. MC540 was added to the liposome solutions to yield a 400:1 lipid:dye molar ratio with a final MC540 concentration of 5 μM. The mixtures were incubated for at least 20 min while being shielded from light. MC540 association to the different liposomes was analyzed by recording the absorbance spectra using a Lambda 25 UV/Vis Spectrometer (Perkin Elmer Instruments). All measurements were performed at room temperature with the exception of DMPC and DMPC + 33 mol % which were measured at 50°C. The DMPC/cholesterol mixture is unstable at room temperature resulting in cloudy solutions, altering the absorbance spectrum due to high levels of light scattering. The background samples were obtained by diluting the SUV stock solutions with PBS to yield the appropriate lipid concentration.

4.2.7 Surface Pressure Measurements

Surface pressure measurements were performed using the Wilhelmy balance from a KSV Instrument Langmuir-Blodgett trough (Minitrough) and a custom designed glass cell which contained 100 mL of PBS buffer as a subphase. DOPC with varying amounts of DOPS was dissolved in $CHCl_3$ and spread dropwise at the air/water interface until the surface pressure reached a value between 29-31 mN/m. Discrete amounts of a 17.9 mM solution of MC540 in water were added while gentle stirring the subphase and allowing the surface pressure to equilibrate (approximately 10-20 min) before recording the subsequent change in the surface pressure. The injection volume of the MC540 solution did not exceed 150 μL to ensure the cell volume was not significantly changed.

4.3 Results and Discussion

4.3.1 MC540 Binding to a Multicomponent MLBA

The CFM has been used here to pattern multicomponent lipid arrays to examine MC540 membrane binding. The array was prepared using six primary lipids (DMPC, POPC, SOPC, DOPC, DSPC and DPPC) differing in the acyl chain length as well as the degree of unsaturation. These parameters influence the T_m which determines the phase state of the lipids (25°C) with DMPC, POPC, SOPC and DOPC existing in the l.c. phase while DSPC and DPPC exist in the gel phase at room temperature. Bilayers were prepared from SUV solutions containing these primary lipids with and without cholesterol. The partitioning of MC540 into the twelve unique lipid compositions is represented by the fluorescence image in Figure 4.2. The fluorescence intensity from

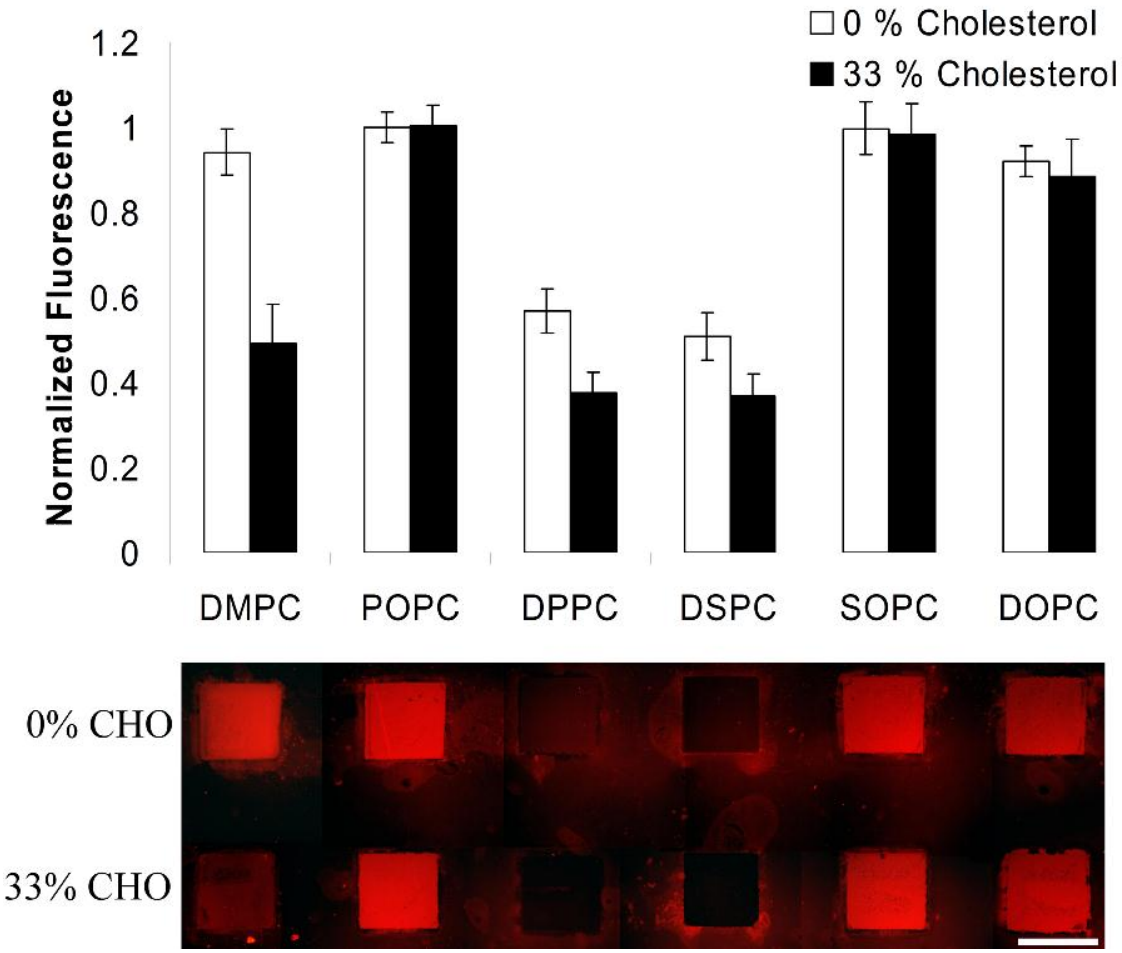

Figure 4.2. Fluorescence image of MC540 binding to a MLBA with the membrane compositions stated in the figure. Quantitative fluorescence values were obtained from three separate experiments with each experiment having duplicated bilayer spots of identical membrane composition prepared on the same substrate (not shown). The data presented in the graph were normalized to MC540 fluorescence on a pure POPC bilayer. The scale bar represents 400 μm.

each bilayer spot was obtained by averaging the fluorescence intensity over the entire bilayer square. The measured fluorescence intensities shown in Figure 4.2, with their respective errors, represent the average and standard deviation of the pooled normalized fluorescence values from three independent binding experiments where each experiment had two bilayer spots of identical bilayer composition on the same substrate for a total of six independent measurements. The fluorescence intensities were normalized to the pure POPC bilayers without any cholesterol present. For the membranes without cholesterol, the fluorescence intensity is approximately two times greater for the more disordered l.c. phase (DMPC, POPC, SOPC and DOPC) lipids than those in the well-ordered gel phase (DSPC and DPPC). The higher fluorescence intensity for the l.c. phase membranes suggest that more dye is penetrating into the hydrophobic core than in gel phase lipid bilayers, in agreement with previous MC540 binding experiments.[4-6] This can be rationalized by the lipid packing in the bilayer relative to its phase. The loosely packed l.c. phase bilayers (60-70 $Å^2$/molecule) allow MC540 to penetrate deeper into the hydrophobic core than the more tightly packed gel phase bilayers (~50 $Å^2$/molecule).[1,4,6] Note that the reported area per molecule values were extrapolated from Langmuir pressure-area isotherms of the appropriate lipid monolayers assuming a surface pressure of 30 mN/m for the MLBAs.[19]

When comparing the fluorescence intensities for the bilayers within the l.c. phase, there is a subtle difference in MC540 binding with respect to the different acyl chain compositions. MC540 fluorescence is ~8% higher in bilayers composed of the mixed chain lipids, POPC (fluorescence intensity = 1.00 ± 0.04) and SOPC (fluorescence intensity = 1.00 ± 0.06), than the bilayers composed of the symmetric acyl chain lipid

DOPC (18:1) (fluorescence intensity = 0.92 ± 0.04). A Student's t-test was performed on the pooled normalized fluorescence values to determine if the different acyl chains had a significant impact on MC540 binding. There is no statistical difference, at the 95% confidence level, in the fluorescence intensities between the mixed chain lipids POPC (16:0-18:1) and SOPC (18:0-18:1) suggesting MC540 binding is insensitive to the difference in the tail length of the saturated chain for lipids in the same phase state. The fluorescence obtained from the bilayer patches prepared with the short, fully saturated DMPC (14:0) lipids falls within error (fluorescence intensity = 0.94 ± 0.05) of the fluorescence signal obtained from the mixed chain lipid bilayers and DOPC bilayers, at the 95% confidence level. These data along with observed uniform fluorescence within the bilayer spots provide evidence that DMPC exists primarily in the l.c. phase at room temperature. Between the gel phase lipids, there is a slight but statistically insignificant decrease in MC540 signal in DSPC (18:0) bilayers relative to the bilayers composed of the shorter chain DPPC (16:0) lipids, at the 95% confidence level. Altogether, these results demonstrate that MC540 binding is sensitive to the phase state of the membrane while not being as sensitive to the changes in chain length and degree of unsaturation of the lipid tails within a certain phase state given the error in our measurements.

The influence of cholesterol on MC540 binding was found to be dependent on the primary lipid composition of the bilayer. Figure 4.2 shows a decrease in MC540 fluorescence in all the saturated lipid bilayers when cholesterol is introduced with a 28, 34 and 50 % attenuation of MC540 fluorescence observed upon addition of 33 mol % CHO to DSPC, DPPC and DMPC bilayers, respectively. The decrease in MC540

binding could be explained by the condensing effect cholesterol has on saturated lipids to decrease the area per lipid molecule.[14] The addition of CHO into DMPC membranes yields the largest reduction in MC540 signal because it induces the greatest change in lipid packing relative to the gel phase DPPC and DSPC bilayers, which already have tightly packed lipids. This physical change in DMPC membranes is apparent in the phase diagram of DMPC + CHO presented by Almeida et al.[20] When high concentrations of cholesterol (>30%) are introduced into DMPC bilayers above the T_m, there is a significant condensing effect on the bilayer, changing the bilayer from the loosely packed l.c. phase to the liquid-order phase exhibiting ordered acyl chains and tighter lipid packing (~50 $Å^2$/molecule) characteristic of the gel phase while still possessing membrane fluidity characteristic of the l.c. phase.[21] In contrast, there was no statistically significant difference in MC540 fluorescence for the remaining l.c. phase + CHO bilayers, at the 95% confidence level. These results were unexpected since a previous study showed a decrease in MC540 fluorescence in SOPC large unilamellar vesicles with increasing cholesterol content.[6] Error bars were not reported by Stillwell et al.,[6] but our results do qualitatively track with their previous study. A slight decrease in MC540 fluorescence in the SOPC + CHO bilayer spot was observed here, but the error in the measurements precludes any strong statements regarding the differences between these systems from being definitively assigned.

The decrease in MC540 binding to CHO containing lipid bilayers correlates with cholesterol's ability to increase the packing density of lipid membranes, most notably in the bilayers prepared with saturated lipids.[21-24] Langmuir film studies have shown that cholesterol at 30 mol % induces a condensing effect on gel phase DPPC monolayers to

further increase the packing density of the film.[22,23] It should also be noted that the bilayers presented here were prepared by the vesicle fusion method which is known to produce more disordered membranes than those prepared on a Langmuir trough.[25] It is likely that cholesterol is increasing the order of the slightly disordered gel phase lipids and simultaneously reducing the number of defects present in the bilayer thereby further prohibiting the incorporation of MC540. This hypothesis is consistent with a study performed by Kim et al.[23] where they characterize Langmuir-Blodgett deposited DPPC monolayers on silanized silicon substrates as a function of CHO content by atomic force microscopy (AFM), ellipsometry and cyclic voltammetry. They found that incorporation of cholesterol (10-30 mol %) into the lipid films yielded more densely packed monolayers with fewer defects than pure DPPC monolayers.

Another contributing factor may be the location of the hydroxyl group on cholesterol at the edge of the polar region of the lipid close to the ester carbonyl group.[26] Thus, cholesterol simply fills up space between the lipids to hinder the insertion of the MC540 butyl chains into the tightly packed bilayers. This is in agreement with literature reports of tetracaine binding to lipid bilayers.[27,28] Tetracaine is a local anesthetic which locates similarly into the membrane as MC540.[27] Zhang et al.[27] observed a reduction in drug binding when 28 mol % cholesterol was added to DPPC lipids at 23°C as a consequence of cholesterol being present at the glycerol backbone where tetracaine would normally locate. It should also be noted that cholesterol can fluidize lipids below their T_m and at high cholesterol concentrations (> 20 mol %). [29] However, it is important to remember that MC540 fluorescence is sensitive to its location in the membrane. Therefore, an increase in fluidity will not

directly result in an increase in MC540 binding if cholesterol is preventing MC540 from penetrating deeper into the hydrophobic core of the membrane. Although cholesterol is most likely condensing the fluid phase lipids, there is still ample space between the lipid headgroups at 33 mol % cholesterol for MC540 binding. This is most apparent for DOPC lipids which are only condensed 6 $Å^2$/molecule, from 66 $Å^2$/molecule, upon the addition of 30 mol % cholesterol at a surface pressure of 30 mN/m, which still provides more space than lipids in the gel phase (~50 $Å^2$/molecule).[21]

4.3.2 Interaction of MC540 with Liposomes

Since there is a lack of statistical data in some of the previous studies on MC540 binding to the various lipid systems, we repeated the MC540 binding experiment with liposomes using UV-Vis absorbance as a control in order to validate the use of the MLBA platform. The absorbance values of MC540 incorporated into SUVs of the same composition as those examined using the MLBA are shown in Figure 4.3. The solution phase vesicle results show similar trends as the MLBA data presented above, namely, an increased monomer concentration in fluid phase bilayers compared to gel phase lipids. However, the absorbance for the gel phase lipids is only ~30 % lower than the l.c. phase lipids as opposed to the ~50 % reduction observed from the fluorescence of MC540 within the PSLBs. It should be noted, however, that SUVs have a looser headgroup packing as a consequence of the small radius of curvature which allows MC540 to better penetrate the gel phase lipid bilayers in vesicle form relative to planar form.[4]

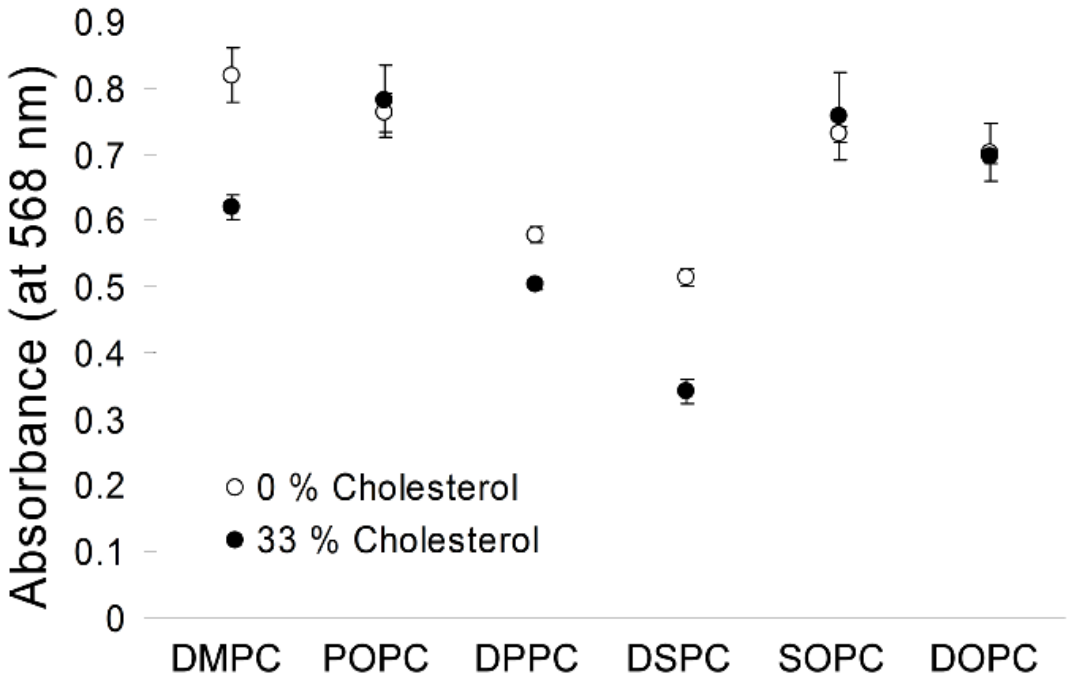

Figure 4.3. Absorbance of MC540 monomer bound to different lipid SUVs with and without cholesterol. The data points represent the average values obtained from three liposome solutions prepared from the same SUV stock solution.

For the l.c. phase lipids, there is no observable difference in MC540 absorbance amongst the mixed chain POPC and SOPC lipids consistent with MC540 binding measured to the MLBAs. DMPC liposomes have the highest MC540 absorbance of all the l.c. phase lipids examined, which was not the case for MC540 adsorption to the MLBAs. This is a possible consequence of the elevated temperature used for the DMPC liposomes (50°C) (see section 4.2.6 for more details). DOPC liposomes have the lowest MC540 absorbance of the liquid phase lipids, agreeing with the MLBA fluorescence data. Similar to MC540 binding to the gel phase MLBAs, the dye penetrates deeper into DPPC liposomes than DSPC liposomes as illustrated by the slightly higher MC540 absorbance for DPPC lipids. With the addition of cholesterol, DMPC liposomes have a significant decrease in MC540 absorbance which is consistent with MC540 binding to the planar bilayers. A considerable decrease in MC540 absorbance was also observed for DPPC and DSPC bilayers when cholesterol is present. Cholesterol in SOPC, POPC and DOPC bilayers did not have a large impact on MC540 absorbance in correlation with the MLBA results discussed above. Based on the strong correlation between the absorbance data from the SUVs and the fluorescence data from the MLBA, it is likely that a decrease in fluorescence signal is strongly attributed to the decrease occurrence of monomers with absorbance maxima at 568 nm. While there is a shift in the monomer-dimer equilibrium constant towards the increased occurrence of dimers with an increase in lipid packing, the fluorescence signal remains relatively low because of their lower quantum efficiencies.[5,8] Overall, the two separate experiments agree very well with only slight discrepancies which could be a result of the high degree of curvature in SUVs.[4,8]

4.3.3 MC540 Binding to Charged Membranes

The negatively charged lipid DOPS was incorporated into DOPC membranes to study the effect on MC540 binding. The image in Figure 4.4a shows MC540 associating into DOPC bilayers with 0, 5, 15, and 25 mol % DOPS. The quantitative fluorescence of each bilayer patch is shown in the plot in Figure 4.4b. The data represent the average of three independent experiments with each MLBA containing two identical bilayer patches prepared from the same SUV stock solution. The graph shows that with increasing negative surface charge density of the membranes there is a correlated decrease in the fluorescence of the anionic dye with a 10, 24 and 40 % reduction in MC540 binding when 5, 15 and 25 mol % DOPS is incorporated into DOPC membranes, respectively. These results support previous studies which found that negatively charged membranes decreases the absorbance and fluorescence of the dye.[9,10] These observations could be explained by the negatively charged membrane electrostatic repelling MC540 monomers from penetrating deep into the membrane as well as changing the amount of dye binding. However, MC540's fluorescence yield is dependent on its surrounding environment so the fluorescence intensity is not entirely related to the amount of MC540 binding to the lipid bilayers.

Since fluorescence measurements do not quantify the surface concentration of MC540 molecules at the bilayer surface, surface pressure measurements were performed in an attempt to correlate the observed changes in MC540 fluorescence to the surface concentration of the dye. Surface pressure measurements are a convenient technique for providing information on molecular adsorption to lipid monolayers.[30-32] The amount of MC540 incorporating into a DOPC monolayer containing varying DOPS

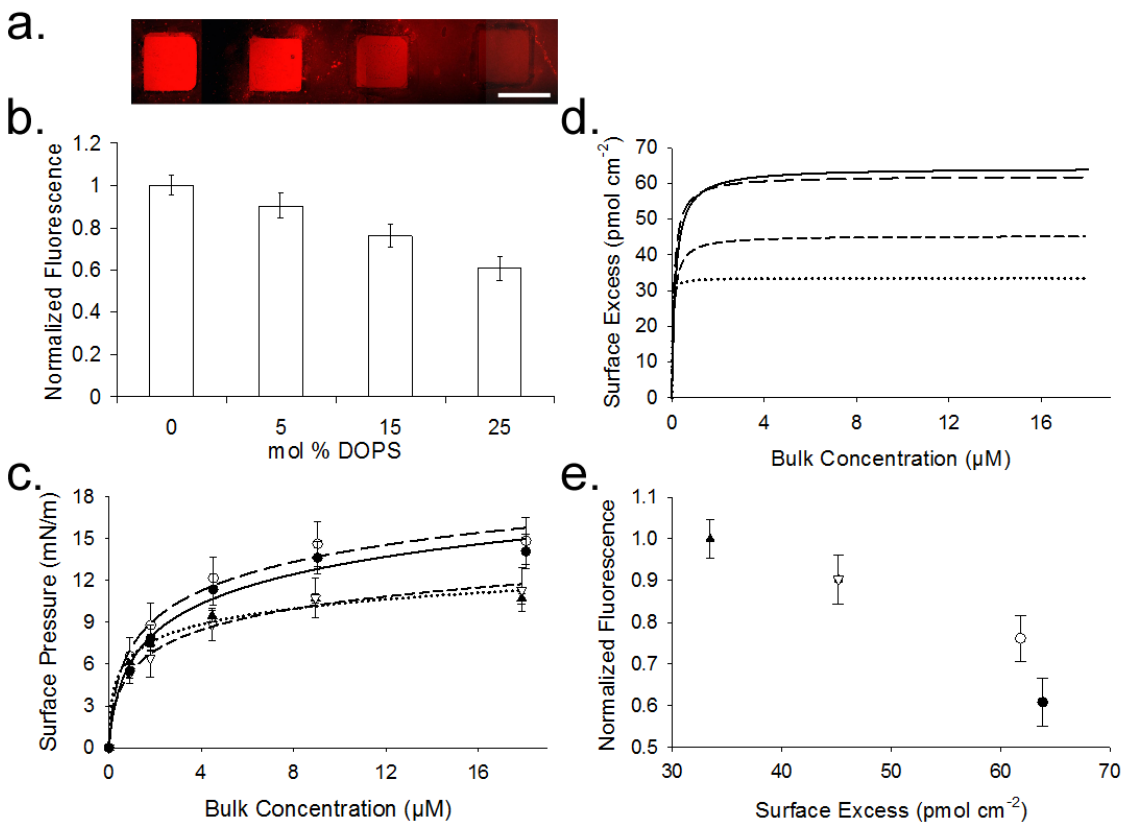

Figure 4.4. (a) Fluorescence image of MLBA prepared with DOPC containing 0, 5, 15 and 25 mol % DOPS from left to right. (b) Fluorescence intensity measured for the different bilayer compositions with the fluorescence normalized to the signal obtained from the pure DOPC bilayers. The data represent the average of three independent experiments performed on freshly prepared MLBAs with each MLBA having two reproduced bilayer spots of identical lipid compositions. (c) Change in surface pressure with increasing bulk concentrations of MC540 for increasing DOPS concentration of 0 (▲), 5 (▽), 15 (○) and 25 (●) mol %. The lines represent the fits to the data for 0 (.....), 5 (- - - - -), 15 (— —) and 25 (——) mol % DOPS using Equation 4.2 with the calculated MC540 surface excess as function of bulk concentration shown in (d). (e) Fluorescence from the MLBA as a function of surface excess with respect to DOPS concentration. The symbols are the same as those represented in (c). Scale bar represents 400 μm.

concentrations was measured by recording the change in surface pressure with respect to the bulk concentration of MC540 (Figure 4.4c). To determine the surface excess concentration (Γ) from the surface pressure data the Gibbs adsorption equation for an electrolyte was used:[33,34]

$$\Gamma_{MC540} = \frac{1}{2RT}\left(\frac{\partial \pi}{\partial ln C_b}\right) \quad (4.1)$$

where C_b is the bulk concentration of MC540, Γ_{MC540} is the surface excess of MC540, and π is the surface pressure. By assuming a Langmuir adsorption process it is possible to obtain an integral form of the surface pressure as a function of bulk concentration, described by:

$$\pi = \Gamma_{max} 2RTln(1 + K_a C_b) \quad (4.2)$$

where Γ_{max} is the maximum surface excess concentration of MC540, R is the molar gas constant, T is temperature and K_a is the binding constant. Equation 4.2 was used to fit the data in 4c and determine the binding affinities of MC540 and Γ_{max}. The K_a for MC540 binding to a DOPC monolayers with 0, 5, 15, and 25 % DOPS was determined to be 56 ± 6, 11 ± 2, 10 ± 4 and 6 ± 1 μM^{-1}, respectively. The decrease in K_a with increasing DOPS means a less favorable free-energy of adsorption of MC540 to the membrane. The surface excess concentration of MC540 (Γ_{MC540}) as a function of the bulk concentration of the dye was determined using the Langmuir isotherm using the values of Γ_{max} and K_a determined from the fits to the data in Figure 4.4c using Equation

4.2, and are plotted in Figure 4.4d. The maximum surface excess concentration was found to increase in the order 34±2, 45±4, 62±1 and 64±4 pmol cm^{-2} with increasing concentration of DOPS from 0 to 25 mol%. An inverse relationship is observed between K_a and Γ_{max}. However, a direct correlation between K_a and Γ_{max} is not necessarily expected because K_a describes the fractional surface coverage with respect to the bulk concentration and therefore does not depend on the absolute concentration (Γ_{max}) in the membrane. The fluorescence intensities of MC540 from the MLBA reported in Figure 4.4b was related to the surface excess concentration of dye (at C_b = 18 μM) in Figure 4.4e. Figure 4.4e shows an inverse relationship between the fluorescence signal and the surface concentration of the dye obtained from surface pressure measurements. This could be explained by the binding mechanism of MC540 in response to a change in the electric field applied across a membrane. It was first proposed by Ross et al.[35] who performed MC540 binding experiments on squid axons, that a change in the applied electric field would shift the monomer-dimer equilibrium constant. The authors observed that when squid nerve axons were depolarized there was an increase in absorbance around 570 nm and decrease at 510 nm, corresponding to an increased concentration of monomers and decreased occurrence of dimers with a shift in equilibrium toward the monomers. This can be accounted for by the drastic reduction in the quantum efficiency of dimerized MC540 relative to the monomer.[35] This hypothesis was later confirmed by fluorescence polarization experiments on hemispherical bilayer membranes performed by Dragsten and Webb.[36] This interpretation is also consistent with absorbance studies of MC540 binding to increasingly charged liposomes performed by Mateašik et al.[9] They found that the

absorbance maxima of MC540 monomers decreased as the surface charge increased with a change in the monomer-dimer equilibrium toward a decreased occurrence of monomers. There was also an accompanied blue shift in the monomer adsorption peak from 568 to 560 nm when 20 % of the negatively charged lipid analog was incorporated into the liposomes. This is indicative of MC540 monomers residing in a slightly more hydrophilic environment. A new absorbance was also observed at 530 nm which was suggested to be the formation of aggregates on the charged membrane. The results presented in Figure 4.4 are consistent with these previous observations.

4.4 Conclusion

MLBAs were used for small molecule-membrane binding experiments to rapidly study the effect different membrane parameters have on MC540 binding. It has been shown that MC540 can distinguish between gel and liquid phase membranes, with measured MC540 fluorescence intensity being twice as great in bilayer spots containing lipids above their T_m. The presence of cholesterol significantly decreased the fluorescence intensity in the saturated DMPC, DPPC and DSPC lipid membranes but had only a minimal impact on MC540 binding to the unsaturated (DOPC) and mixed chain (SOPC and POPC) lipids. The MC540 fluorescence obtained from the MLBAs for the MC540 binding experiments correlated extremely well to experiments using solution phase liposomes. When DOPC membranes were doped with the negatively charged DOPS lipids, MC540 fluorescence was attenuated due to a shift in the monomer-dimer ratio. The reproducibility of the binding experiment with the MLBAs was very good with, on average, <9% relative error for the three separate experiments.

The MLBAs presented here provide a promising platform for small molecule-membrane studies with important applications in areas such as pharmaceutical drug discovery and delivery. For example, coupling lipid bilayer arrays with a label-free imaging technique will provide a high-throughput noninvasive method for investigating how a particular drug interacts with specific membrane components, assisting in the discovery of potential targets for drug binding.

4.5 References

(1) Gennis, R. B. *Biomembranes: Molecular Structure and Function*; Springer-Verlag: New York, 1989.

(2) Schreier, S.; Malheiros, S. V. P.; de Paula, E. *Biochim. Biophys. Acta, Biomembr.* **2000**, *1508*, 210.

(3) Srivastava, R. C.; Nagappa, A. N. *Surface Activity in Drug Action*; Elsevier: Amsterdam, 2005.

(4) Williamson, P.; Mattocks, K.; Schlegel, R. A. *Biochim. Biophys. Acta, Biomembr.* **1983**, *732*, 387.

(5) Lelkes, P. I.; Miller, I. R. *J. Membr. Biol.* **1980**, *52*, 1.

(6) Stillwell, W.; Wassall, S. R.; Dumaual, A. C.; Ehringer, W. D.; Browning, C. W.; Jenski, L. J. *Biochim. Biophys. Acta, Biomembr.* **1993**, *1146*, 136.

(7) Langner, M.; Hui, S. W. *Biochim. Biophys. Acta, Biomembr.* **1999**, *1415*, 323.

(8) Arroyo, J.; Biondi de Lopez, A. C.; Bernik, D. L.; Disalvo, E. A. *J. Colloid Interface Sci.* **1998**, *203*, 106.

(9) Mateasik, A.; Sikurova, L.; Chorvat, D. *Bioelectrochemistry* **2002**, *55*, 173.

(10) Waczulikova, I.; Rozalski, M.; Rievaj, J.; Nagyova, K.; Bryszewska, M.; Watala, C. *Biochim. Biophys. Acta, Biomembr.* **2002**, *1567*, 176.

(11) Tsuchiya, H.; Mizogami, M.; Ueno, T.; Takakura, K. *Inflammopharmacology* **2007**, *15*, 164.

(12) Devaux, P. F.; Seigneuret, M. *Biochim. Biophys. Acta, Rev. Biomembr.* **1985**, *822*, 63.

(13) Small, D. M. *Handbook of Lipid Research: The Physical Chemistry of Lipids, From Alkanes to Phospholipids*; Plenum Press: New York, 1986; Vol. 4.

(14) Yeagle, P. L. *Biochim. Biophys. Acta, Rev. Biomembr.* **1985**, *822*, 267.

(15) Veatch, S. L.; Keller, S. L. *Biophys. J.* **2003**, *85*, 3074.

(16) Masamoto, K.; Matsuura, K.; Itoh, S.; Nishimura, M. *J. Biochem.* **1981**, *89*, 397.

(17) Waggoner, A. S. *Annu. Rev. Biophys. Bioeng.* **1979**, *8*, 47.

(18) Burridge, K. A.; Figa, M. A.; Wong, J. Y. *Langmuir* **2004**, *20*, 10252.

(19) Marsh, D. *Biochim. Biophys. Acta, Rev. Biomembr.* **1996**, *1286*, 183.

(20) Almeida, P. F. F.; Vaz, W. L. C.; Thompson, T. E. *Biochemistry* **1992**, *31*, 6739.

(21) Smaby, J. S.; Momsen, M. M.; Brockman, H. L.; Brown, R. E. *Biophys. J.* **1997**, *73*, 1492.

(22) Sabatini, K.; Mattila, J.-P.; Kinnunen, P. K. J. *Biophys. J.* **2008**, *95*, 2340.

(23) Kim, K.; Kim, C.; Byun, Y. *Langmuir* **2001**, *17*, 5066.

(24) Dynarowicz-Latka, P.; Hac-Wydro, K. *Colloids Surf., B* **2004**, *37*, 21.

(25) Watkins, E. B.; Miller, C. E.; Mulder, D. J.; Kuhl, T. L.; Majewski, J. *Phys. Rev. Lett.* **2009**, *102*, 238101/1.

(26) Worcester, D. L.; Franks, N. P. *J. Mol. Biol.* **1976**, *100*, 359.

(27) Zhang, J.; Hadlock, T.; Gent, A.; Strichartz, G. R. *Biophys. J.* **2007**, *92*, 3988.

(28) Auger, M.; Jarrell, H. C.; Smith, I. C. P. *Biochemistry* **1988**, *27*, 4660.

(29) Rubenstein, J. L. R.; Smith, B. A.; McConnell, H. M. *Proc. Natl. Acad. Sci. U. S. A.* **1979**, *76*, 15.

(30) Trommeshauser, D.; Krol, S.; Bergelson, L. D.; Galla, H. J. *Chem. Phys. Lipids* **2000**, *107*, 83.

(31) Ellison, E. H.; Castellino, F. J. *Biophys J* **1997**, *72*, 2605.

(32) Ellison, E. H.; Castellino, F. J. *Biochemistry* **1998**, *37*, 7997.

(33) Chattoraj, D. K. *Adsorption and the Gibbs Surface Excess*; Plenum Press: New York, 1984.

(34) Rehfeld, S. J. *J. Phys. Chem.* **1967**, *71*, 738.

(35) Ross, W. N.; Salzberg, B. M.; Cohen, L. B.; Davila, H. V. *Biophys. J.* **1974**, *14*, 983.

(36) Dragsten, P. R.; Webb, W. W. *Biochemistry* **1978**, *17*, 5228.

CHAPTER 5

SUM-FREQUENCY VIBRATIONAL IMAGING OF LIPID BILAYER ARRAYS

5.1 Introduction

Thus far, the work presented in this dissertation has utilized fluorescence microscopy to characterize and monitor protein and small molecule-membrane binding to the MLBAs. Fluorescence microscopy is a well-established highly sensitive technique, capable of single molecule detection;[1,2] however, there are many drawbacks to this method. For example, covalently attaching a fluorescent label can modify the native molecule's lipophilicity, charge and size which may alter membrane interactions relative to the unmodified protein, lipid or drug. Labeling biomolecules is also a labor intensive process. In order to use the model membrane arrays discussed in Chapter 1-4 to their full advantage, we need a compatible analytical technique that does not require an extrinsic probe. Our lab has already developed a second harmonic generation (SHG) microscope to monitor the effect of different lipid compositions have on the binding of the anesthetic tetracaine to a MLBA without the use of an external probe.[3] SHG is a

surface specific technique which two photons of the same frequency ω interact to create the second harmonic frequency 2ω. An increase in SHG signal will be observed when the incident ω or SHG 2ω frequency is on resonance with an electronic transition of the drug molecules at the interface. However, SHG is limited in the amount of chemical information that can be attained for the different molecules at the interface. Sum-frequency vibrational generation (SFVG) is another surface specific technique which has the added advantage of providing vibrational selectivity to detect the native lipids and small molecules at the interface. By combining SFVG with imaging, a means of collecting information on lipid properties and structures in a high-throughput label-free method will be possible.

Sum-frequency vibrational spectroscopy (SFVS) is a well-established second-order nonlinear technique which is inherently surface specific and a complete description of its theory can be found in the scientific literature.[4-6] Briefly, SFVS involves the temporal and spatial overlap of a fixed visible (ω_{Vis}) and a tunable IR (ω_{IR}) to produce a third photon at the sum of the two input frequencies (ω_{SFG}). The intensity of the sum frequency signal, I_{SFG}, is given by:

$$I_{SFG} \propto \left|\tilde{f}_{SF} f_{Vis} f_{IR} \chi^{(2)}\right|^2 \tag{5.1}$$

where $\chi^{(2)}$ is the second-order nonlinear susceptibility tensor and $\tilde{f}_{SF}$, f_{Vis} and f_{IR} are the Fresnel coefficients for the sum, visible, and IR fields, respectively. The nonlinear susceptibility tensor has both a resonant (*R*) and non-resonant (*NR*) contribution given by

$$\chi^{(2)} = \chi_R^{(2)} + \chi_{NR}^{(2)} \tag{5.2}$$

with the resonant contribution defined as

$$\chi_R^{(2)} = \sum \frac{NA_i}{\omega_i - \omega_{IR} - i\Gamma_i} \tag{5.3}$$

where N is the number of molecules, A_i is the transition probability, ω_i is the frequency of the transition being probed, ω_{IR} is the frequency of the IR input and Γ_i is the line width of the transition being probed. The above equations show that as the IR frequency approaches the vibrational transition of the molecules at the surface there will be an enhancement in signal. A spectrum containing vibrational information is generated by collecting the sum frequency output as a function of the input IR frequency. SFVS is an ideal technique for probing lipid structure and dynamics due to the symmetry constraints on $\chi^{(2)}$ which prevent SFVS from occurring in systems that possess inversion symmetry.

There have been several examples of sum-frequency vibrational imaging (SFVI) presented in the literature.[7-11] Flörsheimer et al. developed a counter-propagating SFVI system to examine inhomogeneities in Langmuir-Blodgett (LB) monolayers on fused silica.[7,8] Their reported setup utilizes two input beams which arrive at the surface of a prism from opposite directions under total internal reflection and an output SFG beam is collected on the other side of the prism. The counter-propagating setup has the advantage of good spatial separation of the sum-frequency beam from two high

intensity input beams; however, the sum-frequency efficiency is lower when compared to a co-propagating geometry. SFVI microscopy using a co-propagating geometry has been demonstrated and applied to image patterned self-assembled monolayers.[9-11] Baldelli and co-workers have acquired 2D SFVI images of a metal surface that was first microcontact printed with a methyl-terminated alkanethiol and then backfilled with a phenyl-terminated alkanethiol.[10] The researchers tuned the input infrared frequency to be on resonance with the vibrational transitions of either the methyl or phenyl groups to obtain the chemical contrast necessary to generate an image. This application of co-propagating SFVI microscopy relies on the underlying gold substrate to amplify the measured sum-frequency signal through its large non-resonant background. This amplification can be seen upon insertion of Equation 5.1 into Equation 5.2, which results in a non-negligible cross-term containing the product of the resonant and non-resonant susceptibilities.

In this chapter, SFVI was implemented to measure the thermotropic phase transition in model lipid membranes arrays on a dielectric surface, in the absence of non-resonant enhancement effects. As mentioned in Chapter 4, the T_m of phospholipids is a fundamental property influencing the fluidity and permeability of the membrane while also having an impact on the organization of lipids in a membrane.[12] There are several techniques that can monitor the T_m of lipids at a surface such as differential scanning calorimetry (DSC) which can be used to determine the T_m of lipids in solution phase vesicles.[13,14] Fluorescence spectroscopy can be used to infer the T_m based on changes in the emission characteristics of a fluorescent probe.[15,16] Other analytical techniques, such as nuclear magnetic resonance (NMR), Raman, and Fourier transform infrared

spectroscopy (FTIR) can be used to investigate the conformation of the lipid acyl chains to measure the phase transition temperature.[14,17-21] Currently, there is no analytical technique that can obtain information on the T_m of lipid membranes in a high-throughput manner without the use of exogenous chemical reporters. SFVI is presented in this chapter as just such a technique, providing a means to measure the change in phase behavior in an array format with low total surface area samples.

Previous studies using SFVS for the determination of the T_m of amphiphilic molecules have measured changes in the gauche defect content (CH_2 ν_s intensity) of the acyl chains as a function of temperature;[22-25] however, we have previously shown that this method is not appropriate for lipid systems. The close proximity of the lipid acyl chains and the symmetric nature of a lipid bilayer precludes the CH_2 ν_s resonance from providing information on the conformational order of the lipid system, due to complex interferences between adjacent gauche conformers (pair-wise gauche defects) and destructive interference between the proximal and distal leaflets of planar supported lipid bilayers (PSLBs).[26-28] This problem can be circumvented by exploiting these same interferences to measure the T_m using CH_3 ν_s intensity from the termini of the lipid acyl chains. This resonance is extremely sensitive to the symmetry of the bilayer,[29,30] which is influenced by both the distribution of lipids and domains of lipids in the membrane. For a completely homogeneous lipid state, near complete cancellation of the CH_3 ν_s is observed; however, at the T_m, the lipid components segregate into *l.c.* and *gel* state domains to cause a slight dislocation between the domains in the two leaflets of the bilayer.[31] This dislocation is "sensed" by the CH_3 ν_s which manifests as an increase in its relative intensity.[28,32,33] By simply monitoring the CH_3 ν_s as a function of

temperature, one can obtain a spectroscopic measure of the T_m and more importantly the degree of segregation in the lipid film.[32]

In this chapter, SFVS has been coupled with an imaging system to provide the spatial resolution necessary to measure the phase behavior of lipid bilayer arrays of varying composition in a high-throughput manner. A simplified SFVI setup was developed to image lipid asymmetry in micropatterned lipid bilayers. The only optical elements deemed necessary to produce an SFVI image were a single focusing lens in a confocal arrangement along with a combination of interference/notch filters to attenuate the background from the input beams (Figure 5.1). This setup is a simplified version of the SFVI setup presented in the literature[9-11] where most of the optical elements were eliminated (two collimating lenses, microscope objective, grating, tube lens and interference/notch filters). This increased the collection efficiency while also providing a larger field of view.

SFVI for the characterization of lipid structural asymmetry was first characterized using a UV photolithographic patterned PSLB which was asymmetrically prepared using 1,2-distearoyl-*sn*-glycero-3-phosphocholine (DSPC) and its deuterated analog. Both a lens-less and simplified lens setup were initially investigated by collecting images for three different-sized pattern lines (397, 350 and 314 μm). Lens-less images were collected at increasing distances from the sample stage to characterize the propagating SFG beam. The simplified lens setup was used to collect images of the asymmetric bilayer at different frequencies to demonstrate the vibrational selectivity of this technique. Heating and cooling curves were generated from the SFVI images to examine the phase behavior of the DSPC lipids. Finally, SFVI was used to probe the

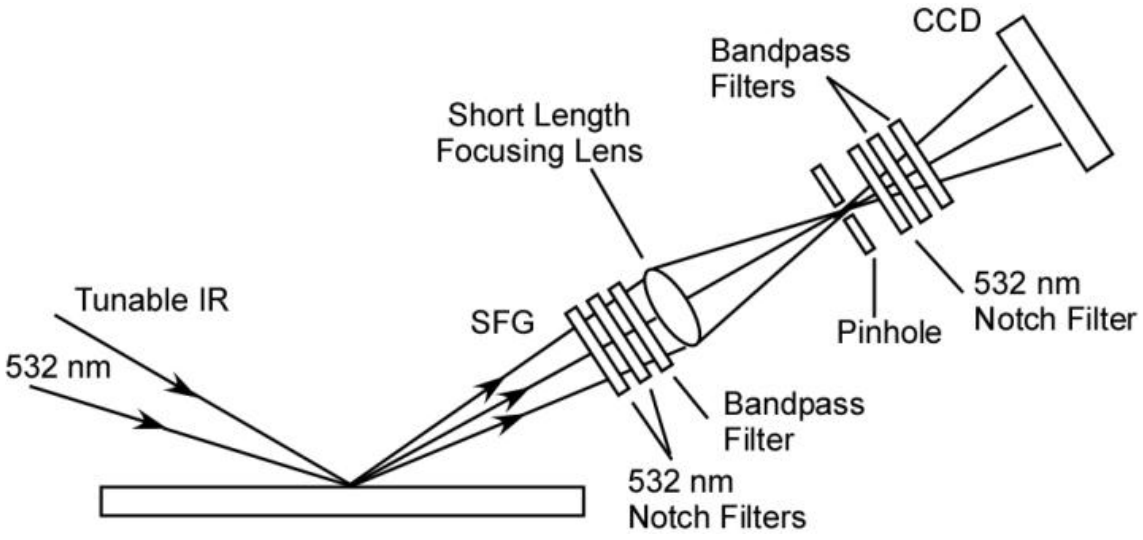

Figure 5.1. Schematic illustration of the simplified SFVI optical setup with the total internal reflections of the input IR and 532 nm laser beams blocked by a series of notch and bandpass filters. The generated SFG image is reconstructed onto a LN cooled CCD camera using a single short length focusing lens (f = 50 mm).

phase behavior of a micropatterned lipid bilayer array (MLBA) of binary phospholipid lipid mixtures using four primary lipids: 1,2-dioleoyl-*sn*-glycero-3-phosphocholine (DOPC), DSPC, 1,2-dipalmitoyl-*sn*-glycero-3-phosphocholine (DPPC) and 1,2-dimyristoyl-*sn*-glycero-3-phosphocholine (DMPC). These lipids were used in equal molar ratios to create three binary mixtures: DOPC:DSPC, DOPC:DPPC and DMPC:DSPC. These experiments showcase the potential application of spatially resolved SFVS for the investigation of lipid bilayer behavior, which can be extended to other system requiring localized vibrational information for characterization and analysis.

5.2 Experimental

5.2.1 Materials

DSPC, 1,2-distearoyl(d70)-*sn*-glycero-3-phosphocholine (DSPC-d_{70}), DOPC, DPPC and DMPC were obtained from Avanti Polar Lipids and used as received. Poly(allylamine hydrochloride) (PAH) (MW 56,000), HPLC grade Methanol and D_2O were purchased from Sigma-Aldrich. Sodium dodecyl sulfate (SDS) was purchased from Fisher Scientific. Spectroscopy grade $CHCl_3$ was obtained from EDM Millipore. Fused silica prisms (Almaz Optics) were used as the solid support for the PSLBs. The water used for bilayer preparation was obtained from a Nanopure Infinity Ultrapure water purification system (nanopure) with a minimum resistivity of 18.2 MΩ·cm.

5.2.2 Asymmetric Lipid Bilayer Preparation

The fused silica prisms were cleaned following the same procedure described in the experimental section of Chapter 2 (section 2.2.3). The asymmetric lipid bilayer was prepared using the Langmuir-Blodgett/Langmuir-Schaefer (LB/LS) method. A 1 mg/mL DSPC lipid solution in chloroform was deposited dropwise on the water subphase of a KSV Instrument Minitrough. The lipid layer was transferred onto a clean silica prism by pulling the substrate vertically out of the subphase at a surface pressure of 35 mN/m. The same prism was then passed horizontally through a monolayer of DSPC-d_{70} at 35 mN/m into the subphase. The bilayer was then placed in a reservoir of water to be patterned using UV photolithography.

A fused silica positive 1951 United States Air Force (USAF) resolution test target (Edmund Optics) with a chrome pattern was used for UV photolithography. The USAF test target was placed directly on top of the lipid bilayer separated by a thin water layer and held in place with electrical tape. A pattern was generated by exposure to UV light from a low pressure mercury vapor grid lamp ultra-violet ozone cleaner (Jelight Co.) for 13 min through the test target where the lipids not protected by the chrome pattern were etched away. The patterned bilayer was then assembled into a custom-built Teflon flow cell and rinsed with D_2O. A thermistor (TE Technologies) inserted into the flow cell was used to monitor the temperature of the bulk solution. A circulating water bath (HAAKE Phoenix II P1, Thermo Fisher Scientific) was used to control the temperature of the flow cell. For the temperature scans, the temperature was increased rapidly (1~2°C/min) and followed by rapid cooling to room temperature.

5.2.3 Small Unilamellar Vesicle Preparation

Equal molar ratios of DOPC:DSPC, DOPC:DPPC and DMPC:DSPC as well as DOPC:DSPC plus 40 mol % cholesterol were premixed in chloroform, evaporated under a stream on N_2 (g) and placed under a vacuum overnight to remove any residual chloroform. The dried lipid film was incubated in phosphate buffer saline (PBS, pH 7.4, 140 mM NaCl, 10 mM KCl, 10 mM Na_2HPO_4, and 2 mM KH_2PO_4) at 65°C for at least 20 min. The lipid film was then resuspended by vortexing and sonication till clarity at 65°C. The final concentration of the small unilamellar vesicle (SUV) solution was 0.25 mg/mL.

5.2.4 MLBA Preparation

Details of the continuous flow microspotter (CFM) construction and MLBA preparation can be found in section 2.2.3. Briefly, the SUV solutions were introduced individually into each microchannel at 65°C and circulated over the substrate for at least 30 min. The SUVs introduced under these conditions (elevated temperature and high salt concentration) will spontaneously fuse forming a symmetric bilayer.[34] Some microchannels circulated only PBS to serve as control spots. The SUV solutions were removed from the inlet wells and the microchannels were rinsed with PBS followed by Nanopure water while making sure the channels never completely emptied. The substrate was removed from the printhead in a reservoir of 1 mg/mL PAH solution and incubated for 20 min. The PAH electrostatically binds to any area of the bare silica surface not covered by PDMS residue, corralling the lipids on the surface preventing them from spreading.[35] PAH was chosen over BSA because of the lack of SFG signal it

produces in the vibrational region of the lipids providing better contrast in the image. The prism was then transferred to a water bath and assembled into a custom built flow cell. The flow cell was rinsed with D_2O before imaging. For the temperature scans, the temperature was brought up to 36°C at a rate of 0.3°C/min and then continued to heat and cool at a rate of 0.75°C/min.

5.2.5 Continuous Lipid Bilayer Preparation by Vesicle Fusion

In order to verify the results obtained from the SFVI of the MLBAs, similar experiments were performed for the three equal molar binary mixtures of 1:1 DOPC:DSPC, 1:1 DOPC:DPPC and 1:1 DMPC:DSPC using SFVS. The bilayers were prepared by vesicle fusion by introducing one of the three binary SUV solutions at 65°C into a dry flow cell assembled with a clean prism. After a 30 min incubation time, the flow cell was rinsed with PBS followed by Nanopure water and a final rinse with D_2O.

5.2.6 SFVI Setup

SFVI was conducted using a custom optical parametric oscillator (OPO)/optical parametric amplifier (OPA) system (LaserVision) pumped by a 10 Hz Surelite Ex NdYAG laser (Continuum) with a 7 ns pulse duration and an energy of about 500 mJ/pulse. This system has been described in detail elsewhere.[29,36] The tunable IR (2750-3050 cm^{-1}) generated from the OPO/OPA was combined with a fixed 532 nm beam at the silica/D_2O interface in a co-propagating manner with incidence angles around 62° and 67°, respectively. The IR and fixed 532 nm beams were collimated to beam areas of ~7 mm^2 with energies of 7 and 9 mJ/pulse, respectively. The SFVI

images were collected with *s*- polarized sum frequency, *s*- polarized visible and *p*-polarized IR (*ssp*). The SFG was collected at the specified IR frequencies using a liquid nitrogen cooled VersArray CCD (Princeton Instruments) with a 512x512 imaging array of 24x24 μm pixels. Three single-band bandpass (447/60 nm Brightline, Semrock) and three single-notch filters (532 nm StopLine, Semrock) were placed before the CCD camera to allow the SFG to pass through while removing any residual 532 nm light. A pinhole was placed at the focal point of the short length focusing lens to block additional scattered light. Image acquisition time varied from 1 to 60 min. The images were analyzed using ImageJ software (http://rsbweb.nih.gov/ij/). The rectangular selection tool in ImageJ was used to select the region of interest which was the entire area of the bilayer's pattern. Background subtractions were performed for each image by blocking the IR and using the same acquisition time to collect each image. The images were then rescaled in the x direction to account for the compression that occurs as a result of imaging at an angle close to 67°. The x scale was chosen such that the vertical line-widths would be equivalent to the horizontal line-widths. The line-widths were defined as the full width at half maximum (FWHM) and calculated using *GRAMS/AI* software.

The MLBA images were flat field corrected to account for the intensity distribution of the IR and 532 nm visible laser beams by normalizing each bilayer image to an image of 10 mM KOH. The background image was collected by first removing the MLBA at the end of the experiment by incubating for 20 min in 125 mM sodium dodecyl sulfate (SDS) solution and rinsing with water. Methanol was then injected and incubated for 5 min followed by an additional water rinse. A 10 mM KOH solution was injected and

imaged at 3100 cm^{-1} with the same exposure time (1 hour) used to acquire the MLBA images. The MLBA images were divided by the KOH images in ImageJ to generate flat field corrected images. Background subtractions were also performed using the average intensity from the control spots to obtain a baseline at zero.

5.2.7 SFVS Setup

A SFVS spectrum was collected for the patterned asymmetric DSPC/DSPC-d_{70} PSLB in order to compare the intensities of the SFVI images acquired for the same bilayer. The SFVS setup is identical to the imaging setup described previously except the CCD was replaced with a photomultiplier tube (PMT) and a boxcar integrator (Stanford Research Systems) to process the SFVS signal. The SFVS spectrum was obtained by tuning the IR wavelength from 2750-3050 cm^{-1} in 2 cm^{-1} steps and integrating for 2 seconds at each step. For the temperature scan experiments, signal was collected at an IR frequency of 2875 cm^{-1} and averaged for 1 second.

SFVS temperature scans were also acquired for continuous bilayers of the binary mixtures (DOPC:DSPC, DOPC:DPPC and DMPC:DSPC). For the temperature scans, the temperature was increased at a rate of 0.3°C/min while continually monitoring the CH_3 ν_s intensity at 2875 cm^{-1}. The heating curves for the three different binary mixtures were normalized using two standardization solutions in order to directly compare the results between the three different experiments. The same procedure used for bilayer removal in the MLBAs described in section 5.2.6 was also used for the removal of the continuous bilayer. For the normalization procedure, the SFG intensities from a 10 mM

KOH (I_{KOH}) solution along with a 150 mM PBS (I_{PBS}) solution were measured at 3100 cm^{-1}. The SFG intensities were then normalized using the following equation:

$$I_{normalized} = \frac{I_{CH_3}}{I_{KOH} - I_{PBS}} \quad (5.4)$$

This corrected the CH_3 v_s intensities between days to account for any changes in alignment, laser power and electronic offsets.

5.3 Results and Discussion

5.3.1 Sum-Frequency Vibrational Imaging

For this study, a simplified imaging system was sought to reduce the loss of photons traveling through unnecessary optics traditionally used in microscopy. For example, traditional microscopy experiments (i.e., fluorescence) produce incoherent light of many frequencies and phases in random directions and are characterized by a large divergence from the point source of emission. Photons emanating from such point sources, like those generated in fluorescence, require the use of an objective to reconstruct the image. In contrast, SFG is a coherent process, meaning the generated photons are of the same frequency, phase and direction producing plane wave fronts (i.e., a monochromatic wave having the same value across a plane perpendicular to the direction of propagation) the collection of an image without the aid of a microscope should be possible, as long as the objects being imaged are several order of magnitude larger than the wavelength of light they emit.[37] Sly and co-workers have already shown the feasibility of lens-less imaging using second harmonic generation (SHG), a special

case of SFG.[38] They were able to collect images of (S)-(+)-1,1'-bi-2-naphthol (SBN) binding to a patterned lipid bilayer using only filters to remove the fundamental light and a CCD for image collection when the detector was placed within the confocal distance of the emitted light from the surface.[38]

Lens-less SFVI was initially attempted using a patterned asymmetric DSPC/DSPC-d_{70} lipid bilayer. The white light images of the USAF test target group-element 0-3, 0-4 and 0-5 with corresponding line-widths of 397, 355 and 314 μm, respectively, used to pattern the lipid bilayer are shown in Figure 5.2a. The asymmetric DSPC/DSPC-d_{70} lipid bilayer was selectively etched using ozone to produce the negative of the test pattern (Figure 5.2b). The SFVI images for each group-element presented in Figure 5.2b were acquired with the CCD camera placed 12 cm away from the sample stage with the ω_{IR} tuned to 2875 cm^{-1} corresponding to the CH_3 ν_s. It should be noted that this distance was much shorter than the confocal distance of the setup. The confocal distance is the point at which the coherent beam is no longer collimated, diverging linearly with distance and the wave front become more spherical. Assuming a Gaussian beam profile, the confocal distance (z) can be defined as follows:[39]

$$z = \frac{\pi w_0^2}{\lambda} \tag{5.4}$$

where λ is the wavelength of the beam and the spot size w defined as the full width at half maximum (FWHM). The confocal distance was calculated to be 67, 86 and 107 cm for the 314, 355 and 397 μm lines, respectively. The SFVI images in Figure 5.2b show distorted images for all the different line-widths. The vertical lines remain

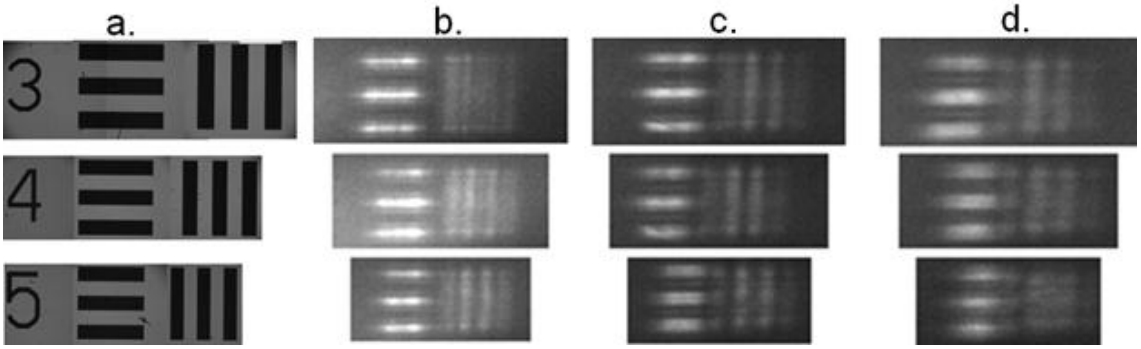

Figure 5.2. (a) The white light image of the USAF test target for group-elements 0-3, 0-4 and 0-5 corresponding to the line-widths of 397, 355 and 314 μm, respectively. (b-d) The lens-less SFVI image of the DSPC/DSPC-d_{70} patterned bilayers prepared using the line-widths shown in (a) and acquired at 2875 cm^{-1}. The lens-less SFVI images were acquired at increasing distances from the sample stage at (b) 12, (c) 20 and (d) 26 cm.

unresolved for the group-elements 0-3 and 0-4 while four blurred vertical lines appear for the 0-5 group-element. While all the horizontal lines remain resolved from one another there exists a nonuniform intensity in both x and y directions with little resemblance to the rectangles shown in the USAF test target. Images were acquired at increasing distances from the substrate to further characterize the propagating SFG beam (Figure 5.2c-d). At 20 cm the lines begin to look more uniform especially for the smaller 0-5 group-element until 26 cm where the images start to blur especially for the 0-5 group-element. This behavior is indicative of diffraction of the emitted sum-frequency light from the surface.

In order to verify diffraction was indeed causing the distortions measured in the SFVI images shown in Figure 5.2, the line profiles obtained from the horizontal lines were compared to Fraunhofer diffraction theory:[40]

$$I = I_0 \left(\frac{\sin \beta}{\beta}\right)^2 \tag{5.5}$$

where $\beta = \frac{1}{2}ka \sin \theta$ with θ defined as the angle of the diffracted rays and a being the width of the slit and $k = 2\pi/\lambda$ where λ is the wavelength of light. The Franuhofer or far-field diffraction equation was used because the objects being measured were much larger than the wavelength of light emitted (~461 nm) and the emitted light is essentially a plane wave. Equation 5.5 was used to plot the intensity distribution from each line-width following normalization with the primary peaks at the appropriate distances of the plot profiles obtained from the SFVI images. The three individual intensity distributions obtained from Figure 5.2 were summed to obtain the intensity

profiles plotted in Figure 5.3. Examination of Figure 5.3 reveals that the Fraunhofer diffraction (grey lines) correlates extremely well with the intensity distribution measured from the SFVI images (black lines). At close distances (12 cm) the calculated and measured intensity distributions both show that the principal maximums have narrower line widths than the USAF test pattern. The lower intensity diffraction peaks observed in the SFVI images, which decrease rapidly off the principal maximum, line up reasonably well with the higher order diffraction peaks predicted by theory. As the distance between the detector and sample is increased the higher order diffraction peaks are not readily resolved in the SFVI images and the line-widths begin to broaden. This too is predicted by the diffraction theory.

The observation of such prominent diffraction was somewhat surprising, as diffraction was not observed in the SHG experiment performed by Sly et al. at distances shorter than the confocal distance for the same line-widths;[38] however, a counter-propagating geometry was used in the SHG experiment. In this geometry, the identical input beams produce an output SHG beam that is emitted normal to the surface with minimal interference. This setup is not viable for these SFVI experiments, due to the vastly different frequencies of the two input beams. Under total internal reflection geometry used here, the resultant SFG beam is being radiated at an angle nearly identical to the 532 nm beam (~67°). The interface between these adjacent wave fronts results in the observed diffraction and renders lens-less imaging impractical for this application.

A confocal spatial filter, consisting of one focusing lens and a pinhole at the focal length, is a convenient way to reconstruct an image of the surface while also removing

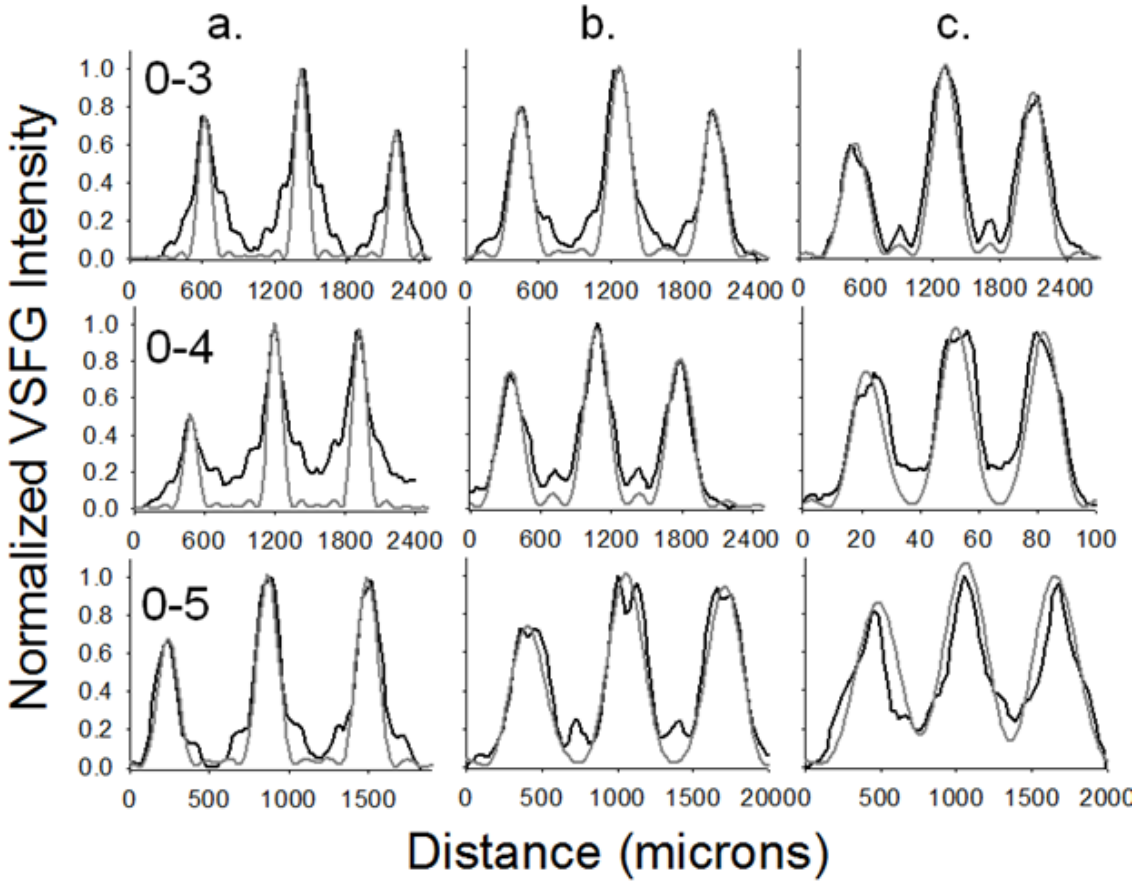

Figure 5.3. (a) The intensity plot profiles for the horizontal lines in Figure 1b are show by the black solid lines as a function of object-detector distance (a) 12, (b) 20 and (c) 26 cm. The grey lines represent the theoretical diffraction pattern produce by the respective line-widths from Equation 5.2.

unwanted background light originating from the incident fundamental at 532 nm and ~3.48 μm.[40] This SFVI setup was initially tested by imaging a pattern created by selectively etching an asymmetric DSPC/DSPC-d_{70} lipid bilayer with ozone using the USAF test target group-element 0-3, 0-4 and 0-5 with corresponding line-widths of 397, 355 and 314 μm, shown in Figure 5.2a. The SFVI images for each group-element were acquired individually at 2875 cm^{-1} and pieced together in Figure 5.4. The SFVI images in Figure 5.4 show well resolved vertical and horizontal lines at all the different line-widths. The non-uniform distribution of intensities between line-widths is likely a consequence of the intensity distribution of the IR and 532 nm visible laser beams. Figure 5.4 also illustrates the ability of this setup to image much smaller line-widths as made apparent by clarity of the individual numbers signifying each element. These numbers have a corresponding line-width of 120 μm. A small air bubble that formed on the second vertical line of group-element 0-4 and destroyed the upper portion of the bilayer is also clearly shown. It should be noted that the CCD camera was placed at a distance from the focal point of the focusing lens to increase the image size to 1.4x its original size.

The resolution of the optical setup was determined by calculating the smallest resolvable feature of the USAF test target which was UV patterned on the asymmetric DSPC/DSPC-d_{70} bilayer (Figure 5.5a). Using the Rayleigh criterion, in which the center maximum of the image of one source falls on the first minimum of the other,[37] the vertical lines remain resolved up to the 2-6 group-element which correspond to 70 μm line-widths (Figure 5.5b). The horizontal lines remain resolved up to the 31 μm line-width (4-1 group-element) (Figure 5.5c). It should be noted that the peaks were

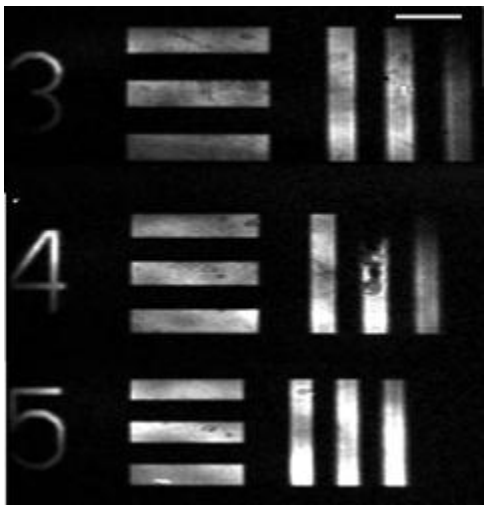

Figure 5.4. The SFVI image taken of a patterned bilayer imaged with a single lens and confocal stop. The CCD was placed an appropriate distance from the lens to produce a 1.4x magnification in the object size. Scale bars represent 1 mm.

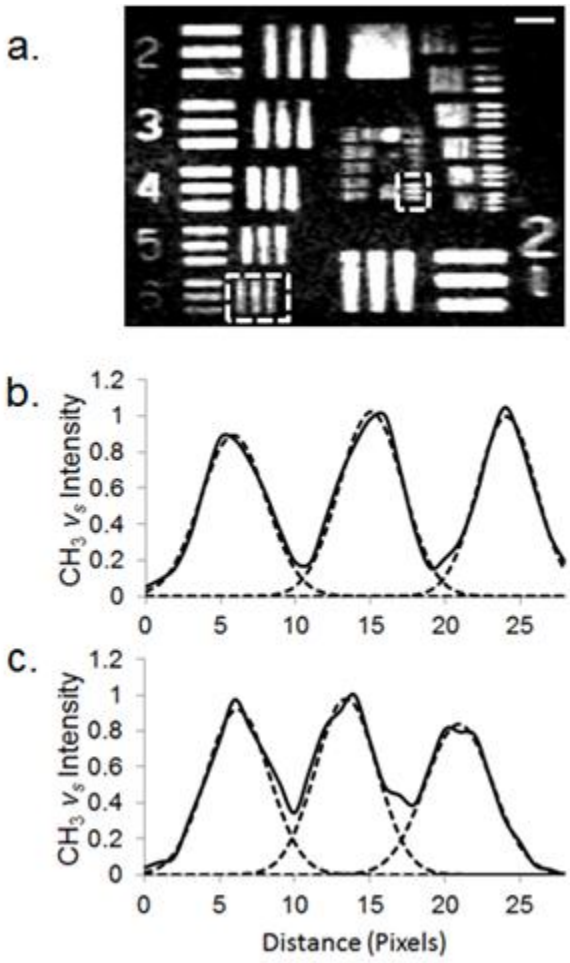

Figure 5.5. (a) The SFVI image of the USAF test target for the group-elements starting at 2-1. (b) The intensity plot profile for the dashed box highlighting the 2-6 group-element vertical lines (70 μm line-width) is shown as the black solid lines with the dashed lines representing the Gaussian peak fitting. (c) The intensity plot profile (black solid line) for the dashed box highlighting the 4-1 horizontal lines (31 μm line-width) and the Gaussian fits (dashed lines) is shown. Scale bars represent 400 μm.

fitted to a Gaussian function in order to provide a simple approximation of the resolution. This anisotropic resolution is expected as a result of imaging at an oblique angle.[9] These results demonstrate that one focusing lens is all that is needed to generate well resolved images with a spatial horizontal and vertical resolution of 70 and 31 μm, respectively. This resolution was acceptable since a setup with a large field of view and efficient photon collection was the desired outcome of the current study, as the application was for the chemical imaging of lipid arrays. It is important to note that the observed resolution in the current study is also based on the quality of the line-widths of the lipid bilayers which is dependent on many factors such as UV exposure time, distance of the substrate from the UV lamps and mobility of the lipids influencing the sharpness of the lines. The resolution of the current lens setup is further limited by the pixel size (24 μm) of the CCD and could be improved by increasing the magnification of the lens setup.

5.3.2 Vibration Spectroscopy and SFVI

In order to test the vibrational selectivity of the SFVI setup, a UV patterned asymmetric DSPC/DSPC-d_{70} bilayer patterned with the USAF test target was imaged at different frequencies and compared to the SFVS signal of an identically prepared bilayer. The spectrum of the patterned bilayer in Figure 5.6 shows predominant peaks from the lipid acyl chains at 2846 cm^{-1}, 2875 cm^{-1} and 2935 cm^{-1} which correlate to the CH_2 symmetric stretch (v_s), CH_3 v_s and the CH_3 Fermi resonance (FR), respectively.[41] Images of the USAF test target patterned asymmetric bilayer using group-element 0-3 corresponding to 397 μm line-widths (Figure 5.6a) were taken at the three peak

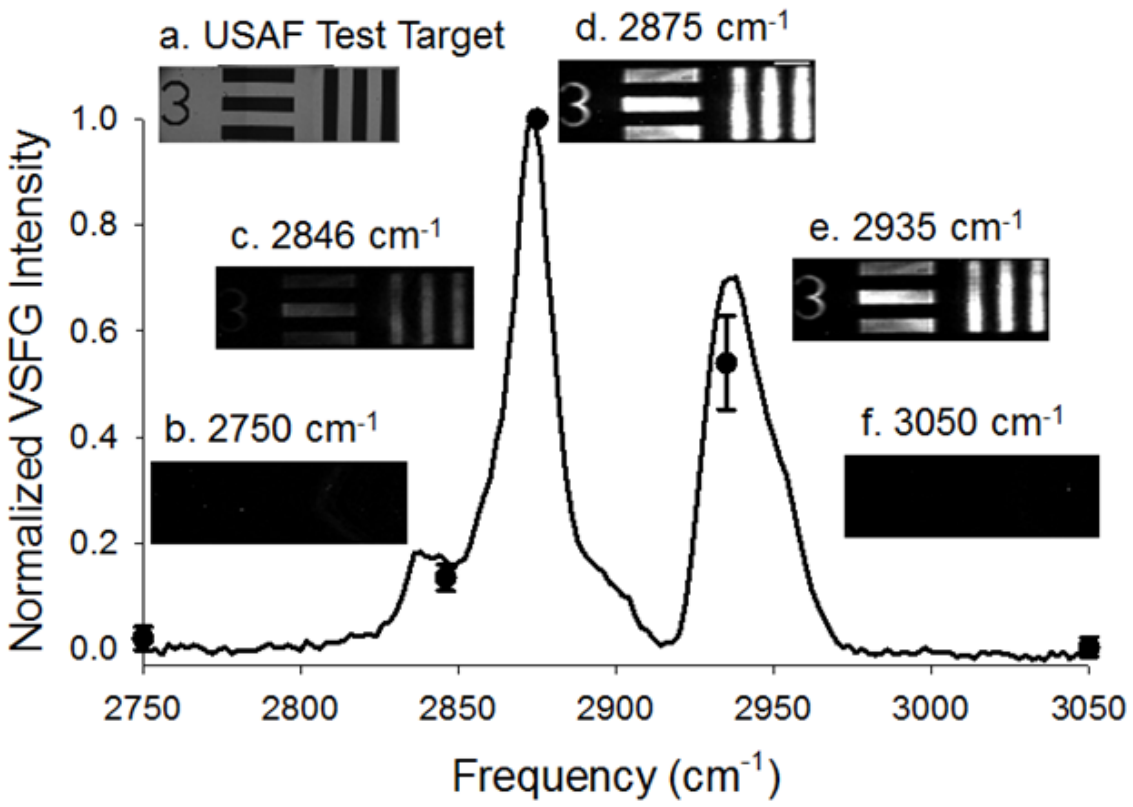

Figure 5.6. SFVI images of a patterned DSPC/DSPC-d_{70} bilayer using (a) USAF test target group-element 0-3 (white light image using a standard laboratory microscope) corresponding to 397 μm line-width acquired at the reported frequencies (b-f). The six line-widths were first individually normalized to their identical initial line-width intensity at 2875 cm^{-1} and reproduced in three separate experiments. The averaged SFVS spectrum from three experiments is also shown for a patterned DSPC/DSPC-d_{70} bilayer (solid black line). The scale bar represents 1 mm.

frequencies along with two off resonance peaks at 2750 and 3050 cm^{-1} and are shown in Figure 5.6b-f. The intensity of the patterned bilayer at the different frequencies was individually normalized to the intensity at 2875 cm^{-1} for each line-width and reproduced in triplicate. The normalized intensities from the images were overlaid with the normalized spectrum of the patterned bilayer. The intensities of the patterned bilayer at 2846 and 2935 cm^{-1} were found to be 12 ± 5 and 46 ± 13 % of the intensity at 2875 cm^{-1}, respectively. These percentages are comparable to the spectral results from the patterned bilayer, which was calculated to be 17 ± 2 and 70 ± 4 % for 2846 and 2936 cm^{-1}, respectively. The differences are insignificant at the 95 % confidence level for the CH_2 v_s/CH_3 v_s ratio but not for the CH_3 $_{FR}$/CH_3 v_s ratio. The discrepancy could be a consequence of the decreasing quantum efficiency (QE) at shorter wavelengths across the SFG wavelengths from 464 to 457 nm (corresponding to ω_{IR} = 2750 to 3050 cm^{-1}) for the CCD device while the PMT's QE increases at these shorter wavelengths. Furthermore, the images acquired off resonance shows a small amount of signal at 2750 cm^{-1} while at 3050 cm^{-1}, no statistically significant intensity above background at the 95 % confidence level was measured. These experiments demonstrate that the SFVI setup can resolve vibrational information with similar results compared to the well-established SFVS technique, but with spatial resolution.

5.3.3 Application of SFVI

SFVI was applied to investigate the conversion of a patterned asymmetric DSPC/DSPC-d_{70} lipid bilayer to a symmetric bilayer as a function of temperature. As the asymmetric DSPC bilayer is heated near its T_m, the lipids undergo a transformation

from the *gel* phase to the *l.c.* phase. This transition is also accompanied by a rapid increase in the rate of lipid translocation, or flip-flop, which results in the conversion of the asymmetric bilayer into a homogenous symmetric bilayer with equal populations of deuterated and proteated DSPC in each leaflet.[30] SFVS has already been used to successfully probe the degree of asymmetry in DSPC/DSPC-d_{83} lipid bilayers as a function of temperature.[32] This application was tested with SFVI by imaging an asymmetric DSPC/DSPC-d_{70} bilayer patterned with 355 μm line-widths from the USAF test target as a function of temperature. The images are shown above the plotted normalized intensities at their respective temperatures in Figure 5.7. The data points were compared to the heating and cooling curves of a patterned bilayer of identical composition obtained using SFVS, shown as solid lines in Figure 5.7. The heating curve (black line) shows a steady decrease in signal until 50°C where the signal falls off sharply and drops to background levels at the T_m (55°C). The results obtained from SFVI (solid triangles) follow a similar trend with respect to temperature with slightly lower average intensities as the temperature approaches the T_m. This could be explained by the difference in integration times between the two techniques: 1 minute for SFVI and 1 second for SFVS. For example, there is a fast rate of lipid flip at 52°C even though it is still below the T_m. The signal will continue to decay during the 1 minute acquisition time resulting in a lower measured intensity.[30] Figure 5.7 also shows that the signal remains at background levels for both techniques when the bilayer is cooled back through its phase transition temperature as a result of the transformed symmetric lipid bilayer.

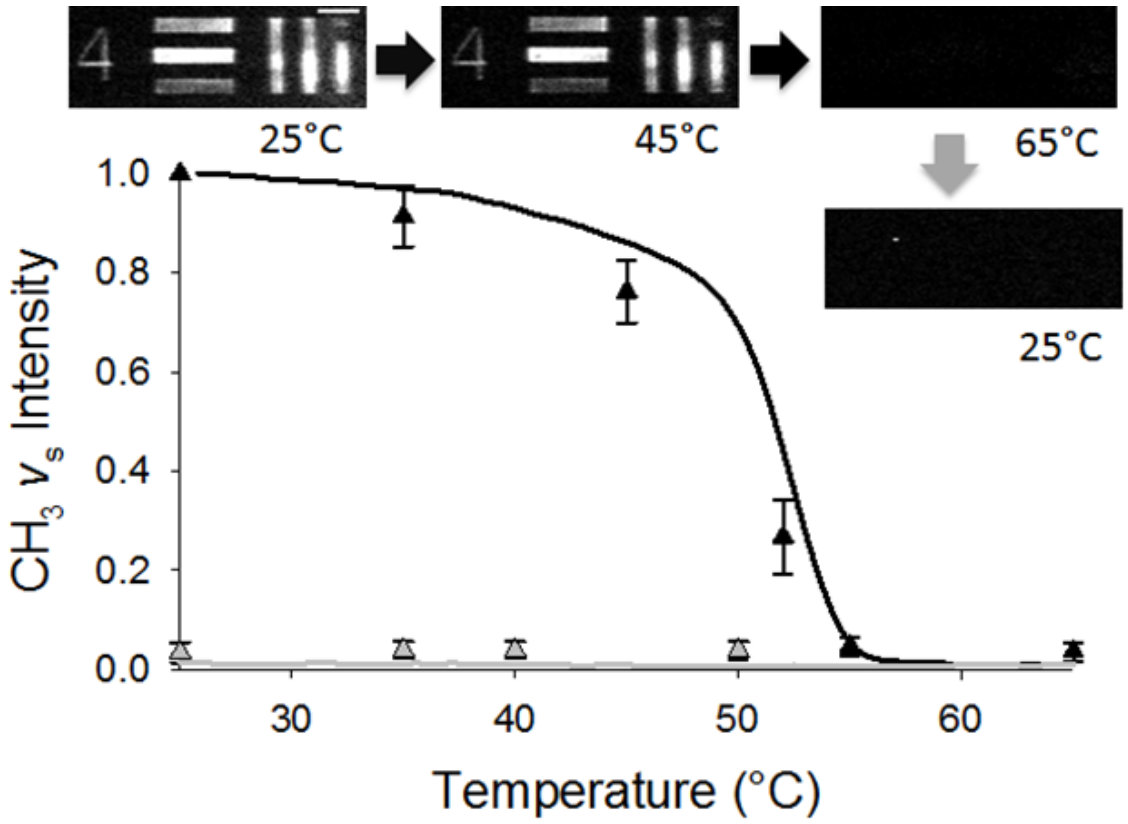

Figure 5.7. SFVI images of the USAF test target group-element 0-4 (355 μm line-width) patterned DSPC/DSPC-d_{70} bilayer acquired at various temperatures measured with an incident IR frequency of 2875 cm^{-1}. The intensities as a function of heating (black) and cooling (grey) are shown as triangles. The data points represent the average intensity measured for of all the lines pooled from three separate experiments which each line first individually normalized to their respective intensity at 25°C. The heating (black) and cooling (grey) curves represent the smoothed data averaged from three separate experiments obtained from a patterned DSPC/DSPC-d_{70} bilayer by SFVS. The scale bar represents 1 mm.

Another potential application of SFVI would be to study the phase behavior of lipid bilayers in a multicomponent MLBAs for high-throughput experiments. Liu et al. have already demonstrated that SFVS is capable of detecting domain disparities between segregated phases in the proximal and distal leaflets of a PSLB.[32] Lipid mixtures with disparate T_ms or a single lipid component bilayer at the T_m create a phase segregated lipid membrane in which distinct lipid domains form in the bilayer. Although this signal is almost an order of magnitude lower than the signal obtained from a fully asymmetric bilayer, it is readily detectable spatially using the SFVI setup described here.[32] To demonstrate the capabilities of our SFVI setup, the phase behavior in a MLBA prepared using the CFM was investigated. Figure 5.8 shows the flat field corrected images obtained at 2875 cm^{-1} of a MLBA composed of DOPC:DSPC, DOPC:DPPC and DMPC:DSPC at various temperatures along with blank spots to serve as controls. It is worth noting that even after a flat field correction, the intensity uniformity within each patch does not compare to the uniformity observed in the fluorescence bilayer spots shown in the previous chapters. This could be a consequence of an irregular distribution of the phase segregated domains unlike the homogeneous distribution of fluorescently labeled lipids. Membranes containing 40 mol % CHO in DOPC:DSPC generate large amount of signal due to an asymmetric distribution of CHO within the membrane and were, therefore, used as position finders in the array.[33]

A significant sum-frequency intensity was observed from DOPC:DSPC (0.28 ± 0.09) and DOPC:DPPC (0.41 ± 0.13) at room temperature while the signal from DMPC:DSPC bilayer patches (0.04 ± 0.04) is not statistically different from the control spots (0.00 ± 0.07). In order to validate our results, SFVS heating curves were obtained

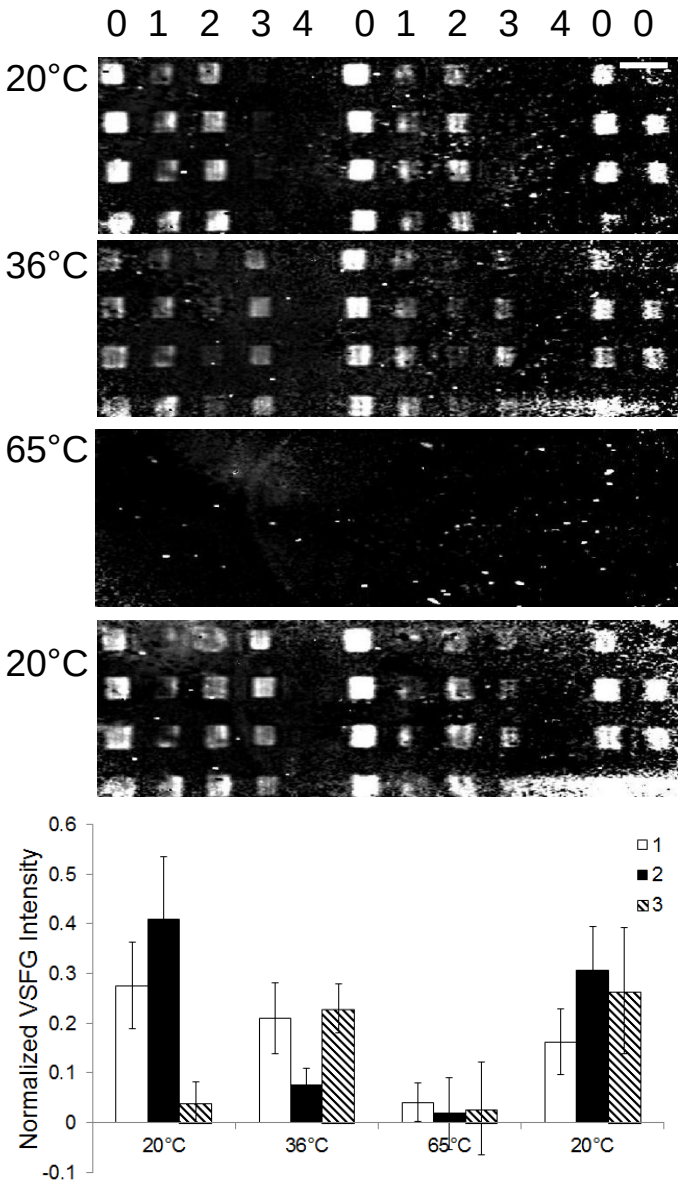

Figure 5.8. The flat field corrected SFVI images of a MLBA composed of a molar ratio of (0) 1:1 DOPC:DSPC with 40 mol % CHO, (1) 1:1 DOPC:DSPC, (2) 1:1 DOPC:DPPC, (3) 1:1 DMPC:DSPC and (4) a control spot acquired at different temperatures at 2875 cm^{-1}. The average VSFG intensities as a function of temperature are shown in the bar graph for columns labeled 1, 2 and 3 with the exception of the bottom right spot located in the second column labeled 3. Scale bar represents 800 μm.

for continuous bilayers having the same binary lipid mixtures used in the MLBAs by monitoring the 2875 cm^{-1} intensity as a function of temperature (Figure 5.9). The results show that a maximum amount of SFG intensity is observed at 20°C for DOPC:DSPC and DOPC:DPPC mixtures while a significantly lower SFG intensity is observed for the DMPC:DSPC bilayer. Both experiments agree well and suggests phase segregation exists between DSPC:DOPC and DOPC:DPPC while DMPC:DSPC are more homogenous at 20°C. This is also consistent with the phase diagrams for these lipid compositions presented in the literature.[32,42,43] At 20°C there is phase coexistence in DOPC:DSPC and DOPC:DPPC bilayers between the *gel* (DSPC/DPPC) and *l.c.* (DOPC) phases while a homogenous *gel* phase exists for the binary DMPC:DSPC mixture.[32,42,43]

When the array is heated to 36°C there is a dramatic attenuation in signal for the DOPC:DPPC bilayer spots from 0.41 ± 0.13 to 0.07 ± 0.03 while there is a fivefold increase in the intensity observed from the DMPC:DSPC spots from 0.04 ± 0.04 to 0.23 ± 0.05. There is a slight but not significant decrease in the sum-frequency intensity for the DOPC:DSPC spots from 0.27 ± 0.09 to 0.21 ± 0.07. This correlates well with the SFVS experiments which show a sharp decrease in the SFG intensity for the DOPC:DPPC bilayer above 26°C. Figure 5.9 also demonstrates that as the DMPC:DSPC binary mixture is heated to 36°C there is a significant increase in the CH_3 ν_s signal while little change is observed for the DOPC:DSPC bilayer. These results are also consistent with the reported T_m for these binary mixtures: 33°C for DPPC in the binary mixture DOPC:DPPC, 27°C for DMPC in DMPC:DSPC mixtures and 48-50°C for DSPC in both DOPC:DSPC and DMPC:DSPC binary mixtures.[32,43] Therefore, at

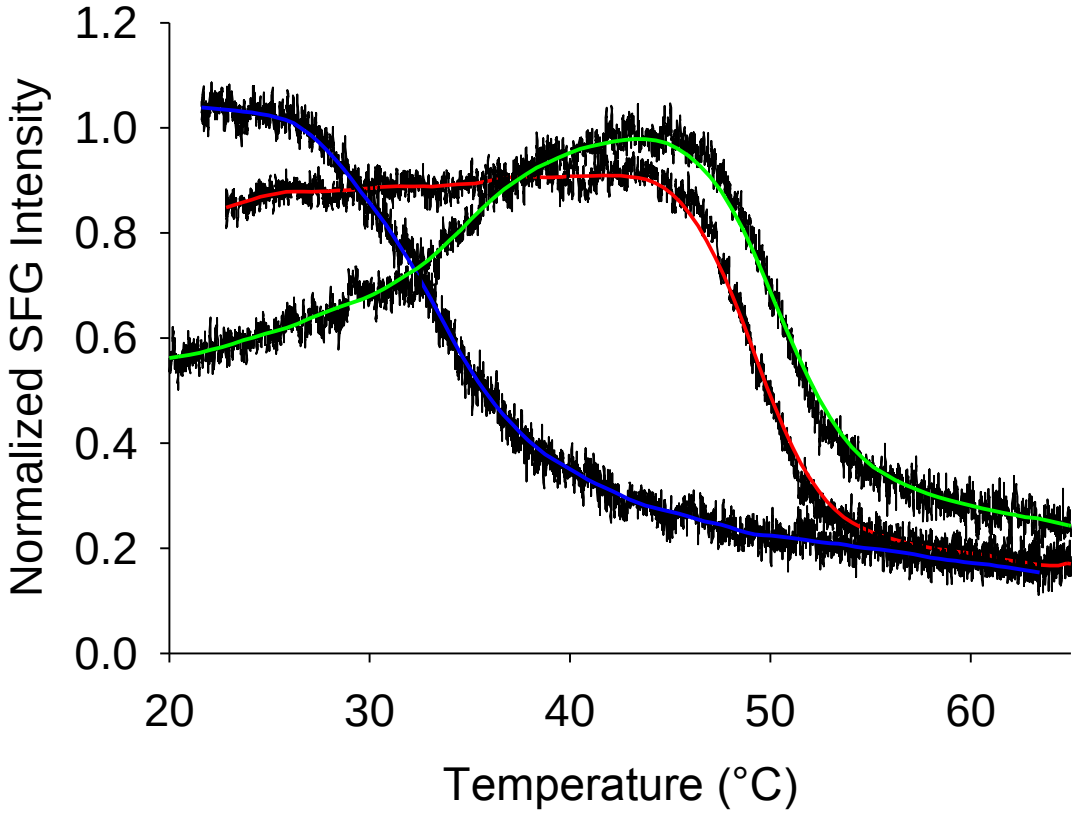

Figure 5.9. CH_3 ν_s intensity as a function of temperature for the binary mixtures 1:1 DOPC:DSPC (—),1:1 DOPC:DPPC (—) and 1:1 DMPC:DSPC (—). The black lines represent the raw data while the color lines are the smooth fits to the data.

36°C DOPC:DPPC becomes a homogenous *l.c.* membrane as DPPC transitions into the *l.c.* phase and there is a subsequent loss in sum-frequency intensity. Meanwhile, there is a significant increase in signal observed for the DMPC:DSPC binary mixtures as DMPC transitions to the *l.c.* phase yielding a two phase coexistence. At this temperature (36°C) there will still be a two phase coexistence in the DOPC:DSPC mixtures although the signal attenuates slightly as a result of increase in temperature approaching the T_m of DSPC. When the temperature is further increased to 65°C there is a significant reduction in signal observed from all the binary lipid mixtures which are all within error of the control spots. This is consistent with the SFVS experiment validating that the minimum values for all the binary mixtures are observed at 65°C. The subsequent loss of signal is the result of all the lipid membranes being in the *l.c.* phase.

When the MLBA is cooled back down to 20°C there is an almost full recovery of the original intensities for DOPC:DSPC (0.16 ± 0.06) and DOPC:DPPC (0.31 ± 0.09). The slightly lower intensities observed for DOPC:DSPC and DOPC:DPPC bilayer spots could be a consequence of the temperature sweeps through the T_m of the lipids which is known to disrupt membrane structure and increase defects in the membrane upon cooling.[44,45] In contrast, the intensity from the DMPC:DSPC bilayer patches (0.26 ± 0.13) are comparable to signal intensity observed when the sample was first heated to 36°C. This could be a result of a hysteresis where lipids can exhibit a lower T_m as a result of cooling the sample during temperature sweeps. For example, Ohlsson et al. used quartz crystal microbalance with dissipation (QCM-D) to measure the T_m of 1,2-ditridecanoyl-s*n*-glycero-3-phosphocholine (DTPC) lipids and observed a 1.5°C

hysteresis at a cooling rate of 0.2°C/min.[46] Furthermore, they reported a linear dependence between the rate of cooling and the hysteresis with a faster rate yielding a larger hysteresis.[46]

With only one optical element used to construct images, the SFVI setup described here had the signal to noise ratio necessary to detect domain disparities between the *l.c.* and *gel* phase lipids. This is nontrivial given the low amount of SFG signal generated from this type of asymmetry. Also, without the use of an objective, the SFVI setup allowed for a larger field of view equivalent to a 5 x 12 mm^2 area. These experiments highlight this simplified SFVI setup as a high-throughput platform capable of simultaneously detecting the phase behavior in up to 48 unique lipid bilayer spots.

5.4 Conclusion

The SFVI setup described here, utilizes a single focusing lens in conjunction with a confocal stop, is capable of resolving both vertical and horizontal line-widths of varying sizes on the μm scale. It was also shown that SFVI can be used to probe the different vibrational resonances of the lipid bilayer with its vibrational sensitivity comparable to SFVS. SFVI was capable of resolving up to 48 400 x 400 μm^2 spots along with the sensitivity of measuring the phase behavior in binary lipid bilayer mixtures. The phase transition temperatures of three different binary mixtures (DOPC:DSPC, DOPC:DPPC and DSPC:DMPC) were successfully probed using the IR sensitivity and spatial resolution afforded by SFVI. The capability of this technique to study inhomogeneities of biological surfaces with IR selectivity and sub-IR resolution could be extended to a

broad range of important applications in many fields such as drug discovery and clinical diagnostics.

5.5 References

(1) Xie, X. S.; Lu, H. P. *Journal of Biological Chemistry* **1999**, *274*, 15967.

(2) Weiss, S. *Science* **1999**, *283*, 1676.

(3) Nguyen, T. T.; Conboy, J. C. *Analytical Chemistry* **2011**, *83*, 5979.

(4) Lambert, A. G.; Davies, P. B.; Neivandt, D. J. *Applied Spectroscopy Reviews* **2005**, *40*, 103.

(5) Shen, Y. R. *Nature (London, United Kingdom)* **1989**, *337*, 519.

(6) Shen, Y. R. *The Principles of Nonlinear Optics*; John Wiley and Sons: New York, 1984.

(7) Floersheimer, M.; Brillert, C.; Fuchs, H. *Langmuir* **1999**, *15*, 5437.

(8) Florsheimer, M.; Brillert, C.; Fuchs, H. *Materials Science & Engineering, C: Biomimetic and Supramolecular Systems* **1999**, *C8-C9*, 335.

(9) Hoffmann, D. M. P.; Kuhnke, K.; Kern, K. *Review of Scientific Instruments* **2002**, *73*, 3221.

(10) Cimatu, K.; Baldelli, S. *J. Phys. Chem. B* **2006**, *110*, 1807.

(11) Kuhnke, K.; Hoffmann, D. M. P.; Wu, X. C.; Bittner, A. M.; Kern, K. *Applied Physics Letters* **2003**, *83*, 3830.

(12) Chapman, D.; Williams, R. M.; Ladbrooke, B. D. *Chemistry and Physics of Lipids* **1967**, *1*, 445.

(13) Rinia, H. A.; Boots, J.-W. P.; Rijkers, D. T. S.; Kik, R. A.; Snel, M. M. E.; Demel, R. A.; Killian, J. A.; Van der Eerden, J. P. J. M.; de Kruijff, B. *Biochemistry* **2002**, *41*, 2814.

(14) Koynova, R.; Caffrey, M. *Biochimica et Biophysica Acta* **1998**, *1376*, 91.

(15) Smith, L. M.; Weis, R. M.; McConnell, H. M. *Biophysical Journal* **1981**, *36*, 73.

(16) Von Tscharner, V.; McConnell, H. M. *Biophysical Journal* **1981**, *36*, 409.

(17) Brown, K. G.; Peticolas, W. L.; Brown, E. *Biochemical and Biophysical Research Communications* **1973**, *54*, 358.

(18) Snyder, R. G.; Strauss, H. L.; Elliger, C. A. *Journal of Physical Chemistry* **1982**, *86*, 5145.

(19) Yan, W.-H.; Strauss, H. L.; Snyder, R. G. *Journal of Physical Chemistry B* **2000**, *104*, 4229.

(20) Mendelsohn, R.; Moore, D. J. *Chemistry and Physics of Lipids* **1998**, *96*, 141.

(21) Tamm, L. K.; Tatulian, S. A. *Quarterly Reviews of Biophysics* **1997**, *30*, 365.

(22) Varga, I.; Keszthelyi, T.; Meszaros, R.; Hakkel, O.; Gilanyi, T. *Journal of Physical Chemistry B* **2005**, *109*, 872.

(23) Harp, G. P.; Rangwalla, H.; Yeganeh, M. S.; Dhinojwala, A. *Journal of the American Chemical Society* **2003**, *125*, 11283.

(24) Zhang, D.; Gutow, J. H.; Eisenthal, K. B. *Journal of the Chemical Society, Faraday Transactions* **1996**, *92*, 539.

(25) Braun, R.; Casson, B. D.; Bain, C. D. *Chemical Physics Letters* **1995**, *245*, 326.

(26) Liu, J.; Conboy, J. C. *Langmuir* **2005**, *21*, 9091.

(27) Liu, J.; Conboy, J. C. *J. Phys. Chem. B.* **2007**, *111*, 11.

(28) Liu, J.; Conboy, J. C. *J. Am. Chem. Soc.* **2004**, *126*, 8894.

(29) Liu, J.; Conboy, J. C. *Biophysical Journal* **2005**, *89*, 2522.

(30) Liu, J.; Conboy John, C. *Journal of the American Chemical Society* **2004**, *126*, 8376.

(31) Garg, S.; Rühe, J.; Lüdtke, K.; Jordan, R.; Naumann, C. A. *Biophysical Journal* **2007**, *92*, 1263.

(32) Liu, J.; Conboy, J. C. *Journal of Physical Chemistry C* **2007**, *111*, 8988.

(33) Liu, J.; Conboy, J. C. *Vibrational Spectroscopy* **2009**, *50*, 106.

(34) Wacklin, H. P. *Langmuir* **2011**, *27*, 7698.

(35) Burridge, K. A.; Figa, M. A.; Wong, J. Y. *Langmuir* **2004**, *20*, 10252.

(36) Brown, K. L.; Conboy, J. C. *J. Am. Chem. Soc.* **2011**, *133*, 8794.

(37) Milonni, P. W.; Eberly, J. H. *Lasers*; John Wiley and Sons: New York, 1988.

(38) Sly, K. L.; Nguyen, T. T.; Conboy, J. C. *Submitted to Optical Express* **2012**.

(39) Hecht, E. *Optics*; Addison Wesley: San Francisco, 2002.

(40) Fowles, G. R. *Introduction to Modern Optics*; 2nd ed. ed.; Holt, Rinehart and Winston: New York, 1975.

(41) Tamm, L. K.; Tatulian, S. A. *Quarterly Reviews of Biophysics* **1997**, *30*, 365.

(42) Almeida, P. F. F.; Vaz, W. L. C.; Thompson, T. E. *Biophys. J.* **1993**, *64*, 399.

(43) Lentz, B. R.; Barenholz, Y.; Thompson, T. E. *Biochemistry* **1976**, *15*, 4529.

(44) Xie, A. F.; Yamada, R.; Gewirth, A. A.; Granick, S. *Physical Review Letters* **2002**, *89*, 246103/1.

(45) Tamm, L. K.; McConnell, H. M. *Biophysical Journal* **1985**, *47*, 105.

(46) Ohlsson, G.; Tigerstroem, A.; Hoeoek, F.; Kasemo, B. *Soft Matter* **2011**, *7*, 10749.

CHAPTER 6

CONCLUSION

The development and application of MLBAs prepared by a CFM has been described in this dissertation. It has been presented as a simple alternative to generate multicomponent lipid arrays. In Chapter 2 the MLBAs created by the CFM were shown to maintain the 2D fluidity and structure of biological membranes. Experimental evidence was also presented to demonstrate the accurate, reproducible transfer of the lipid composition from vesicle to PSLB form. Three different fluorescently labeled lipids were used to show that each microchannel is individually addressable, allowing for discrete lipid compositions to be transferred to the substrate in a controlled manner. The functionality of these arrays was also demonstrated by the successful execution of a ligand-protein binding assay. The multiplexed ligand array targeted its specific protein while showing minimal cross-reactivity and nonspecific binding. Furthermore, the amount of each protein bound correlated to the ligand concentration doped into each membrane. These binding assays were shown to be reproducible and agreed well with similar ligand-protein assays on PSLBs presented in the literature. The MLBAs were well characterized in Chapter 2, demonstrating the success of this new technique for generating MLBAs and its potential applications for performing high information biological assays.

For MLBAs to be commercially useful as a multiplexed biosensor platform, the durability of these arrays must be improved. Chapter 3 focused on creating stable MLBAs by incorporating a poly(lipid) into the membrane. MLBAs prepared with the polymerizable lipid, poly(bis-SorbPC) were shown to be stable when exposed to an air-water interface while the fluid lipid bilayer patches prepared with unpolymerizable lipids completely desorbed from the surface. The practical use of these polymerized lipid arrays was tested using a multicomponent ligand-protein binding assay. GM_1 and biotin functionalized lipids were doped into poly(bis-SorbPC) lipids and selectively bound their fluorescently labeled protein counterparts. The results showed minimal cross-reactivity and nonspecific binding of the CTb. There was a significant amount of nonspecific adsorption of the streptavidin to the poly(bis-SorbPC) bilayers but it was comparable to that observed for fluid unpolymerizable lipids. These stable ligand arrays were also shown to be reusable by introducing them to a denaturing solution as well as an air-water interface. The binding assays were regenerated and proved to be reproducible, demonstrating their durability. Chapter 3 presents a more practical MLBA format with the added stability necessary for applications outside the laboratory.

Small molecules represent an important class of interactions occurring at the cell membrane. In Chapter 4 small molecule-membrane binding to the MLBAs was modeled using MC540. Fifteen membrane compositions were used and results showed that MC540 fluorescence intensity was greatest for fluid phase lipids while significant attenuation in fluorescence was observed in gel phase lipid spots. Cholesterol was also shown to have minimal impact on the MC540 fluorescence in fluid phase bilayers while decreasing MC540 fluorescence even further in gel phase lipid bilayer patches. These

results correlated well with previous studies reported on MC540 binding to lipid bilayers. Binding to negatively charged membranes containing PS headgroup lipids was also investigated. MC540 fluorescence intensity was attenuated with increasing PS concentration as a result of electrostatic repulsion. This work demonstrates that MLBAs are viable models for small molecule-membrane interactions with the potential to be incorporated in a wide variety of applications such as pharmaceutical screening.

In Chapter 5, the combination of high-throughput imaging and the label-free surface specific technique SFVG was discussed. This SFVI technique has the unique ability to study lipid properties without the use of a perturbing fluorophore while also providing the spatial resolution necessary to investigate lipid bilayer arrays. A simplified SFVI apparatus was developed and characterized with UV photolithographic patterned asymmetric PSLBs. The CH_2 ν_s, CH_3 ν_s and $CH_{3\,FR}$ vibrational resonances were imaged and correlated to the established SFVS intensities. The T_ms of these patterns were also successfully investigated and were found to have heating and cooling curves similar to that observed with SFVS. The phase behavior of three binary mixtures, DOPC:DSPC, DOPC:DPPC and DMPC:DSPC, was also investigated in the MLBAs. Significant SFG signal was observed for the DOPC:DSPC and DOPC:DPPC binary mixtures at room temperature while no SFG signal was observed for the DMPC:DSPC lipid bilayer spots. When the MLBA was heated to 36°C, significant SFG signal was still observed from the DOPC:DSPC bilayer patches, while the signal from the DOPC:DPPC spots diminished below background signal and the DMPC:DSPC spot's signal became observable. Above 65°C the SFG signal from all the binary mixtures dropped below background noise and cooling resulted in the return of SFG intensity for all the bilayer

spots. These results were consistent with the previously reported phase behavior of these compositions. One powerful application of SFVI is towards studying phase segregation as it provides a way to collect the vibrational spectra of the molecules at the surface for unique membrane compositions.

It has been shown in this dissertation that MLBAs have a diverse range of applications ranging from their use in multiple protein-ligand assays to their applications in the investigations of small molecule-membrane interactions with fluorescence microscopy. The lipid arrays were also used to study lipid phase behavior in multi-composition bilayers using nonlinear imaging techniques. The development of SFVI in combination with the MLBAs has greatly enhanced the potential applications of these arrays by eliminating the need for an extrinsic probe. This has opened the possibility of imaging a wide variety of analytes that have a vibrational resonance in the mid-IR region, as well as investigating their perturbing effects on the structure and dynamics of multicomponent lipid membranes. In particular, the influence of pharmaceutical drugs on the lipids' thermotropic phase behavior, which may be important to the primary function of the drug in addition to any potential side effects, can be explored in a noninvasive high-throughput manner. The studies reported here highlight MLBAs as a powerful tool for a broad range of applications.